



**Dottorato di Ricerca in Ingegneria Civile**  
***Graduate School in Civil Engineering***

Sede: Facoltà di Ingegneria - Università di Pavia - via Ferrata 1 – 27100 Pavia – Italy

Dottorato di Ricerca in Ingegneria Civile VIII Nuova serie (XXIV Ciclo)

**Structural Monitoring and System Control Using a  
Wireless Sensor Network**

Tesi di Dottorato  
ZhiCong Chen

*Advisor:*

Prof. Fabio Casciati

*Reviser:*

Prof. Roberto Sala

Pavia, October 2011

*To My Parent, Wife and Upcoming Child*



## ***Acknowledgements***

I wish to express my sincere and profound gratitude to Professor Fabio Casciati for constantly providing his enthusiastic support, scientific knowledge, patient guidance, and human experience during the whole PhD study period as a coordinator of the PhD school in Civil Engineering, and for his useful and valuable suggestions and encouragement in the preparation of this thesis, as an advisor. Without his support, the author would have missed the opportunities to participate several conferences and the 2010 asia-pacific summer school on smart structures technology. The detailed revisions and friendly collaboration from Prof. Lucia Faravelli, Prof. Fabio Casciati and Doctor Sara Casciati on writing the accademic articles during PhD study are also greatly acknowledged.

I am grateful to my colleagues for helping me with various aspects of my life and research in the university of Pavia, including the colleagues from the department of structural mechanics: Clement Fuggini, Raed Alsaleh, Alessandro Marzi, Paolo Basso, Matilde Notarangelo, Krzysztof Hinc and Umut Yildirim; the colleagues from department of hydraulic and environmental engineering: Mariacristina Collivignarelli, Alessandro Abbà, Barbara Marianna Crotti, Veronica Cornalba and Matteo Canato.

Lastly, the support of my family is gratefully acknowledged. Especially, I would like to thank my wife Lijun Wu for her support, encourage, assistance and inspiration.



## Dottorato di Ricerca in Ingegneria Civile

<b>Settore:</b> <b>Field:</b>	Ingegneria Engineering
<b>Sede Amministrativa non consortile:</b> <b>Administrative location:</b>	Università degli Studi di PAVIA University of Pavia
<b>Durata del dottorato:</b> <b>Duration:</b>	3 anni 3 years
<b>Periodo formativo estero:</b> <b>Period in foreign organization:</b>	come previsto dal regolamento del Dottorato di Ricerca as required by the school's rules
<b>Numero minimo di corsi:</b> <b>Minimum number of courses:</b>	6 6

## Recapiti - Addresses



Dipartimento di Meccanica Strutturale  
via Ferrata 1 - 27100 Pavia - Italy  
Tel. 0382 / 985458      Fax 0382 / 528422



Dipartimento di Ingegneria Idraulica e Ambientale  
via Ferrata 1 - 27100 Pavia - Italy  
Tel. 0382 / 505300      Fax 0382 / 505589

## Coordinatore – Coordinator

CASCIATI Fabio - Professore Ordinario di Scienza delle Costruzioni (ICAR/08)

Dipartimento di Meccanica Strutturale  
via Ferrata 1 - 27100 Pavia – Italy      Tel. 0382 / 985458      Fax 0382 / 528422  
e-mail: [fabio@dipmec.unipv.it](mailto:fabio@dipmec.unipv.it)

## Collegio dei Docenti – Teaching Staff

CIAPONI Carlo	Professore Straordinario (ICAR/02)
DEL GROSSO Andrea	Professore Ordinario, Unige (ICAR/09)
FARAVELLI Lucia	Professore Ordinario (ICAR/08)
GALLATI Mario	Professore Ordinario (ICAR/01)
GOBETTI Armando	Professore Associato (ICAR/08)
MOISELLO Ugo	Professore Ordinario (ICAR/02)
PAPIRI Sergio	Professore Associato (ICAR/02)
SALA Roberto	Professore Associato (ING-IND/08)
MARCELLINI Alberto	Dirigente di Ricerca. CNR – Milano



## Organizzazione del corso

Il dottorato di ricerca in *Ingegneria Civile* presso la Scuola di Dottorato in Scienze dell'Ingegneria dell'Università degli Studi di Pavia è stato istituito nell'anno accademico 1994/95 (X ciclo).

Il corso consente al dottorando di scegliere tra quattro curricula: idraulico, sanitario, sismico e strutturale. Il dottorando svolge la propria attività di ricerca presso il Dipartimento di Ingegneria Idraulica e Ambientale per i primi due curricula o quello di Meccanica Strutturale per gli ultimi due.

Durante i primi due anni sono previsti almeno sei corsi, seguiti da rispettivi esami, che il dottorando è tenuto a sostenere. Il Collegio dei Docenti, composto da professori dei due Dipartimenti e da alcuni esterni all'Università di Pavia, organizza i corsi con lo scopo di fornire allo studente di dottorato opportunità di approfondimento su alcune delle discipline di base per le varie componenti. Corsi e seminari vengono tenuti da docenti di Università nazionali ed estere.

Il Collegio dei Docenti, cui spetta la pianificazione della didattica, si è orientato ad attivare ad anni alterni corsi sui seguenti temi:

- Meccanica dei solidi e dei fluidi
- Metodi numerici per la meccanica dei solidi e dei fluidi
- Rischio strutturale e ambientale
- Metodi sperimentali per la meccanica dei solidi e dei fluidi
- Intelligenza artificiale

più corsi specifici di indirizzo.

Al termine dei corsi del primo anno il Collegio dei Docenti assegna al dottorando un tema di ricerca da sviluppare sotto forma di tesina entro la fine del secondo anno; il tema, non necessariamente legato all'argomento della tesi finale, è di norma coerente con il curriculum, scelto dal dottorando.

All'inizio del secondo anno il dottorando discute con il Coordinatore l'argomento della tesi di dottorato, la cui assegnazione definitiva viene deliberata dal Collegio dei Docenti.

Alla fine di ogni anno i dottorandi devono presentare una relazione particolareggiata (scritta e orale) sull'attività svolta. Sulla base di tale relazione il Collegio dei Docenti, "previa valutazione della assiduità e dell'operosità dimostrata dall'iscritto", ne propone al Rettore l'esclusione dal corso o il passaggio all'anno successivo.

Il dottorando può svolgere attività di ricerca sia di tipo teorico che sperimentale, grazie ai laboratori di cui entrambi i Dipartimenti dispongono, nonché al Laboratorio Numerico di Ingegneria delle Infrastrutture.

Il “Laboratorio didattico sperimentale” del Dipartimento di Meccanica Strutturale dispone di:

1. una tavola vibrante che consente di effettuare prove dinamiche su prototipi strutturali;
2. opportuni sensori e un sistema di acquisizione dati per la misura della risposta strutturale;
3. strumentazione per la progettazione di sistemi di controllo attivo e loro verifica sperimentale;
4. strumentazione per la caratterizzazione dei materiali, attraverso prove statiche e dinamiche.

Il laboratorio del Dipartimento di Ingegneria Idraulica e Ambientale dispone di:

1. un circuito in pressione che consente di effettuare simulazioni di moto vario;
2. un tunnel idrodinamico per lo studio di problemi di cavitazione;
3. canalette per lo studio delle correnti a pelo libero.

## Course Organization

The Graduate School of Civil Engineering, a branch of the Doctorate School in Engineering Science, was established at the University of Pavia in the Academic Year of 1994/95 (X cycle). The School allows the student to select one of the four offered curricula: Hydraulics, Environment, Seismic Engineering and Structural Mechanics. Each student develops his research activity either at the Department of Hydraulics and Environmental Engineering or at the Department of Structural Mechanics. During the first two years, a minimum of six courses must be selected and their examinations successfully passed. The Faculty, made by Professors of the two Departments and by internationally recognized external scientists, organizes courses and provides the students with opportunities to enlarge their basic knowledge. Courses and seminars are held by University Professors from all over the country and abroad. The Faculty starts up, in alternate years, common courses on the following subjects:

- solid and fluid mechanics,
- numerical methods for solid and fluid mechanics,
- structural and environmental risk,
- experimental methods for solid and fluid mechanics,
- artificial intelligence.

More specific courses are devoted to students of the single curricula.

At the end of each course, for the first year the Faculty assigns the student a research argument to develop, in the form of report, by the end of the second year; the topic, not necessarily part of the final doctorate thesis, should be consistent with the curriculum selected by the student. At the beginning of the second year the student discusses with his Coordinator the subject of the thesis and, eventually, the Faculty assigns it to the student. At the end of every year, the student has to present a complete report on his research activity, on the basis of which the Faculty proposes to the Rector his admission to the next academic year or to the final examination. The student is supposed to develop either

theoretical or experimental research activities, and therefore has access to the Department Experimental Laboratories, even to the Numerical Laboratory of Infrastructure Engineering. The Experimental Teaching Laboratory of the Department of Structural Mechanics offers:

1. a shaking table which permits one to conduct dynamic tests on structural prototypes;
2. sensors and acquisition data system for the structural response measurements;
3. instrumentation for the design of active control system and their experimental checks;
4. an universal testing machine for material characterization through static and dynamic tests.

The Department of Hydraulics and Environmental Engineering offers:

1. a pressure circuit simulating various movements;
2. a hydrodynamic tunnel studying cavitation problems;
3. a micro-channels studying free currents.

## **Elenco delle tesi – Previous PhD Theses**

Marco Battaini (X ciclo)	Sistemi strutturali controllati: progettazione e affidabilità. (February 1998).
Claudia Mariani (X ciclo)	Problemi di ottimizzazione per strutture bidimensionali anisotrope. (February 1998).
Antonella Negri (X ciclo)	Stima delle perdite idrologiche nei bacini di drenaggio urbani. (February 1999).
Aurora Angela Pisano (XI ciclo)	Structural System Identification : Advanced Approaches and Applications. (February 1999).
Carla Saltalippi (XI ciclo)	Preannuncio delle piene in tempo reale nei corsi d'acqua naturali. (February 1999).
Eugenio Barbieri (XI ciclo)	Thermo fluid Dynamics and Topology: Optimization of an Active Thermal Insulation Structure. (February 2000).
Barbolini Massimiliano (XII ciclo)	Dense Snow Avalanches: Computational Models, Hazard Mapping and Related Uncertainties. (February 2000).
Espa Paolo (XII ciclo)	Moti atmosferici generati da forze di galleggiamento: simulazioni numeriche e studio su modello fisico. (February 2000).
Petrini Lorenza (XII ciclo)	Shape Memory Alloys: Modelling the Martensitic Phase Behaviour for Structural Engineering Exploitation. (February 2000).
Podestà Stefano (XIV ciclo)	Risposta sismica di antichi edifici religiosi: una nuova proposta per un modello di vulnerabilità. (February 2002).

- Sturla Daniele (XIV ciclo) Simulazioni lagrangiane di flussi rapidamente variati nell'approssimazione di acque poco profonde. (February 2002).
- Marazzi Francesco (XV ciclo) Semi -active Control of Civil Structures: Implementation Aspects. (February 2003).
- Nascimbene Roberto (XV ciclo) Sail Modelling for Maximal Speed Optimum Design. (February 2003).
- Giudici Massimo (XVI ciclo) Progettazione in regime non lineare di strutture in CAP a cavi aderenti e non aderenti. (February 2004).
- Mutti Matteo (XVI ciclo) Stability Analysis of Stratified Three—phase Flows in Pipes. (February 2004).
- Petaccia Gabriella (XVI ciclo) Propagazione di onde a fronte ripido per rottura di sbarramenti in alvei naturali. (February 2004).
- Casciati Sara (XVII ciclo) Damage Detection and Localization in the Space of the Observed Variables. (February 2005).
- D'Amico Tiziana (XVI ciclo) Ricerca e sviluppo di metodologie diagnostiche per il recupero di edifici monumentali: prove vibroacustiche sul tufo. (February 2005).
- Barco Olga Janet (XVII ciclo) Modeling the Quantity and Quality of Storm Water Runoff Using SWMM. (February 2005).
- Boguniewicz Joanna (XVIII ciclo) Integration of Monitoring and Modelling in the Surface Water State Evaluation Process of a Sub-Alpine Lake Watershed. (February 2006).

Bornatici Laura (XVIII ciclo)	L'impiego degli algoritmi generici per la risoluzione dei problemi di progetto di reti di distribuzione idrica. (February 2006).
Collivignarelli Maria Cristina (XVIII ciclo)	Trattamento di rifiuti liquidi mediante processi biologici aerobici termofili e mesofili e processi avanzati di ossidazione chimica in diversa. (February 2006).
Domaneschi Marco (XVIII ciclo)	Structural Control of Cable-stayed and Suspended Bridges. (February 2006).
Ráduly Botond (XVIII ciclo)	Artificial Neural Network applications in Urban Water Quality Modeling. (February 2006).
Cappabianca Federica (XVIII ciclo)	La valutazione del rischio valanghivo attraverso la modellazione dinamica. (February 2006).
Callegari Arianna (XVIII ciclo)	Applicazione di tecnologie di monitoraggio on-line per la gestione dei processi di trattamento reflui. (February 2006).
Gazzola Elisa (XVIII ciclo)	Applicazione di processi biologici anaerobici al trattamento di acque reflue e fanghi di depurazione: aspetti tecnici ed energetici. (February 2006).
Antoci Carla (XVIII ciclo)	Simulazione numerica dell'interazione fluido-struttura con la tecnica SPH. (July 2006).
Giuliano Fabio (XIX ciclo)	Performance Based Design and Structural Control for Cable Suspension Bridges. (February 2007).
Maranca Federica (XVIII ciclo)	Valutazione del ciclo di vita (LCA): confronto tra sistemi di trasporto gas via gasdotto. (February 2007).

Falappi Stefano (XIX ciclo)	Simulazioni numeriche di flussi di fluidi viscosi e materiali granulari con la tecnica SPH (February 2007).
Zanaboni Sabrina (XIX ciclo)	Pre-trattamento di rifiuti liquidi industriali mediante ossidazione ad umido. (February 2007).
Matteo Bruggi (XX ciclo)	Topology optimization using mixed finite elements. (February 2008).
Gian Paolo Cimellaro (XX ciclo)	Passive Control of Industrial Structures for Natural Hazard Mitigation: Analytical Studies and Applications. (February 2008).
Alessandro Abbà (XXI ciclo)	Il recupero dei rifiuti speciali nel settore delle costruzioni: studio delle possibilità di recupero e valutazione dei meccanismi di lisciviazione. (February 2009).
Karim Hamdaoui (XXI ciclo)	Experimental Applications on Cu-based Shape Memory Alloys: Retrofitting of Historical Monuments and Base Isolation (February 2009).
Thomas Messervey (XXI ciclo)	Integration of Structural Health Monitorin into the Design, Assessment, and Management of Civil Infrastructure (February 2009).
Filippo Ubertini (XXI ciclo)	Wind Effects on Bridges: Response, Stability and Control (February 2009).
Fuggini Clemente (XXII Ciclo)	Using Satellites Systems for Structural Monitoring: Accuracy, Uncertainty, and Reliability(February 2010)
Raboni Massimo (XXII Ciclo)	Impiego di tecniche numeriche e sperimentali per l'analisi di fenomeni multiphysics(July 2010)
Alessandro Marzi(XXIII Ciclo)	Impianti in materiale plastic per il trasporto dei fluidi nel settore navale (February 2011).



- Barbara Marianna Crotti(XXIII Ciclo) Verifiche di funzionalità e criteri di ottimizzazione degli impianti di potabilizzazione: alcuni casi di studio (February 2011)
- Luigi Franchioli(XXIII Ciclo) Analisi prestazionale dei sistemi di distribuzione idrica e calcolo della loro affidabilità (February 2011)
- Raed Alsaleh(XXIII Ciclo) Verification of Wind Pressure and Wind Induced Response of a Supertall Structure Using a Long Term Structural Health Monitoring System (February 2011).



# Table of Contents

Introduction and main motivation .....	1
Abstract.....	5
Chapter 1	
Some Typical Sensors-Design Constraints on a Wireless Sensing Unit...	7
1.1 Introduction .....	7
1.2 Typical Sensors for Measuring Structural Dynamics.....	7
1.2.1 Accelerometer.....	7
1.2.2 Strain Gauge .....	12
1.2.3 Load Cell .....	16
1.2.4 Laser Distance Sensor .....	17
1.3 Design Constraints.....	19
1.3.1 Power Supply Constraint.....	19
1.3.2 Signal Conditioning Constraint .....	20
1.3.3 Resolution Constraint .....	21
1.4 Summary.....	22
Chapter 2	
State of the Art of the Wireless Sensor Networks for Structural	
Monitoring Applications .....	23
2.1 Introduction .....	23
2.2 Some Recent Wireless Sensor Networks.....	25
2.2.1 Illinois Imote2 .....	25
2.2.2 Stanford Unit .....	28
2.2.3 EMPA .....	30
2.2.4 Narada.....	32
2.2.5 MicroStrain.....	33
2.2.6 WiseSPOT .....	34
2.2.7 XMU unit.....	36
2.3 Summary.....	36
Chapter 3	
Design and Implementation of a Wireless Sensor and its Application in	
Structural Monitoring .....	39
3.1 Introduction .....	39

3.2 Architecture of the proposed Wireless Structural Monitoring System.....	40
3.3 Frequency Division Multiplexing.....	41
3.4 Hardware Design of the Wireless Sensing Unit .....	44
3.4.1 Overview of the wireless sensing unit .....	45
3.4.2 Signal Conditioning and ADC .....	46
3.4.3 Microcontroller and RF transceiver .....	51
3.4.4 Power Management .....	53
3.5 Software Design of the Wireless Sensing Unit.....	62
3.5.1 Integrated Development Environment.....	62
3.5.2 Communication Protocol .....	64
3.5.3 Sampling and Data transmission.....	69
3.6 Experimental Validation .....	72
3.7 Summary .....	76
Chapter 4	
an Active Mass Damper using a digital DC motor PID controller and wireless sensors.....	79
4.1 Introduction.....	79
4.2 Active Mass Damper.....	79
4.3 Real Time Wireless Sensing .....	83
4.4 PID Position Controller for a DC motor .....	85
4.5 Experimental Validation .....	90
4.6 Summary .....	92
Chapter 5	
Energy Harvesting and Storage .....	95
5.1 Introduction.....	95
5.2 Ambient Energy Source and Harvester.....	96
5.3 Power Management .....	101
5.4 Energy Storage.....	102
5.5 Low Power Electronics .....	102
5.6 Hardware Design and Implementation of a Smart Energy Harvesting and Storage Unit Prototype .....	103
5.7 Summary .....	104
Chapter 6	
Summary, Conclusions and Future Directions .....	105

6.1 Summary and Conclusions .....	105
6.2 Future Directions .....	107
Bibliography .....	109



## **Introduction and main motivation**

Various civil and machinery structures, including buildings, bridges, dams, offshore oil platforms, aircrafts, ships etc., are playing a very important role in the development of our economy and society. Due to various problems, such as aging, overloading and natural catastrophe, the safety and durability are becoming more and more publicly concerned. Traditionally, visual and non-destructive inspections are used to detect structural damage. An inherent drawback of visual inspections is that only the damage visible on the surface of the structure can be observed. The damage located below surface can be detected by non-destructive evaluation (NDE) inspection technologies, like ultrasonic inspection. However, the NDE inspection technologies generally require a trained professional to operate in the field, thereby raising the costs. Furthermore, the operator must have knowledge of potential damage regions to prioritize inspection of the complete structure. As a promising solution to overcome the drawbacks of visual and NDE inspections, the concept of structural health monitoring (SHM) is emerging and has been attracting more and more research interest. In addition to automatically detect structural damage by SHM system, structural control concept is also proposed to enhance or actively protect structures when extreme excitation occurs.

Structural Health Monitoring (SHM) system can augment or potentially replace visual inspections. It combines structural monitoring and analytical methods (damage detection algorithms) to quickly and automatically predict, identify and even locate the onset of structural damage, thus increasing the safety to public and facilitating the structural maintenance. On the other hand, structural control system adopts passive and/or active devices to apply forces to the structure or to introduce appropriate changes in the mass, damping, and stiffness properties of the structure, so that excessive structural responses can be mitigated during external excitations, such as earthquake and strong wind (Spencer and Nagarajaiah 2003; Casciati, Rodellar and Yildirim 2011).

Structural control technology can be classified into four types: passive, semi-active, active, hybrid according to the energy requirement.

Structural health monitoring systems and structural control systems except the passive type, require the installation of sensors on structure to measure the response. In a conventional structural monitoring system, sensors are separately connected to a centralized data acquisition device by coaxial cables which provide not only the communication but also the power supply links. Although a wired connection offers reliable and high-quality communication, the cable installation and maintenance is labor-intensive, time-consuming and expensive. For example, the cost of installing over 350 sensing channels upon the Tsing Ma suspension bridge in Hong Kong is estimated to have exceeded US\$8 million (Farrar 2001) .

With the fast development of wireless communication and microelectronic technology, the low cost and low power wireless sensor is emerging as a promising alternative solution for rapid and low-cost sensor deployment in a structural monitoring system. Some academic and commercial wireless sensing systems have been proposed to eradicate the extensive lengths of wires associated with tethered systems (Lynch 2006). Furthermore, researchers also realized that wireless sensors have computational resources allowing for parallel and distributed data processing to reduce the data traffic (Spencer, Ruiz-Sandoval and Kurata 2004). However, wireless sensor networks are in their infancy in many respects, some key issues need to be investigated before the wireless monitoring systems can serve as economical substitutes to the traditional wire-based monitoring systems, such as unreliable communication, limited data rate, limited energy supply, communication delay, time synchronization etc.

Civil and mechanical experiments requires some features for the sensor and data acquisition system to be respected (such as sampling points in the range 50-250 per second, low frequency accuracy, suitable cut-off frequency and so on) which are achieved with sensors presently used in a wired form and in time division multiplexing. This thesis is to remove the wires and avoid the time



delay by adopting frequency division multiplexing wireless communication(Casciati and Chen 2011).

In this thesis, a wireless sensor unit capable of interfacing with various sensors is designed and applied in a structural monitoring system and a structural control system. The main feature of the wireless sensor network is the real time communication which is required by the control system.

The thesis is organized as follows:

Chapter 1 introduces some typical sensors for measuring structural dynamics in civil engineering applications and their constraints to the design of a wireless sensing unit. The main constraints are associated with power supply and signal conditioning.

Chapter 2 reviews the recent advances on the wireless sensor network for civil engineering applications. Some recent wireless sensor networks will be introduced from the hardware, software and algorithm aspects, including the Imote2, Stanford unit, EMPA unit, Narada, MicroStrain unit and WiseSPOT.

Chapter 3 describes the wireless sensing unit designed by the author and its applications in a structural monitoring system. The wireless sensing unit consists of power management module, signal conditioning module and system on chip (SoC) Radio Frequency (RF) transceiver module. It is compatible with the sensors described in Chapter 1. The structural monitoring system consists of wireless sensor, base station, USB hub, computer and the data acquisition software called HyperTerminal.

Chapter 4 presents the application of the wireless sensor unit in a structural control system in which real time communication is required. The real time communication is achieved by frequency division multiplexing method. The structural control system is an active mass damper for a three-storey frame mounted on a single-axis shaking table. It consists of four wireless sensors, four corresponding receiver units, a controller, a PID position controller for DC motor, a mass driven by a DC motor and installed on the top of the frame.

Chapter 5 introduces the energy harvesting and storage technologies for wireless sensor networks. This kind of technology is a promising solution for the power supply bottleneck of wireless sensor networks. Energy harvester can

scavenge energy from ambience, such as light, heat, vibration, wind etc. The harvested energy can be stored in rechargeable batteries or super capacitor.

Chapter 6 serves as a summary to the thesis and discusses possible future research directions.

## **Abstract**

With the increasing emphasis on structural safety, structural control and health monitoring have attracted much research interest over recent few decades. The traditional cable connection between sensor and data acquisition device is broadly identified as one of main limitations. With the fast development of wireless communication and microelectronics, low cost and low power wireless sensor network is emerging as a promising alternative to the wired sensor. In addition to wireless data acquisition, wireless sensor also has computation resource supporting parallel distributed engineering analysis.

In this dissertation, a wireless sensing unit prototype is developed and validated by its application in a structural monitoring system and a structural control system. The prototype is designed to be compatible with some sensors already available in the laboratory to which the author has access and common in civil engineering, including accelerometer, strain gauge, load cell and displacement sensor. In order to ensure real time multi-channel data transmission, mainly for structural control application, the wireless sensor can work in many frequency channels supporting frequency division multiplexing.

Two applications using this prototype were implemented. A structural monitoring system was assembled to monitor structural response. The wireless sensing unit is also utilized to replace the cable feedback in an active mass damper (AMD) installed on the top of a three-storey frame which is mounted on a single axis shaking table simulating the excitation. In this AMD, a DC motor is used as the actuator. The motor was previously driven by an analog PID controller which is not power efficient. In order to save the energy for actuation, a digital PID controller is developed to improve the energy efficiency. Another advantage of the digital controller is its small size. These two advantages make battery powered structural control feasible for a small scale structure.

Batteries are commonly used as the energy supply for a wireless sensor node. However, due to the limited energy, they need to be regularly replaced. As a promising solution to eradicate this maintenance problem, energy harvesting and storage technology is emerging. In this dissertation, recent advances in this field are investigated and a power harvester prototype using solar cell or wind turbine is developed.



# **Chapter 1**

## **Some Typical Sensors-Design Constraints on a Wireless Sensing Unit**

### ***1.1 Introduction***

In a structural control or health monitoring system, the deployed sensors play a basic role serving as a data source of response. A sensor is a device that measures a physical quantity and converts it into a signal (typically, electrical signal) which can be read by an observer or by an instrument.

In this chapter, the principles and main characters of some typical sensors in civil engineering are discussed. The constraints these sensors put on a wireless sensing unit are proposed. The wireless sensing unit is developed to serve as interface for all the sensors and it is required to be compatible with all the sensors.

### ***1.2 Typical Sensors for Measuring Structural Dynamics***

In a structure, several dynamic variables, including displacement, acceleration, strain and force, can be monitored by their corresponding sensors. In this section, some accelerometers, strain gauges, load cells and a laser distance sensor are described.

#### **1.2.1 Accelerometer**

An accelerometer measures its own acceleration, which is the acceleration it experiences relative to freefall and is the acceleration felt by people and objects mounting it. According to the operating principles, there are many types of accelerometer, such as resistive accelerometer, capacitive accelerometer and piezoelectric sensor. In this section, 3 types of accelerometer commonly adopted in structural monitoring are introduced: CXL01LF03 from Crossbow technology, FBA-11 and FBA ES-T from Kinemetrics. All of the three accelerometers are of a capacitive type. The CXL01LF03 is a Micro-electromechanical system (MEMS) accelerometer.

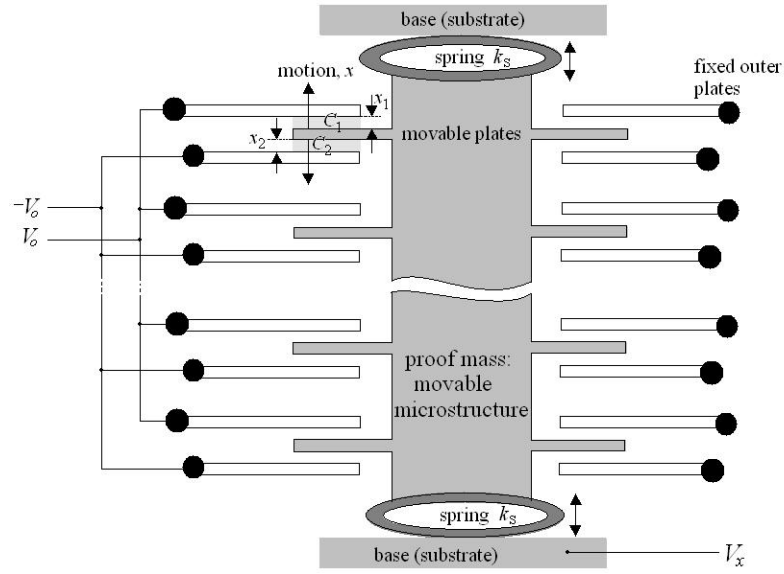


Fig. 1.1, MEMS Accelerometer structure.

Due to small size, low power, low cost and robust sensing, MEMS accelerometers are broadly used in industry. A typical MEMS accelerometer is composed of movable proof mass with plates that is attached through a mechanical suspension system to a reference frame, as shown in the Figure 1.1 (Andrejašić 2008). Movable plates and fixed outer plates represent capacitors. The deflection of the proof mass is measured using the capacitance difference.

Capacitive sensing is independent of the base material and relies on the variation of capacitance when the geometry of a capacitor is changing. Neglecting the fringing effect near the edges, the parallel-plate capacitance is:

$$C_0 = \epsilon_0 \epsilon \frac{A}{d} = \epsilon_A \frac{1}{d} \quad (1.1)$$

Where  $\epsilon_A = \epsilon_0 \epsilon A$ ,  $A$  is the area of the electrodes,  $d$  the distance between them,  $\epsilon_0$  the permittivity of vacuum and  $\epsilon$  the permittivity of the material separating them.

Every sensor has a lot of capacitor sets. All upper capacitors are wired parallel for an overall capacitance  $C_1$  and, likewise, all lower ones for an overall capacitance  $C_2$ , otherwise the capacitance difference would be too negligible to be detected. The free-space (air) capacitances between the movable plate and two stationary outer plates  $C_1$  and  $C_2$  are functions of the corresponding displacements  $x_1$  and  $x_2$ :

$$C_1 = \epsilon_A \frac{1}{x_1} = \epsilon_A \frac{1}{d+x} = C_0 - \Delta C \quad (1.2)$$

$$C_2 = \epsilon_A \frac{1}{x_2} = \epsilon_A \frac{1}{d-x} = C_0 + \Delta C \quad (1.3)$$

If the acceleration is zero, the capacitances  $C_1$  and  $C_2$  are equal because  $x_1=x_2$ . The proof mass displacement  $x$  appears in the presence acceleration. If  $x \neq 0$ , the capacitance difference is found to be:

$$C_2 - C_1 = 2\Delta C = 2\epsilon_A \frac{x}{d^2 - x^2} \quad (1.4)$$

Measuring  $\Delta C$ , one finds the displacement  $x$  by solving the nonlinear algebraic equation:

$$\Delta C x^2 + \epsilon_A x - \Delta C d^2 = 0 \quad (1.5)$$

This equation can be simplified. For small displacements, the term  $\Delta C x^2$  is negligible. Thus,  $\Delta C x^2$  can be omitted.

$$x \approx \frac{d^2}{\epsilon_A} \Delta C = d \frac{\Delta C}{C_0} \quad (1.6)$$

For an ideal spring, according to Hook's law, the spring exhibit a restoring force  $F_s$  which is proportional to the displacement  $x$ . Thus,  $F_s = k_s x$ , where  $k_s$  is the spring constant. From Newton's second law of motion, neglecting the air friction (which is negligibly small), the following differential equation results  $ma = m d^2 x / dt^2 = k_s x$ . Thus, the acceleration, as a function of the displacement, is

$$a = \frac{k_s}{m} x \quad (1.7)$$

Then, from the equation 1.6 and 1.7, one concludes that the acceleration is approximately proportional to the capacitance difference  $\Delta C$ .

CXL01LF03 belongs to high sensitivity LF series accelerometers provided by Crossbow Technology. It is a three axis, precise,  $\pm 1$  g acceleration sensors. Common applications include instrumentation, modal analysis, and orientation measurements. The LF Series sensing element is a bulk micro-machined three layer silicon structure. The three layers form a differential capacitor with low noise. The sensor is bonded to a high-quality ceramic substrate where it is coupled to signal conditioning electronics. The entire package design is optimized for minimal thermal hysteresis, yielding superior DC response. The LF Series operates on a single 5 VDC or a 6 - 30 VDC unregulated supply with the -R option. The -R option also provides 10ms over voltage and reverse voltage protection. The LF Series sensor provides a direct high-level analog voltage signal output. The output requires no external signal conditioning and is easy to interface to standard data acquisition systems. Each module's offset and scale factor are factory calibrated and tested. Standard modules have a bandwidth of 50 Hz. The module should be securely attached using screws or adhesive. The LF Series accelerometers are available in two package options - nylon (both single and tri-axial), and high temperature aluminum (both single and tri-axial).

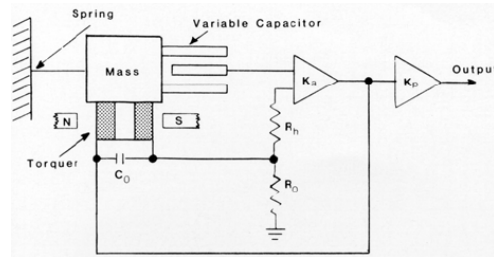


Fig.1.2 Schematic of the Kinemetrics's force balance accelerometers

The FBA-11, one of Kinemetrics' line of force balance accelerometers, is a spring-mass device using variable capacitance transduction and electromagnetic feedback, as shown in Fig.1.2. The output is fed back to the torquer coil, which is an integral part of the mass. From the coil, the feedback loop is completed through resistors  $R_h$  and  $R_0$ . This stiffens the system, thereby increasing the natural frequency to 50 Hz. Resistor  $R_0$  and capacitor  $C_0$  control the damping,



normally adjusted to 70% of the critical value. The acceleration sensitivity is controlled by the gain  $K_p$  of the post-amplifier. Aluminum pivot support blocks are used to maintain long-term drift-free stability of the accelerometer mass.

The FBA-11 uniaxial accelerometer housing can be mounted to either a horizontal or vertical surface using flanges or bolt slots which are part of the molded casting; thus there is no need to reorient the accelerometer when a horizontal mounting surface is not available. The FBA-23 has three accelerometers orthogonally mounted on an internal deck plate. Each of these units, housed in cast aluminum base and cover, is sealed to prevent the entrance of moisture and dirt.

The EpiSensor FBA ES-T is a three-axial accelerometer optimized for earthquake recording applications. Inside the waterproof anodized-aluminum housing there are three orthogonally mounted low-noise EpiSensor force balance accelerometer modules. The EpiSensor has user-selectable full-scale recording ranges of  $\pm 4g$ ,  $\pm 2g$ ,  $\pm 1g$ ,  $\pm 1/2g$  or  $\pm 1/4g$ . The EpiSensor bandwidth of DC to 200 Hz is a significant improvement over earlier generations of sensors. The output voltage levels are user-selectable at either  $\pm 2.5V$  or  $\pm 10V$  single-ended, or  $\pm 5V$  or  $\pm 20V$  differential. The EpiSensor is normally powered with a  $\pm 12V$  external DC power source. It is optionally available with a single  $+12V$  supply option. The one in the laboratory to which the author has access is configured to be  $\pm 2.5V$  single-ended voltage output and be powered with a  $\pm 12V$  external DC power source.

The main technical specifications of these three accelerometers are summarized in the following table.

Table 1.1 Main technical specifications of the three analyzed accelerometers

	CXL01LF03	FBA-11	FBA ES-T
Supply Voltage(Volts)	$+5 \pm 0.25$	$\pm 12$	$\pm 12$ , low noise, ripple $<50mV$
Supply Current (mA)	2/axis	2.5/axis	30 (Max.)
Zero g Output (Volts)	$+2.5 \pm 0.15$	$\pm 0.025$	$\pm 0.025$
Input Range(g)	$\pm 1$	$\pm 2$	$\pm 1$
Sensitivity (Volts/g)	2	1.25	2.5
Bandwidth(Hz)	DC-50	DC-50	DC-200
Noise	0.5mg	$2 \mu g$	Low Noise

### 1.2.2 Strain Gauge

A structure is designed with the lowest amount of material. For a transportation tool, like airplane, train or automobile, this also means to attain a faster running speed and a less fuel consumption. However, the safety will be compromised unless the required strength is maintained.

The stress however is a state variable and cannot be measured. It can be estimated in the linear range by strain measurements. The strain can be measured on the body surface and strain gages are the most common sensing element to measure surface strain.

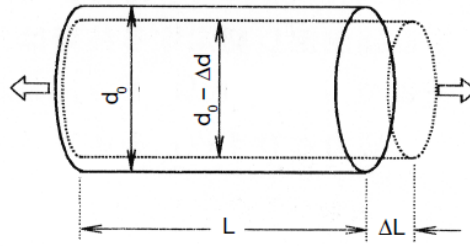


Fig. 1.3 Strain in a tensioned bar

When a bar is tensioned (see the Fig. 1.3), it elongates by  $\Delta L$ , and thus it lengthens to  $L$  (original length) +  $\Delta L$  (change in length). The ratio of this elongation (or contraction),  $\Delta L$ , to the original length,  $L$ , is called strain, which is denoted as  $\epsilon$  and it is a dimensionless quantity:

$$\epsilon_1 = \frac{\Delta L}{L} \quad (1.8)$$

The strain in the same tensile (or compressive) direction as the external force is called longitudinal strain. Usually, the ratio is an extremely small value, and thus a strain value is expressed by suffixing “ $\times 10^{-6}$  (parts per million) strain,” “ $\mu\text{m/m}$ ” or “ $\mu\epsilon$ .”

The tensioned bar becomes thinner while lengthening. Suppose that the original diameter,  $d_0$ , is made thinner by  $\Delta d$ . Then, the strain in the diametrical direction is:

$$\varepsilon_2 = \frac{-\Delta d}{d_0} \quad (1.9)$$

The strain in the direction orthogonal to the external force is called lateral strain. Each material has a certain ratio of lateral strain to longitudinal strain, with most materials showing a value around 0.3. This ratio is called Poisson's ratio, which is marked in  $\nu$  (nu):

$$\nu = \left| \frac{\varepsilon_2}{\varepsilon_1} \right| = 0.3 \quad (1.10)$$

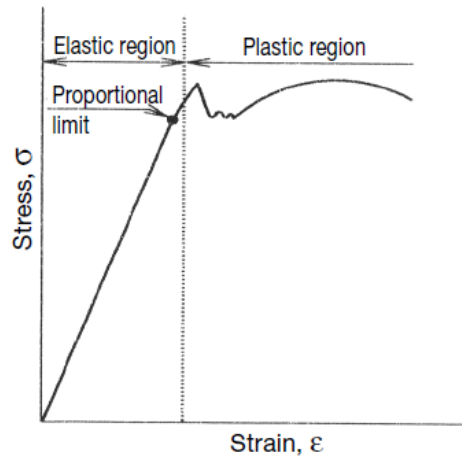


Fig. 1.4 The relation between strain and stress

Fig. 1.4 graphs a typical relation between stress and strain on common steel (mild steel). The region where stress and strain have a linear relation is called the proportional limit, which satisfies the Hooke's law.

$$\sigma = E \cdot \varepsilon \text{ or } \frac{\sigma}{\varepsilon} = E \quad (1.11)$$

The proportional constant,  $E$ , between stress and strain in the equation 1.11 is called the modulus of longitudinal elasticity or Young's modulus, the value of

which depends on the materials. Thus the stress can be estimated through measurement of the strain initiated by external force, even though it cannot be measured directly.

The strain gauge is tightly bonded to a measuring object so that the sensing element (metallic resistive foil) may elongate or contract according to the strain borne by the measuring object. When bearing mechanical elongation or contraction, most metals undergo a change in electric resistance. The strain gauge applies this principle to strain measurement through the resistance change. Generally, the sensing element of the strain gauge is made of a constantan (copper-nickel alloy) foil. The alloy foil has a rate of resistance change proportional to the strain with a certain constant called gauge factor.

The principle can be expressed as follows:

$$\frac{\Delta R}{R} = K \cdot \varepsilon \quad (1.12)$$

where,

$R$ : Original resistance of strain gauge,  $\Omega$  (ohm)

$\Delta R$ : Elongation- or contraction-initiated resistance change,  $\Omega$  (ohm)

$K$ : Proportional constant (called gauge factor)

$\varepsilon$ : Strain

The gauge factor,  $K$ , differs depending on the metallic materials. The copper-nickel alloy (Advance) provides a gage factor around 2. Thus, a strain gauge using this alloy for the sensing element enables conversion of mechanical strain to a corresponding electrical resistance change. However, since the strain is very small, the resistance change caused by the strain is extremely small and cannot be measured with a conventional ohmmeter. Accordingly, such minute resistance changes can be measured with a dedicated strain amplifier using an electric circuit called Wheatstone bridge.

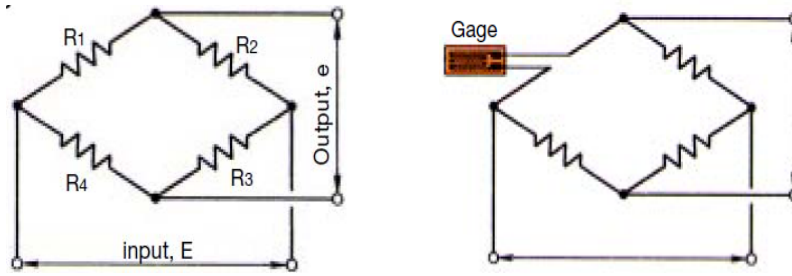


Fig. 1.5 Wheatstone bridge (a) without gage (b) with a strain gage

The Wheatstone bridge is an electric circuit suitable for detecting modest resistance changes. It is therefore used to measure resistance changes of a strain gauge. The bridge is configured by combining four resistors as shown in Fig.1.5(a).

Suppose:

$$R1 = R2 = R3 = R4, \text{ or, } R1 \times R3 = R2 \times R4 \quad (1.13)$$

Then, whatever voltage is applied to the input, the output,  $e$ , is zero. Such a bridge status is called “balanced.” When the bridge loses the balance, it outputs a voltage corresponding to the resistance change. As shown in Fig. 1.5(b), a strain gage is connected in place of  $R1$  in the circuit. When the gage bears strain and initiates a resistance change,  $\Delta R$ , the bridge outputs a corresponding voltage,  $e$ .

$$e = \frac{1}{4} \cdot \frac{\Delta R}{R} \cdot E \quad (1.14)$$

That is,

$$e = \frac{1}{4} \cdot K \cdot \varepsilon \cdot E \quad (1.15)$$

Since values other than  $\varepsilon$  are known values, the strain,  $\varepsilon$ , can be determined by measuring the bridge output voltage.

The structure described above is called a 1-gauge system since only one gauge is connected to the bridge. Besides the 1-gauge system, there are 2-gauge and 4-gauge systems. Furthermore, one of the problems of strain measurement is the thermal effect. Besides the external force, an increase (decrease) of temperatures elongates or contracts the measuring object with a certain linear expansion coefficient. Accordingly, a strain gage bonded to the object bears

thermally-induced apparent strain. Temperature compensation solves this problem. (KYOWA)

Two types of HBM strain gauges are available in the the laboratory to which the author has access, 1-LY11-1.5/120 and 1-LY41-0.6/120.

Table 1.2. stain gauges considered in the implementation

	1-LY11-1.5/120	1-LY41-0.6/120
Nominal Resistance( $\Omega$ )	120	120
Maximum Permanent Effective Bridge Excitation Voltage(V)	2.5	1.5
Gauge Factor	Approximate 2	Approximate 2

### 1.2.3 Load Cell

A load cell is a transducer that is used to convert a force into an electrical signal. This conversion is indirect and happens in two stages. Through a mechanical arrangement, the force being sensed deforms a strain gauge. The strain gauge measures the deformation. The sensing or spring element is the main structural component of the load cell. The element is designed in such a way that it develops a strain, directly proportional to the load applied. Sensing elements are normally made of high strength alloy steels (nickel plated for environmental protection), precipitation-hardened stainless steels, heat treated aluminium alloys, or beryllium copper alloys. By bonding strain gages to a precisely machined element, the force applied can be identified in terms of resistance change. The strain gages, usually four or a multiple of four, are connected into a Wheatstone bridge configuration in order to convert the very small change in resistance into a usable electrical signal which is typically in the order of a few millivolts and requires amplification by an instrumentation amplifier before it can be used. Passive components such as resistors and temperature depending wires are used to compensate and calibrate the bridge output signal.

The main specifications of the two FUTEK donut load cells available in the laboratory to which the author has access are summarized in the following table 1.3.

Table 1.3. load cells considered in the implementation

	LTH300	LTH350
Rated Output	2mV/V nominal	2mV/V nominal
Capacity	222N	445N
Excitation(VDC or VAC)	18V Max.	18V Max.
Bridge Resistance	700 $\Omega$	700 $\Omega$

#### 1.2.4 Laser Distance Sensor

Wenglor YT89MGV80 is a photoelectric sensor based on transit time for measuring distance. This kind of sensor measures the distance between the sensor and the object. They function in accordance with the principle of transit time measurement. For this reason, the object's color, shape and surface characteristics have practically no influence on measurement results. Even dark objects can be reliably recognized against bright backgrounds. Large working ranges and distances are achieved by these sensors. They are aligned directly to the object. The main specification of Wenglor YT89MGV80 is shown in the Table 1.4.

Table 1.4. Main specification of YT89MGV80

Power Supply	18-30V DC
Current Supply	Less than 80mA
Analogue Output	0-10V
Cut-Off Frequency	60Hz
Working Range	300-3700mm
Measuring Range	3000mm
Resolution	1mm

The principle of transit time, also called time-of-flight (TOF), distance measurement is quite simple. A short laser pulse is projected to a target. The time it takes for the pulse to travel to the target and back is measured. The distance to the target is calculated from the TOF and the speed of the light in the medium. The basic setup for a TOF distance measurement device is shown in Fig.1.6. Knowing the speed of light, the distance to the target can be determined from the TOF by:

$$2d = ct \quad (1.16)$$

Where  $d$  is the distance from the sensor to the target,  $c$  is the speed of light and  $t$  is the TOF of the laser pulse.

For the distance measurement to be unambiguous, the TOF ( $t$ ) should be greater than the pulse width ( $T_p$ ) and less than the pulse repetition period ( $T_r$ ). Thus,

$$T_p < t < T_r \quad (1.17)$$

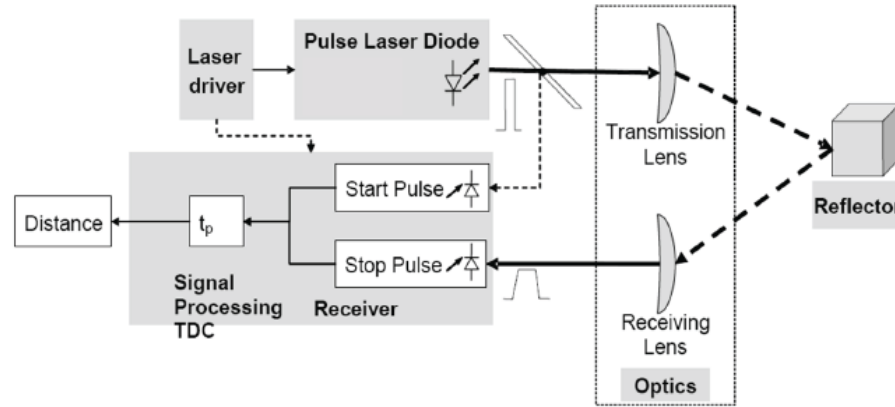


Fig. 1.6 Basic setup of a TOF laser distance measurement system

The most important part of a TOF distance measurement system is the time calculation unit. Light travels at 299,792,458 m/s in a vacuum; in 1ns light travels about 30cm in a vacuum. If a measurement has an error of  $\Delta t = 1\text{ns}$ , it is relayed as an error in distance of 15cm.

An important part of a precision time measurement system is the time discriminator. The main task of the time discriminator is to deliver a trigger signal at the right instant. Commonly used principles in discriminator design



include leading edge timing (constant amplitude), zero crossing timing (derivation), first moment timing (integration) and constant fraction timing. The time elapsed between the start and stop pulses is measured with a time-to-digital converter, which is a fast, accurate and stable time-interval measuring device that uses, e.g., a digital counting technique together with an analog or digital interpolation method.

### 1.3 Design Constraints

#### 1.3.1 Power Supply Constraint

Based on the description in the previous section, some requirements for the power supply are summarized in the following table. Since the wireless sensing unit should be compatible with all the sensors, it should be able to provide appropriate power to them. The wireless sensing unit is supposed to be powered by an energy source like batteries. In order to have all the required voltages, various voltage regulators are used to make conversion. The power management module in the wireless sensing unit mainly consists of various voltage regulators.

Table 1.5. Power Consumption of the Three Sensors

	Supply Voltage (Volt)	Supply Current (mA)	Power Consumption (mW)
FBA-11	$\pm 12$	2.5mA	60mW
FBA-EST	$\pm 12$	35mA	840mW
CXL01LF3	+5V	12mA	60mW
YT89MGV80	+18 (+18~+30)	<80mA	1440mW
LTH300/LTH350	+5V(Max:18V)	7.1mA	35.5mW
1-LY11-1.5/120	+2.5V	20.8mA	52mW

In order to make the unit suitable for both low-power sensors (CXL01LF3) and non-low-power sensors (FBA-EST and YT89MGV80), there are four main principles to be considered in the design of the power management module:

(1) Highly efficient power conversion. Since the power management module itself will consume some power, higher conversion efficiency means less wasted power.

(2) Adjustable output voltage. Although the required voltages for the three sensors are determined, in order to make the wireless sensing unit suitable for other sensors, it is better to make the output voltage of the regulators adjustable.

(3) Medium output power. The output voltage of the regulators will not maintain its prefixed value if the required current is too high, so the output current should be considered as well when selecting the regulators. Medium output power is required because the wireless sensing unit is also intended for non-low-power sensors, such as FBA-EST and YT89MGV80.

(4) Ability to sleep with low power consumption. In the structural monitoring application, the wireless sensors are not required to acquire data continuously. Since many current sensors are not able to sleep, it is a good method to cut off its power supply when the data acquisition is not required in order to reduce the power consumption as much as possible. Therefore, the power management module should be able to sleep with little power consumption.

### 1.3.2 Signal Conditioning Constraint

The various sensors have different output offset and range, which should all be met by the sensing unit. Therefore, the signal condition module should be carefully designed.

(1) DC/AC Coupling. DC (Direct Current) coupling represents that the output signal of the sensor including both the DC component and AC (Alternative Current) component is directly connected to the input of the wireless sensing unit. AC coupling represents that the output signal of the sensor is connected to a high pass filter to remove the DC component before entering other parts of the signal conditioner in the wireless sensing unit. Both DC/AC coupling are required in the design of the wireless sensing unit. DC coupling can obtain both the DC component and AC component of the signal from the sensor. However, the sensor might have a useless high offset and a small desirable AC signal, since the structural response is small in civil engineering. In this case, if the gain of the amplifier will be limited by the offset so that the small desirable AC signal cannot be amplified enough to have a better quality. For example, the offset of the accelerometer CXL01LF3 could be 2.5V. Assuming the input range of the ADC is 0 to 5V, the gain is limited to be less than 2 if DC coupling is used. Therefore, if the sensor offset is useless, AC coupling can be adopted to only obtain the AC signal component. When the AC signal component is quite small, a high-gain amplifier can be used to improve the signal quality.

(2) Differential Input. Although the accelerometers and laser distance sensor have single-ended output, the load cell and strain gauge has differential output. The single-ended output can be connected to differential input; however differential output cannot be connected to single-ended input. Therefore, differential input is preferred in the design of the wireless sensing unit.

(3) Adjustable Gain Amplifier. An amplifier is required to improve signal qualify especially when the signal is quite small. Since different sensors have different sensitivity and output range and the structural response depends on the excitation, the gain of the amplifier should be adjustable to better match the signal range.

(4) Anti-aliasing Filter. According to Nyquist theorem, the sampling frequency should be higher than twice the highest frequency component in the sampled signal, otherwise the signal component with frequency higher than half sampling frequency will be folded back into the lower frequency band, thus introducing an aliasing error. In order to avoid aliasing, a low-pass filter is required before ADC if the signal has undesirable component higher than half sampling frequency.

### 1.3.3 Resolution Constraint

Sensor resolution refers to the smallest detectable increment of a sensor signal. But, in a sensor data sheet, this parameter is usually not mentioned. Instead, the parameters noise or noise spectral density are given. The relationship of noise and resolution is that noise determines the highest resolution. The noise of a sensor is associated with the bandwidth. The noise power spectral density, defined as the noise power per unit of bandwidth, is the parameter to show the relation of the noise and bandwidth. Thus, usually a larger bandwidth will lead to a higher noise and a lower resolution. Reducing the bandwidth can reduce the noise and improve the resolution. For example, the relationship of resolution and bandwidth of Freescale accelerometers is (Freescale Semiconductor 2007):

$$R = N\sqrt{BW_{LPF}} \times 1.6 \quad (1.18)$$

Where R is resolution, N is noise spectral density in the unit of  $\frac{\mu g}{\sqrt{Hz}}$ ,  $BW_{LPF}$  is the bandwidth of the accelerometer low pass filter.

The resolution of an A/D converter is the smallest detectable voltage. If the A/D converter resolution is less than the sensor resolution, then the system will be limited by the A/D converter. Otherwise the limitation is due to sensor resolution. In order to obtain as much as possible information from sensor, the ADC resolution should be higher than sensor resolution. When the amplifier is used in signal conditioner, the relation between the ADC resolution and the sensor resolution is that the ADC resolution should be better than the sensor resolution multiplied by the gain.

### ***1.4 Summary***

In this chapter, the principles and main characteristics of several sensors for measuring structural dynamics, including accelerometer, strain gage, load cell and laser distance sensor, are described and their constraints to a wireless sensing unit are proposed.

The main specifications of a sensor considered in designing a generally compatible wireless sensing unit include power supply (voltage and current supply) and the bandwidth, resolution, offset and range of the output signal.

Four constraints for the power supply are proposed, including: (1) Highly efficient power conversion; (2) Adjustable output voltage; (3) Medium output power; (4) Ability to sleep with micro power consumption. Four constraints for the signal conditioning are proposed, including: (1) DC/AC Coupling; (2) Differential Input; (3) Adjustable Gain Amplifier; (4) Anti-aliasing Filter. Moreover, the ADC resolution should be better than the signal resolution multiplied by the gain.

## **Chapter 2**

# **State of the Art of the Wireless Sensor Networks for Structural Monitoring Applications**

### ***2.1 Introduction***

A wireless sensor network (WSN) consists of spatially distributed autonomous wireless sensors to *monitor* physical or environmental conditions, such as temperature, sound, vibration, pressure, motion or pollutants and to cooperatively pass their data through the wireless network to a main location. The development of wireless sensor networks was motivated by military applications such as battlefield surveillance; today such networks are used in many industrial and consumer applications, such as industrial process monitoring and control, structural health monitoring, and so on.

The WSN is built of some nodes– from a few to several hundreds or even thousands-where each node is connected to one (or sometimes several) sensors. Each sensor network node has typically several parts: a radio transceiver with an internal antenna or connection to an external antenna, a microcontroller with some memory, an analog to digital converter (ADC), a signal conditioner for interfacing with the sensors, a power management and an energy source, usually a battery or an embedded form of energy harvesting, as shown in Fig. 2.1. The topology of the WSNs can vary from a simple star network to an advanced multi-hop wireless mesh network. The propagation technique between the hops of the network can be routing or flooding.(Wikipedia)

There are many broadly used standard wireless technologies which can be used for a wireless sensor, like Cellular network, Wi-Fi and Bluetooth. Although they are mature and popular, these technologies don't feature low cost and low power. These two features are addressed by IEEE802.15.4 and ZigBee. The emerging ZigBee™ protocol is a specification for a suite of high level communication protocols using small, low-power digital radio based on the IEEE 802.15.4 standard for wireless personal area networks (WPANs). ZigBee™ is poised to become the global control/sensor network standard. It can be simply implemented and contains features like low power consumption and low data rate. The focus of ZigBee™ technique is to define a general-purpose, low cost, low power, self-organizing mesh network that can be used for various applications where low data transfer rate is sufficient. The low cost allows the

technology to be widely deployed in wireless control and monitoring applications. Low power allows longer life with smaller batteries. Mesh networking provides high reliability and more extensive range.

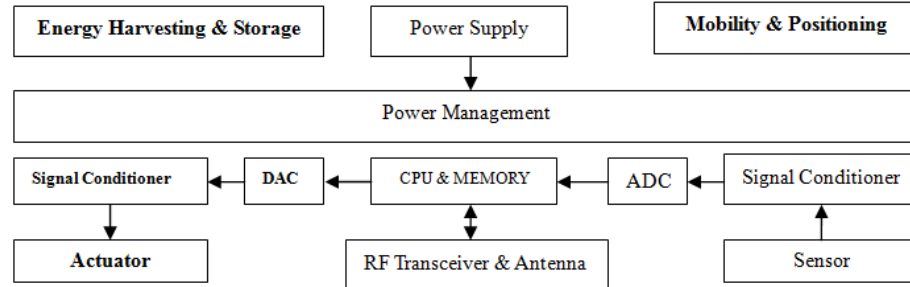


Fig. 2.1 The block diagram of an ideal autonomous wireless sensor

In recent years, besides the typical components, some new concepts marked in bold in the figure 2.1 for a WSN are emerging: actuator management, energy harvesting and storage for self-powered perpetual wireless sensor, self-positioning and mobility.

Conventional wireless sensor network can only offer monitoring function. However, its functionality can be extended to include actuation capabilities by integrating an actuation signal generation module for controlling an actuator. Lynch et al. (2008) proposed a wireless sensor prototype capable of data acquisition, computational analysis and actuation for use in a structure control system with a semi-active magnetorheological (MR) damper as the actuator.

Besides integration of actuator in a wireless sensor network, mobility is another attractive function for structural health monitoring. Compared with static sensors, mobile sensor networks offer flexible system architectures with adaptive spatial resolutions. The authors (Zhu, Yi, Wang, Lee and Guo 2010) propose a mobile sensing node that is capable of maneuvering on structures built with ferromagnetic materials. The mobile sensing node can also attach/detach an accelerometer onto/from the structural surface. There are also many other bio-inspired robot techniques which have the potential to provide mobility for wireless sensor. The authors (Unver, P. Murphy and Sitti 2005) propose two small-scale agile wall climbing robots, Geckobot and Waalbot, able to navigate on smooth vertical surfaces which use adhesive materials for attachment. Geckobot is a lizard-inspired climbing robot with similar kinematics to a gecko climbing gait. Waalbot uses two actuated legs with rotary motion and two passive revolute joints at each foot. The authors

(Saunders, Goldman, Full and Buehler. 2006) propose a RiSE robot which is a biologically inspired, six legged climbing robot, designed for general mobility in scansorial (vertical walls, horizontal ledges, ground level) environments. The authors (Kim, Spenko, Trujillo, Heyneman, Mattoli and Cutkosky 2007) propose a new bio-inspired climbing robot designed to scale smooth vertical surfaces using directional adhesive materials. The robot, called Stickybot, draws its inspiration from geckos and other climbing lizards and employs similar compliance and force control strategies to climb smooth vertical surfaces including glass, tile and plastic panels.

Self-positioning is another desirable feature for a wireless sensor. Position itself is an importance physical variable for a wireless sensor. In structural monitoring, the positioning sensor can be used to monitor the deformation or displacement of a structure (Casciati and Chen 2009). Combining the feature of mobility and self-positioning, it is possible for the wireless sensor to autonomously move to a designated location.

There are many positioning technologies available with different accuracy. Besides the well known and broadly used out-door GPS technique, there are many other methods appropriate for in-door positioning, including received signal strength (RSS), angle of arrival (AOA), time of arrival (TOA), round trip time of flight (RTOF) and time difference of arrival (TDOA) (Liu, Darabi, Banerjee and Liu 2007). Especially, the IEEE802.15.4 physical layers standard is updated to IEEE802.15.4a which is capable of TOA distance measurement through two additional physical layers using ultra-wideband (UWB) and chirp spread spectrum (CSS). (IEEE Computer Society 2007)

In the following, some typical wireless sensor networks adopted in SHM are summarized, including Illinois Imote2, Stanford unit, EMPA unit, Narada, MicroStrain Unit and WiseSpot. Most of them are based on the IEEE802.15.4 standard compliant transceiver operating in the license-free ISM frequency band 2.4GHz, supporting the standard ZigBee protocol.

## ***2.2 Some Recent Wireless Sensor Networks***

### ***2.2.1 Illinois Imote2***

Spencer et al. (2010) proposed a wireless smart sensor network (WSSN) based on the Intel Imote2 platform and the sensor board SHM-A designed for SHM.



Fig. 2.2 Imote2 with battery board and external antenna

The Imote2, pictured in Fig. 2.2, is a high-performance wireless smart sensor platform, integrating an Intel's PXA271 XScale® low power processor, the IEEE802.15.4 compliant low power RF transceiver CC2420 from Texas Instrument and large memory. It can provide intense data acquisition and processing required for dynamic structural monitoring. The processor speed can be adjusted from 13 to 416MHz. Higher speed will produce higher performance, but at the cost of higher power consumption. Thus, the power consumption can be minimized through smart power management according to the specific requirement of application. The memory size is increased significantly from the previous generation of motes, having 256 kB SRAM, 32 MB FLASH and 32 MB SDRAM, which enables longer measurements, as well as the on-board computation.

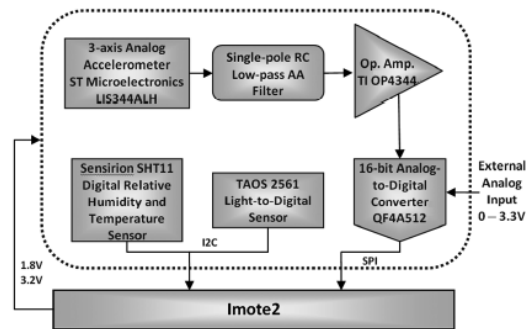


Fig. 2.3 Block diagram of SHM-A board



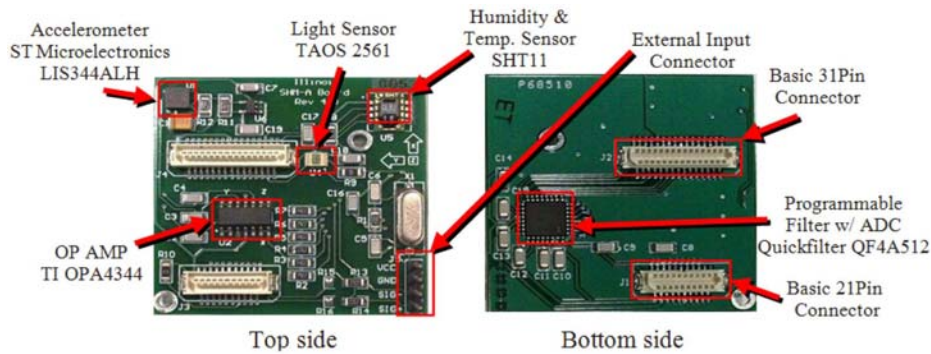


Fig. 2.4 SHM-A board, Top and Bottom side

Since the only commercial accelerometer sensor board (ITS400C) that interfaces with Imote2 does not have high enough resolution and accurate enough sample rate, a SHM-A was designed, as shown in Fig. 2.3 and 2.4. The SHM-A sensor board mainly consists of a 3 axis analog accelerometer LIS344ALH from ST Microelectronics, a 16-bit analog to digital converter QF4A512, a relative humidity and temperature sensor SHT11 and a light sensor TAOS 2561.

The open-source operating system TinyOS specific for WSN is adopted in Imote2. The application software development is based on a service-oriented architecture (SOA) that is modular, reusable and extensible, thus allowing engineers to more readily realize the potential of smart sensor technology. Furthermore, the ISHMP Toolsuite is designed to tackle the complexity associated with creating WSSN applications based on SOA design principle, which is open-source and available for public use at <http://shm.cs.uiuc.edu/software.html>. The hardware and software of the WSSN were validated on a cable-stayed bridge (the 2<sup>nd</sup> Jindo Bridge) in South Korea.

## 2.2.2 Stanford Unit

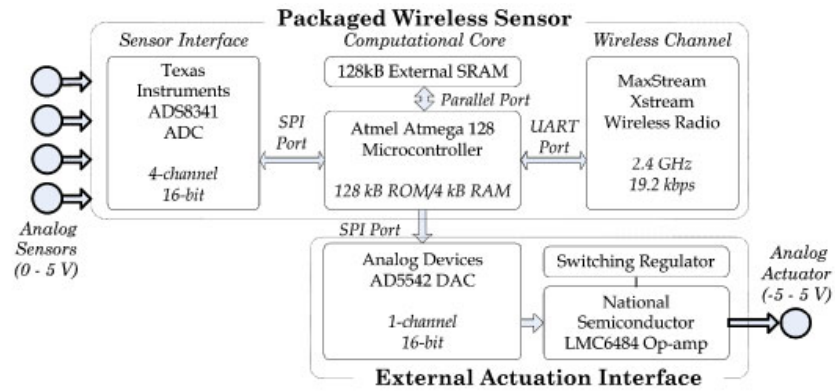


Fig. 2.5 Block diagram of the hardware of the Stanford Wireless Sensing Unit

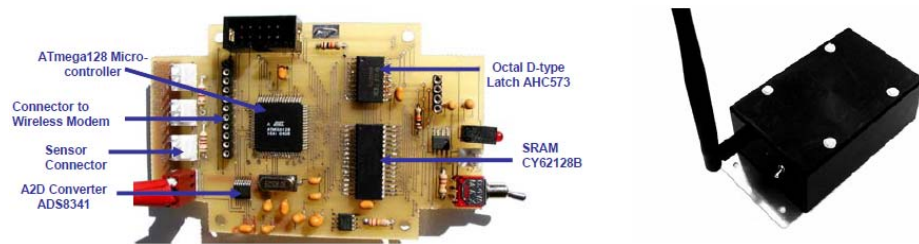


Fig. 2.6 (Left) final printed circuit board and (right) fully assembled wireless sensing unit prototype

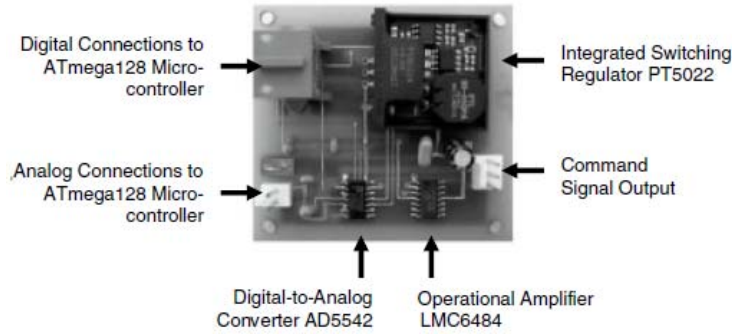


Fig. 2.7 Stand-alone actuation interface circuit

Wang et al. have proposed a wireless sensing unit suitable for both structural monitoring and control (Wang, Lynch and Law 2005) (Lynch, Wang, Swartz, Lu and Loh 2008), as shown in the Fig. 2.5 and Fig. 2.6. For the sensing interface, a four channel Texas Instrument ADS8341 16-bit ADC is selected to convert analog sensor signals to digital formats for use by the microcontroller. For the computational core, the low-power 8-bit Atmel ATmega128 AVR microcontroller is selected. The microcontroller has 128 kB of ROM, which is sufficient for storing damage detection software. In addition to ROM, 4 kB of SRAM is integrated with the microcontroller; however, this amount of SRAM is insufficient to store all the collected data. An additional 128 kB of SRAM (Cypress CY62128B) is interfaced with the microcontroller for the storage of measurement data. The MaxStream 9XCite wireless modem (which operates on the 900 MHz radio band and is capable of data rates as high as 38.4 kbps) or MaxStream 24XStream wireless modem (which operates on the 2.4G band and is capable of data rates 9600bps or 19200bps) can be used to be the RF transceiver.

In order to use the wireless sensor in structural control, an actuation interface was extended, as shown both in Fig. 2.5 and 2.6, which mainly consists of the digital-to-analog converter (DAC) AD5542 from Analog Devices (which is single channel, 16-bit and with a maximum sample rate of up to 1 MHz) and an additional operational amplifier LMC6484 (which is used to broaden the 0-5V output range of the DAC to -5 to 5 V). The -5V supply is generated by a Texas Instruments PT5022 switching regulator which converts the regulated 5V power supply from the wireless sensor to a -5V supply.

### 2.2.3 EMPA

Meyer et al. from EMPA designed a wireless sensor network for long term SHM (Meyer, Bischoff, Feltrin and Motavalli 2007; Feltrin, Meyer, Bischoff and Motavalli 2009). The platform features modular design of network nodes where sensor conditioning, data processing unit and wireless communication module each forms a separate subsystem. The sensor node was based on the commercial WiseNode which is replaced by Tmote Sky wireless sensor platform recently (Feltrin 2010). Here, both of them are introduced.

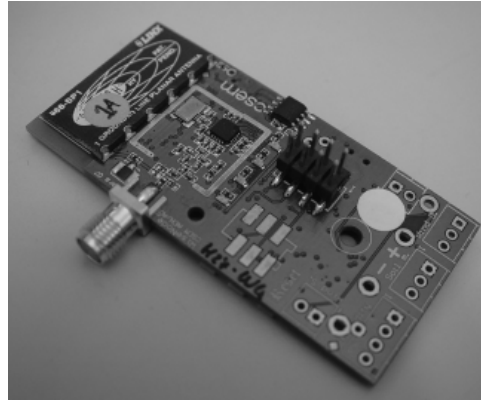


Fig. 2.8 WiseNode wireless sensor module

As shown in Fig. 2.8, the WiseNode platform is based on the MSP430F1611 microcontroller, and on the radio transceiver CC1100 operating at 868/915 MHz. WiseMAC, a low power wireless and dedicated medium access protocol and a tree routing protocol are implemented on the WiseNode's microcontroller. The WiseMAC protocol is providing a very energy efficient radio communication by coordinating the medium usage, locally synchronizing communication activities (duty cycle) of the neighboring nodes, reducing the energy loss due to the packet collisions, idle listening and packet overhearing (El-Hoiydi and Decotignie, 2004). The node also runs a clock synchronization algorithm to give a common acquisition reference to all nodes. The network self organizes from the root node.

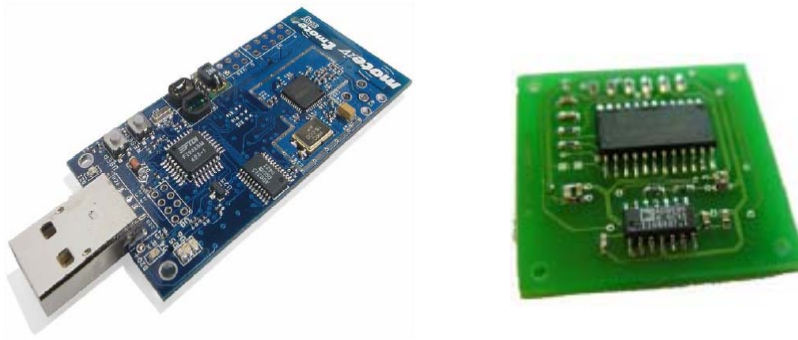


Fig. 2.9 Tmote sky wireless sensor module (left),  
LIS3L02 Module (right)

As shown in Fig. 2.9 (left), the main components of the Tmote Sky sensor node platform are the ultra low power TI MSP430F1611 microcontroller, the FTDI FT232BM USB-interface, which allows for programming the microcontroller over USB (Universal Serial Bus), and the Chipcon CC2420 low power radio chip. The network is self-configuration (also called “ad hoc” network). The data from sensor node is sent to the sink node by multi-hop routing. The advantages of the wireless sensor network are fast deployment (limitations are mounting of the sensors), easily scalable and little interference with surroundings.

Some decentralized data processing algorithm is also implemented to reduce the energy consumption due to large data transmission, such as FFT and Peak Picking.

One of the sensors they used is the LIS3L02 capacitive MEMS acceleration sensor of ST Microelectronics that can be operated with a power supply of 3 V and has a power consumption of 4mW, as shown in Fig. 2.9 (right). The frequency range is from DC up to 1.5 KHz.

## 2.2.4 Narada

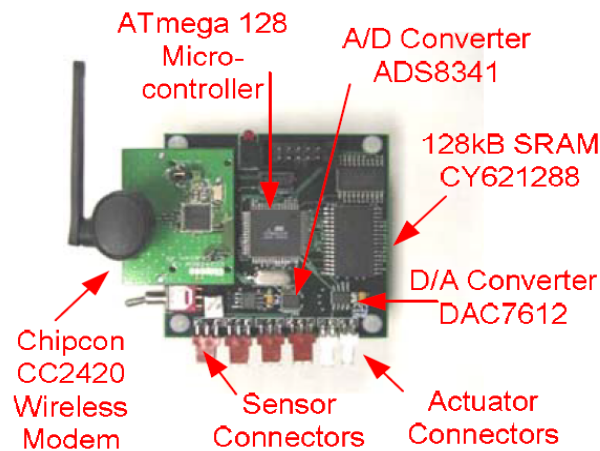


Fig. 2.10 Narada wireless sensing/control unit

Swartz and Lynch designed a wireless sensor platform, termed Narada as shown in Fig. 2.10, for a variety of monitoring and control applications (Swartz and Lynch 2006; Swartz and Lynch 2009). Narada unit consists of four functional modules: sensor signal digitization, computational core, wireless communication, and actuation signal generation. The sensor signal digitization module, which consists of the Texas Instrument 16-bit A/D converter ADS8341, converts analog sensor signals into digital data. Sensor data are then transferred to the computational core, which consists of a low-power 8-bit Atmel ATmega128 microcontroller. An external 128kB Static Random Access Memory is integrated with the computational core for additional data storage and interrogation. The wireless unit communicates with other units or server through the wireless transceiver, Chipcon CC2420, which takes about 1.5~2ms to transmit a 10-byte packet. Analog signals as control commands are sent to structural actuators through the Texas Instruments D/A converter DAC7612. Up to two structural actuators can be commanded by a single Narada unit.

## 2.2.5 MicroStrain

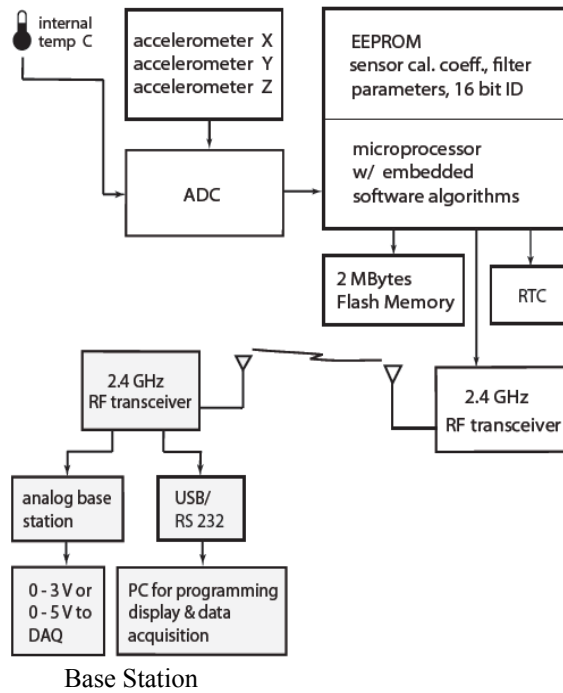


Fig. 2.11 Block diagram of the G-Link® -mXRS™ Accelerometer and WSDA® -Base(MicroStrain)

MicroStrain Inc. has a series of wireless sensor node suitable for structural monitoring, such as SG-Link® -mXRS™ Strain, G-Link® -mXRS™ Accelerometer, DVRT-Link™ -mXRS™ Displacement etc. Combining signal conditioning, embedded processing, extended range wireless communications, and precision timekeeping, all the three wireless nodes operate within a fast, synchronized, scalable network of wireless sensor nodes located up to 1 km from the WSDA® -Base. SG-Link® -mXRS™ node measures strain, torque, load, pressure and magnetic fields through a connector to user-supplied bridge sensors; G-Link® -mXRS™ node measures accelerations, vibrations, and tilt angles with its embedded accelerometers; DVRT-Link™ -mXRS™ node provides wireless data acquisition from all MicroStrain DVRT® displacement

sensors. The block diagram of the G-Link® -mXRS™ Accelerometer and WSDA® -Base is shown in Fig. 2.11

At the heart of MicroStrain's extended range synchronized (mXRS™) system is the WSDA® -Base, which uses the exclusive beaconing protocols to synch precision timekeepers embedded within each sensor node in the network. The WSDA® -Base also coordinates data collection from all sensor nodes. Users can easily program each node on the scalable network for simultaneous, periodic, or burst mode sampling with our Node Commander® software, which then automatically configures network radio communications to maximize the aggregate sample rate.

All the three types of nodes use 2.4GHz IEEE802.15.4 standard compliant transceiver and have the following features in common:

- Support for hundreds of simultaneous sampling wireless sensor nodes
- Node to node synchronization of +/- 32 microseconds
- Ultra-stable on-board precision timing reference of +/- 3ppm over industrial temperature range
- Extended wireless communication range to 1 km.

### 2.2.6 WiseSPOT

WiseSPOT is a research project which aims to develop a new generation of miniature low-power wireless sensor nodes that will utilize advanced smart antenna technology for continuous monitoring, localization and tracking of events in the network environment (i.e, crack detection in large structures, land movements in landslide prediction etc.).(SignalGeneriX)

Compared to conventional wireless sensor networks, the proposed innovative architecture, illustrated in Fig. 2.12, can achieve longer range, less power consumption, less interference and even localization through the smart antenna which consists of 4 directional antennas to be selected via antenna switching. The WiseSPOT wireless node is based on the M2110 MEMSIC's IRIS OEM Edition module, which provides a functional integration of the microprocessor, memory and the wireless transceiver.



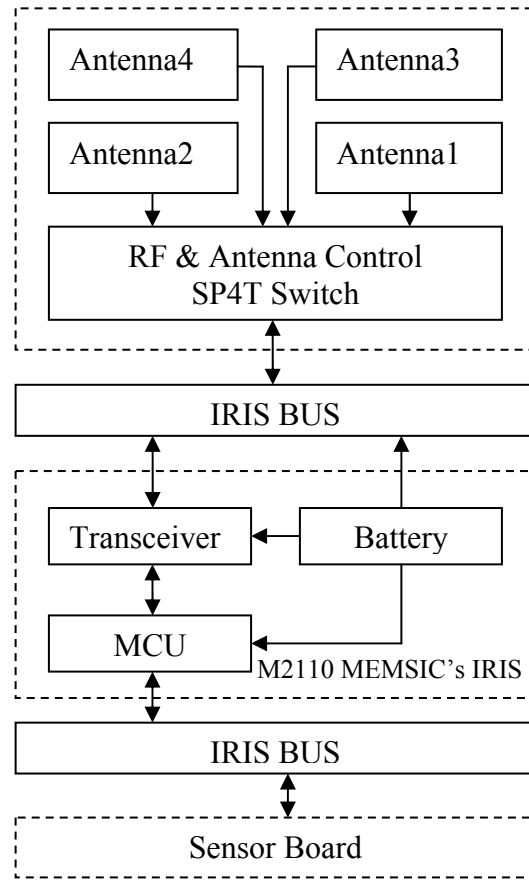


Fig. 2.12 WiseSPOT Node Architecture

In the framework of WiseSPOT project, a localization algorithm which combines RSSI (Received Signal Strength Indication) and AOA (Angle of Arrival) techniques was designed. The localization algorithm processes antenna signals using a switch to select each of the node's four directional antennas. The localization mechanism is based on the existence of three or more, static nodes at pre-known locations having some neighbor-nodes in common, as shown in Fig. 2.13. The position of each node in relation to the base nodes is estimated and their exact position in the network is then calculated using a triangulation-based technique.

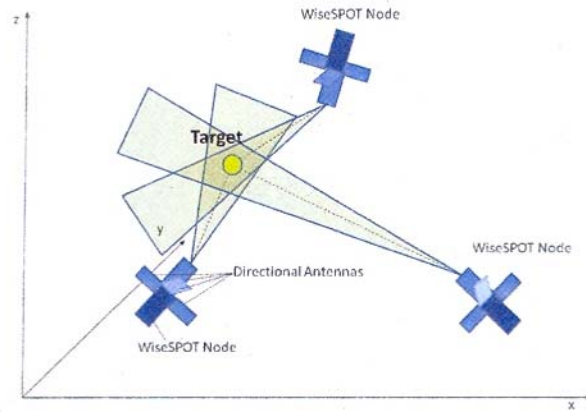


Fig. 2.13 WiseSPOT localization approach

### 2.2.7 XMU unit

Lei et al. designed a ZigBee-based wireless sensor network for structural monitoring (Jiang, Tang and Lei 2009). The wireless sensor node consists of four modules: sensors (such as accelerometer, strain gauge, anemometer and so on), signal conditioner, Computational module and wireless communication module. In the signal conditioner module, there are amplifier, anti-aliasing filter, voltage offsetting, and the 16-bit ADC ADS8341 which has 4 input channels and a sampling frequency up to 100 KHz. The computational module mainly consists of the 8-bit Atmel ATmega128L microcontroller and a 128kB SRAM (Cypress CY62128B) for storing measurement data. The CC2430 from Texas Instrument is selected to be the wireless transceiver, which is a true System-on-Chip (SoC) solution specifically tailored for IEEE 802.15.4 and ZigBee applications. It enables ZigBee nodes to be built with very low total bill-of-material costs. In the wireless sensor node, some engineering analysis algorithms are embedded, such as Auto-regression Analysis, FFT and Peak picking. The TPSN algorithm is adopted to realize time synchronization.

## 2.3 Summary

Main components of the above mentioned WSNs (except the MicroStrain one) and the WSN designed by the authors are summarized in Table 2.1.

Table 2.1. Main components of the abovementioned WSNs

	Microprocessor	RAM	ADC	RF Transceiver
Illinois IMOTE2 with SHM-A	PXA271	256 KB SRAM 32 MB SDRAM	QF4A512	CC2420
EMPA (Tmote Sky)	MSP430F1611	10K	Integrated in $\mu$ P	CC2420
WiseSPOT (IRIS M2110CA)	Atmega 1281	8K	Integrated in $\mu$ P	AT86RF230
Stanford Unit	ATmega128	132KB	ADS8341	9XCite or 24XStream
Narada	ATmega128	132KB	ADS8341	CC2420
XMU Unit	ATmega128	132KB	ADS8341	CC2430
Pavia Unit	Enhanced 8051 In the CC1110	4KB	ADS8343	CC1110

Most WSNs utilizes IEEE802.15.4 compliant transceiver operating on 2.4GHz ISM frequency band and the standard ZigBee protocol, except the Stanford unit. Among these WSNs, Imote2 features high-speed computation and large data storage ability, and the WiseSPOT features smart antenna and localization. However none of the WSNs support general wireless data acquisition for common sensors, that is, none of them is able to directly interface with various conventional sensors used in wired DAQ systems.



## **Chapter 3**

### **Design and Implementation of a Wireless Sensor and its Application in Structural Monitoring**

Based on the design constraints analysis in chapter 1 and the investigation of existing wireless sensor network technologies in Chapter2, the following work were performed and presented in this chapter:

- (1) Design and implementation of a new wireless sensor network platform which features the compatibility with many typical sensors broadly adopted in Civil Engineering.
- (2) Design and implementation of a 4-channels wireless structural monitoring system which features real-time. The feature is implemented by the frequency division multiplexing method.
- (3) The wireless sensing unit and wireless structural monitoring system were validated by some laboratory tests.

#### ***3.1 Introduction***

A structural monitoring system is a fundamental component in a SHM system and it used to monitor the behavior of structures during forced vibration testing or natural excitation for the consequent structural health analysis and diagnosis. It includes some sensors installed on a structure and a centralized data acquisition device. The sensors are responsible to convert the structural response into electrical signal. The data acquisition device is responsible to sample the electrical signal output from the sensors and store the sampled data in a central data repository.

In order to guarantee reliable and high quality signal sampling, structural monitoring systems employ coaxial wires as the link between sensors and the centralized data acquisition device. While coaxial wires provide a very reliable link, their installation in structures can be expensive and labor-intensive. If few sensors are installed and they are close to the data acquisition device, a coaxial cable link is suitable. However, when many sensors are required and they are far from the data acquisition device, coaxial cable link is inconvenient. Besides the expensive and labor-intensive installation, the cost of coaxial cable itself is also very high and a long cable will also attenuate the signal and power supply.

As a promising solution to the drawbacks of conventional structural monitoring system, wireless structural monitoring systems are emerging. A wireless structural monitoring system consists of some wireless sensors installed on a structure and a base station receiving the sampled data from all the sensors through wireless links. The power supply of the wireless sensors are usually batteries, sometimes with energy harvesting device.

A wireless sensor and a structural monitoring system based on it are designed and validated in this chapter. This chapter is based on the previous researches (Faravelli and Chen 2009; Casciati, Faravelli and Chen 2009a, 2009b, 2010a, 2010b, 2010c, 2010d). The rest of this chapter is organized as follows: Firstly, the architecture and function of the proposed wireless structural monitoring system is introduced to give an overview of the design; Secondly, the hardware design of the wireless sensor is described in detail; Thirdly, the software design of the wireless sensor is presented. Lastly, a laboratory experiment is performed to validate the whole wireless structural monitoring system.

### 3.2 Architecture of the proposed Wireless Structural Monitoring System

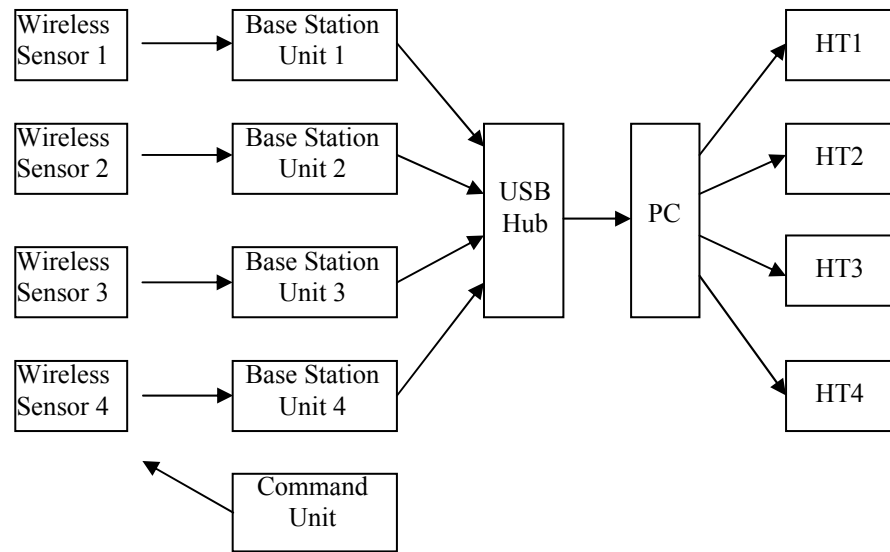


Fig. 3.1 Architecture of the wireless structural monitoring system.

A wireless structural monitoring system is built for facilitating the laboratorial structural monitoring experiments in the laboratory to which the author has access. The wireless structural monitoring system can adopt various sensors, accelerometers, strain gauge, load cell and laser distance sensor, as described in chapter1. In order to achieve real time monitoring, the frequency division multiplexing (FDM) method is adopted. Different wireless sensors operate in different frequency channels without any conflict. Through this method, the overall time delay is the same as the time delay of one channel.

As shown in Fig. 3.1, the proposed wireless structural monitoring system consists of sensors, wireless sensing units, base station units, one command unit, one USB hub, one computer and the software HyperTerminal. The sensors take the power from and output the analog signal to the wireless sensing units. The wireless sensing units sample and convert the analog signal into data and then send the data to their corresponding base station unit by wireless communication. When the data are received, the base station unit sends it to the computer through a virtual COM implemented by an UART-USB bridge. Since each wireless sensor has its own base station unit, there will be as many base station units connected to the computer as the wireless sensors are. Due to the limited number of USB interface in the computer, an USB hub is utilized to increase the USB interfaces. In the computer, the software, called HyperTerminal, is adopted to acquire the COM data and save them into a txt file.

In order to be able to manually start, stop and synchronize wireless data acquisition from the sensors, a command unit is arranged. The command unit operates in a preset command channel and has two buttons, one is for starting DAQ and the other one is for stopping DAQ. When one of the buttons is pressed, the corresponding wireless command will be broadcast to all the wireless sensors. Each wireless sensor has two operating channel, one is the common command channel and the other channel is its private channel. Each wireless sensor will change to operate in command channel right after finishing a data packet to its base station unit, and will return to its private channel when a new data packet is ready to be sent.

### ***3.3 Frequency Division Multiplexing***

Frequency division multiplexing (FDM) is a kind of physical layer multiplexing approach where the available total frequency bandwidth is divided

into several separate frequency slots which correspond to different frequency channels dedicated to the transmission of different signals. Since the occupied frequency bands of different slots are non-overlapping, the signals of different channels can really be transmitted simultaneously without introducing any delay due to the transmission in series of the other signals.

In order to implement an FDM approach, a transceiver equipped with a programmable frequency synthesizer and a bandwidth-programmable band-pass channel filter is usually required. The programmable frequency synthesizer is used to produce different carrier frequencies for different channels, while the channel filter is used to filter the undesired signals from other channels. The RF transceivers CC1110 and CC2510 from Texas Instrument are of this type. Both of them can operate in a large frequency range covering most of the ISM/SRD frequency bands (ISM: industrial, scientific, medical; SRD: short range device). Moreover, they have a programmable channel filter and a frequency synthesizer which support the multi-channel application. The CC1110 can operate in the frequency range below 1 GHz (namely, in the ranges of 300-348 MHz, 391-464 MHz, and 782-928 MHz) and the CC2510 can operate in the frequency range of 2.4 GHz (from 2400 to 2483.5 MHz).

In order to design a system complying with the current legal regulations, the wireless transceivers should operate within the limited license-free frequency bands enforced in each geographical area. In particular, while the 2.4 GHz frequency band is globally license-free, the license-free frequency band below 1 GHz is regionally dependent. For example, in Europe the license-free frequency bands below 1 GHz include the ranges of 433.05-434.79 MHz and 863-870 MHz, while in USA the range is 902-928 MHz. The advantages and disadvantages of either adopting the globally accepted 2.4 GHz frequency band or the regionally limited sub 1 GHz frequency band are summarized in table below.

Table 3.1. Comparison between the available licence-free frequency bands.

Frequency bands	Advantages	Drawbacks
2.4 GHz	<ul style="list-style-type: none"> <li>• Same solution worldwide</li> <li>• Large bandwidth</li> <li>• 100% duty cycle allowed</li> </ul>	<ul style="list-style-type: none"> <li>• Shorter range</li> <li>• Crowded</li> </ul>
Below 1 GHz	<ul style="list-style-type: none"> <li>• Better range</li> <li>• Less crowded</li> </ul>	<ul style="list-style-type: none"> <li>• Custom solutions</li> <li>• Limitations in "performance"</li> <li>• Duty cycle restrictions</li> </ul>

In order to cover most of the license-free frequency bands and to optimize the communication performance, both the RF transceivers CC1110 and CC2510



can be utilized. Although the hardware is different, the CC1110 and CC2510 modules have the same hardware interface and the same embedded software, which is tailored to different frequency configurations. Due to their similarities, the design of their modules can be unified.

The resulting number of channels that can be used for wireless data transmission is calculated by dividing the total available bandwidth ( $TB$ ) by the channel bandwidth ( $CB$ ). To achieve the best performance, it is recommended that the necessary channel bandwidth must occupy at most 80% of the actually configured total available bandwidth. Therefore, the number of channels,  $N$ , is determined as:

$$N = \frac{80\% \times TB}{CB} \quad (3.1)$$

When either the modulation approach of FSK (frequency shift keying) or GFSK (Gauss frequency shift keying) is adopted, the necessary  $CB$  is given by

$$CB = DR + FS + 4 \times X \times F \quad (3.2)$$

Where  $DR$  indicates the data rate;  $FS$  the frequency separation value;  $X$  the tolerance of the crystal oscillator; and  $F$  is the average frequency of the carrier.

Since the 2.4 GHz frequency band is globally license-free and it has loose limitations, the calculation of the available number of channels is performed in this bandwidth to provide an example. The following values are assumed for the parameters in Eq. (3.2):  $X = \pm 20$  ppm,  $DR = 100$  kHz,  $FS = 130$  kHz, and the carrier frequency is 2441.7 MHz which is the center of the 2.4 GHz frequency band. Using Eq. (3.2), the  $CB$  is calculated to be equal to 536 KHz. The nearest channel filter bandwidth configuration available in CC2510 is 541 kHz. From Eq.(3.1), the corresponding number of channels,  $N$ , is 154 when a total bandwidth of 83.5MHz is considered. However, guard bands between two adjacent channels are required due to the imperfect filters and the interference. Therefore, the resulting number of the actually available channels is less than its theoretical value. Furthermore, since many devices are working on the 2.4 GHz frequency band, particularly the WiFi, the number of usable channels also depends on the specific occasion.

Another aspect relevant for the application of wireless communication in the monitoring of large-scale structures is the communication range. In the ideal free space, where there are no obstacles between the transmitter and the receiver

and the signal can propagate along a straight line between the two, the path gain  $P_G$  is given by

$$P_G = 10 \log_{10} \frac{P_r}{P_t} = 10 \log_{10} \frac{G_t \lambda^2}{(4\pi d)^2} \quad (3.3)$$

where  $P_r$  is the power of the received signal,  $P_t$  is the power of the transmitted signal,  $G_t$  is the product of the antenna gains of the transmitter and the receiver in the direction of the line of sight,  $d$  is the distance between the transmitter and the receiver, and  $\lambda$  is the wave length of the signal.

Equation (3.3) shows that the power of the received signal is inversely proportional to the square of the distance and directly proportional to the square of the wave length. Therefore, operating in the frequency band sub-1GHz results into a better communication range than the one that can be achieved in the 2.4 GHz band. Another problem encountered in the implementation of wireless communication systems is the conflict between the receiver sensitivity and its bandwidth; indeed, a large bandwidth decreases the sensitivity. For example, the receiver sensitivity of CC1110 at 433 MHz is equal to: -110 dBm with a data rate of 1.2 kBaud, -102 dBm with 38.4 kBaud, and -95 dBm with 250 kBaud. Therefore, reducing the data rate can increase the communication range, but the communication delay and the power consumption are also consequently increased. In the proposed wireless system, when the data rate is set to 100 kBaud, a stable communication range can be up to 150 m. If a longer communication distance is required, a relay unit can be utilized. Nevertheless, a more accurate estimate of the actual range can be formulated only at the end of the testing process, when in-field applications are implemented.

### 3.4 Hardware Design of the Wireless Sensing Unit

As described in the chapter 2, a wireless sensor node usually is composed of sensor, signal conditioner, analog to digital converter, microcontroller and a RF transceiver. The wireless sensor node which will be described in this section includes all the basic components. It is under the design constraints presented in the chapter1, which mainly focus on the power management and signal conditioning modules. Unlike most of the typical wireless sensor node introduced in chapter2, the RF transceiver (CC1110) adopted in this wireless sensing unit operates in ISM sub-1GHz instead of 2.4GHz, and uses its

proprietary communication protocol instead of the commonly used standard ZigBee. However, the sub-1GHz transceiver can be replaced a 2.4GHz IEEE802.15.4 compliant RF transceiver (CC2430), since both of them has the same pin configuration.

### 3.4.1 Overview of the wireless sensing unit

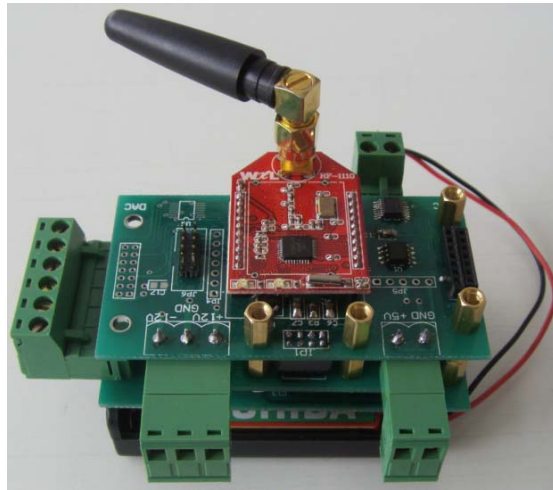
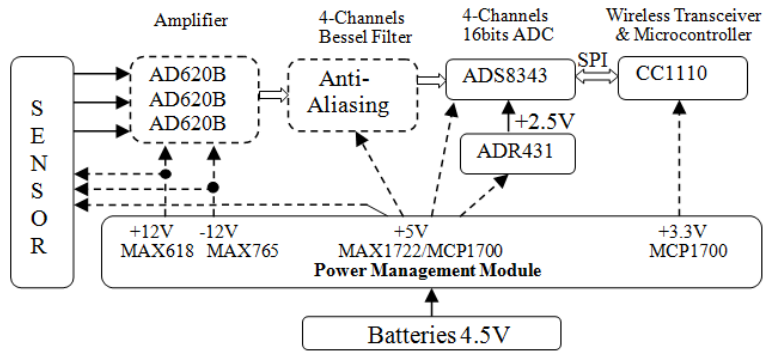


Fig. 3.2 Component level block diagram (Top) and prototype (Bottom) of the wireless sensing unit

As shown in Fig. 3.2, the wireless sensing unit consists of three amplifiers (AD620B) for three input channels, a 4-channel anti-aliasing Bessel filter, a 4-channel 16 bits ADC (ADS8343), a System on Chip (SoC) RF transceiver (CC1110), and a multiple outputs power management module with a 4.5Volts batteries power supply.

The amplifier role is to amplify the analog signal output from the sensor. The amplification can indirectly help to improve the signal sampling resolution. Thus, a relatively lower resolution ADC is adequate. In addition, a low-pass filter is required to avoid the aliasing when there are signal components with frequency higher than half the ADC sampling frequency. The ADC role is to convert an analog signal into a digital series for consequent data processing algorithm. The SoC RF transceiver CC1110 includes not only a RF transceiver which is for RF wireless communication, but also a 8051 integrated microcontroller, such that another external microcontroller is not necessary. The microcontroller controls the activities of the wireless sensing unit through executing the embedded program. Since different sensors have different power supply requirement, a multiple output power management module is required. As shown in the Fig. 3.2, there are many power supply outputs in the power management module, including  $\pm 12V$ ,  $+5V$  and  $+3.3V$ . The output of  $\pm 12V$  power supplies are adjustable in a wide range, (The output voltage of the  $+12V$  power supply can be adjusted from input voltage up to  $+28V$ ; The output voltage of the  $-12V$  power can be adjusted from  $-1V$  to  $-16V$ ).

### 3.4.2 Signal Conditioning and ADC

#### (1) Amplifier AD620B

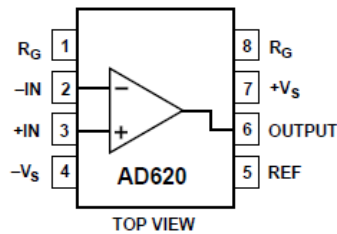


Fig. 3.3 Connection Diagram of AD620

AD620 is a low-power low-cost instrumentation amplifier, as shown in Fig.3.3. It features high integration, easy to use, gain set with one external resistor (gain range 1 to 1000), wide power supply range ( $\pm 2.3$  V to  $\pm 18$  V), and low power (max supply current: 1.3 mA). In addition, its output offset can be configured by the pin REF to match the ADC input range. Due to the high integration, one AD620 with only 1 external resistor is enough to form the amplifier for one input channel. Thus, it is appropriate for the wireless sensor application.

Its gain can be configured by the resistor  $R_G$  between the two  $R_G$  pins. The relation between the gain and  $R_G$  is given by the following equation 3.4.

$$G = \frac{49.4 \text{ k}\Omega}{R_G} + 1 \quad (3.4)$$

## (2) 5 order Anti-aliasing Bessel filter

A low pass 5 order Bessel filter is designed to perform the anti-aliasing before an ADC. The ADC is usually operated with fixed sampling rate  $f_s$ . The Nyquist theorem states that the sampling rate must be greater than twice the highest frequency component of the measured signal to accurately reconstruct the waveform. Specifically, the frequency components below  $f_s/2$  can be reliably recorded while the ones above  $f_s/2$  will be folded back to the spectrum of interest leading to a false alias lower frequency component with the same amplitude. This phenomenon of aliasing is illustrated in the following Fig.3.4. The left part shows the analog input signal consisting of 5 frequency components. Only the component (1) resides in the segment  $N=0$  spanning from DC (direct current) to  $f_s/2$  where the signal can be reliably recorded. The other components (2) to (5) in the segments  $N=1$  to  $N=4$  will be folded back into segment  $N=0$  appearing as lower frequencies with the following equation 3.5. The final sampled signal is present in the right part of Figure3.

$$f_{\text{aliased}} = |f_{\text{in}} - N \times f_s| \quad (3.5)$$

Where  $f_{\text{in}}$  is the signal with frequency higher than  $f_s/2$ ;  $f_s$  is the sampling frequency;  $N$  is the integer which make  $f_{\text{aliased}}$  less than  $f_s/2$ .

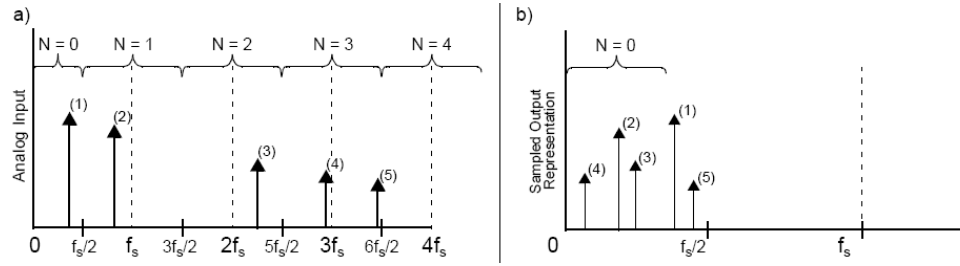


Figure 3.4. Illustration of the aliasing phenomenon in frequency domain.

The aliasing phenomenon can be eliminated or significantly reduced by using a low pass filter before the ADC to attenuate the frequency components above one half of the sampling rate. The ideal low pass filter is illustrated in the left part of the Fig. 3.5, for which all the frequency components above the cut-off frequency will be completely eliminated suddenly. However, this kind of filter with ideal performance is impossible in practice. The actual performance of low pass filter is illustrated in the right part of Figure 3.5. The  $f_{\text{CUT-OFF}}$  is defined as the frequency with a gain of -3 dB less than DC for the Butterworth and Bessel low pass filter while  $f_{\text{STOP}}$  is the frequency at which a minimum gain is acceptable. The frequency region that span from DC to the cut-off frequency is defined as the Pass Band while the frequency region above the  $f_{\text{STOP}}$  is defined as the Stop Band. Unlike to the ideal low pass filter, there is a Transition Band that spans from  $f_{\text{CUT-OFF}}$  to  $f_{\text{STOP}}$  in the practical filter. The bandwidth of the transition band is determined by the filter design (Butterworth, Bessel, Chebyshev, etc.) and the order of the filter. The filter order is determined by the number of poles in the transfer function. Generally, the transition bandwidth will become smaller when more poles are used to implement the filter design.

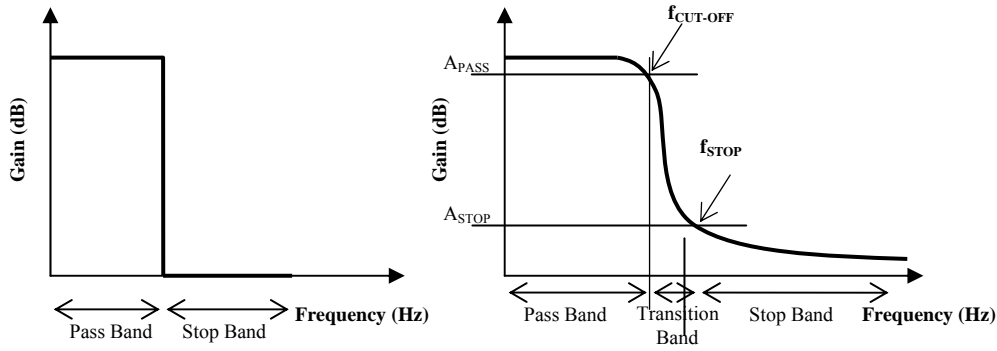


Figure 3.5. The features of ideal and practical low pass filter

When a low-pass filter is used for the anti-aliasing, the signal frequency component in the pass band will all pass the filter with little influence while the component in the stop band will be greatly attenuated to an acceptable level. However, the frequency component in the transition band will be differently attenuated depending on frequency value. If the  $f_s/2$  is between the  $f_{\text{CUT-OFF}}$  and  $f_{\text{STOP}}$ , the frequency component from  $f_s/2$  to  $f_{\text{STOP}}$  will still be folded back into the pass band significantly. Therefore, in the design of anti-aliasing filter, the  $f_{\text{STOP}}$  should be lower than one half of the sampling frequency. Moreover, the minimum gain  $A_{\text{STOP}}$  at the  $f_{\text{STOP}}$  should be less than the signal to noise ratio (SNR) of the data acquisition system. For instance, if a 12-bit A/D Converter is used, the ideal SNR is 74dB. The filter should be designed so that its gain at  $f_{\text{STOP}}$  is at least 74dB less than the pass band gain.

According to the principle discussed above, a 5 order Bessel filter with a  $f_{\text{CUT-OFF}}$  of 25Hz is designed using the tool FilterLab provided by Microchip [13]. Its schematic is present in the Figure 3.6. The Figure 3.7 is the theoretical amplitude-frequency and phase-frequency response and figure 3.8 is the implementation of this filter of 4 channels.

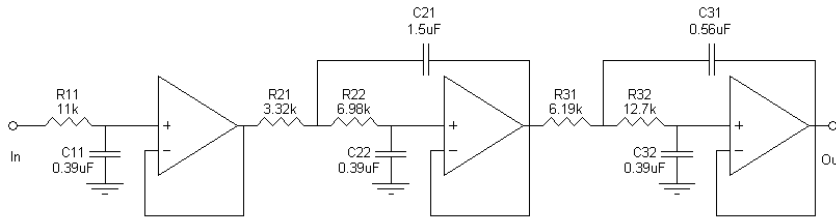


Figure 3.6. Schematic of the 5 order Bessel Filter

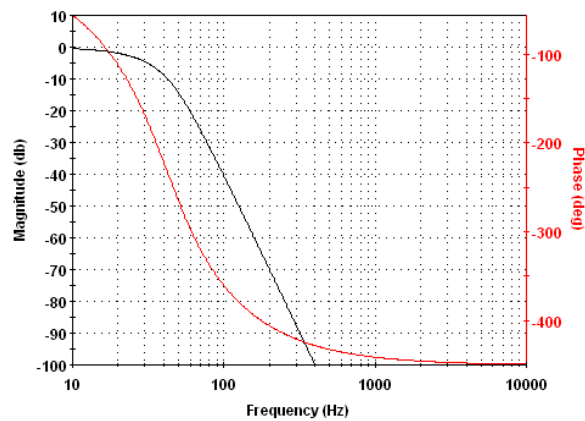


Figure 3.7. The simulation of amplitude/phase-frequency of the designed filter

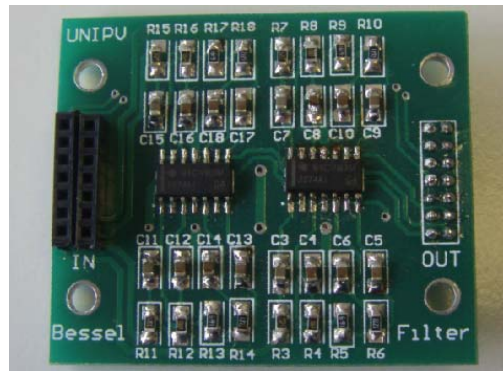


Figure 3.8. The implemented filter

### (3) Analog to Digital Converter ADS8343

ADS8343 is a 16-bit, 4-channel sampling analog-to-digital converter with a synchronous serial interface. The conversion rate is up to 100KHz. The power supply can vary from 2.7V to 5V. The typical power dissipation is 8mW at a 100kHz throughput rate and a +5V supply. The reference voltage ( $V_{REF}$ ) can be varied between 500mV and  $V_{CC}/2$ , providing a corresponding input voltage range of  $\pm V_{REF}$ . The device includes a shutdown mode which reduces power dissipation to under 15 $\mu$ W. The ADS8343 is ensured down to 2.7V operation.



### 3.4.3 Microcontroller and RF transceiver

The CC1110 is a low-power sub-1 GHz system-on-chip (SoC) designed for low power wireless applications, as shown in Fig.3.9. It combines the excellent performance of the state-of-the-art RF transceiver CC1101 with an industry-standard enhanced 8051 MCU, up to 32 kB of in-system programmable flash memory and up to 4 kB of RAM, and many other powerful features. Based on the CC1110, the CC1111 SoC transceiver integrates a full-speed USB 2.0 interface. Interfacing to a PC using the USB interface is quick and easy, and the high data rate (12 Mbps) of the USB interface avoids the bottlenecks of RS-232 or low-speed USB interfaces. Thus, The CC1111 could be adopted for the base station unit.

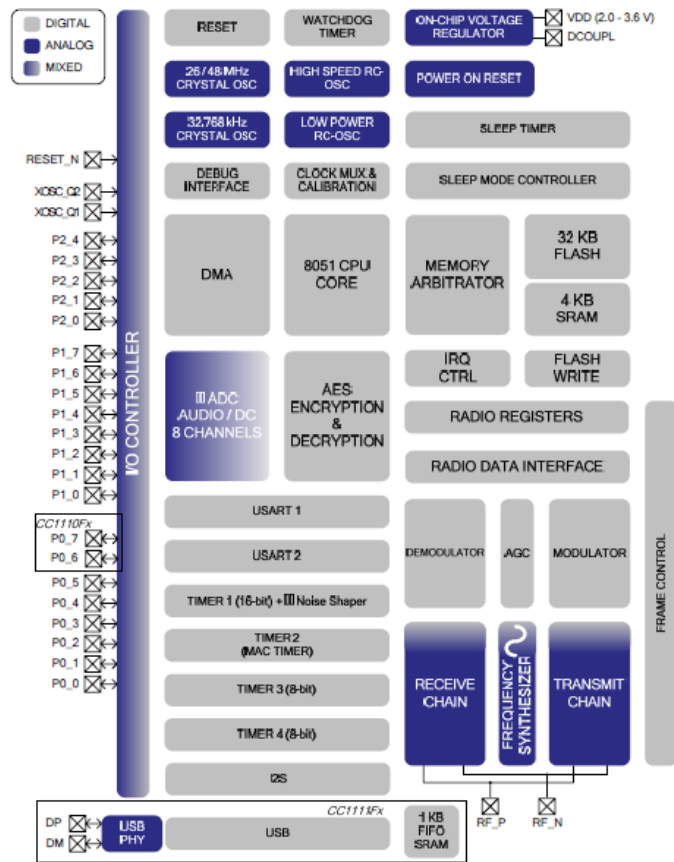


Fig. 3.9 Architecture of the CC1110 or CC1111RF transceiver

The high-performance RF transceiver integrated in CC1110 is based on the CC1101 RF transceiver. It features excellent receiver selectivity and blocking performance; high sensitivity (-110 dBm at 1.2 kBaud); programmable data rate up to 500 kBaud; programmable output power up to +10 dBm for all supported frequencies; frequency range: 300-348 MHz, 391-464 MHz and 782-928 MHz; digital RSSI / LQI support. In addition, this transceiver is low power: Low current consumption (RX: 16.2 mA @ 1.2 kBaud, TX: 16 mA @ -6 dBm output power); 0.3  $\mu$ A in PM3 (operating mode with the lowest power consumption, only external interrupt wakeup); 0.5  $\mu$ A in PM2 (operating mode with the second lowest power consumption, timer or external interrupt wakeup).

Besides the high performance and low power 8051 microcontroller core, there are many peripherals, mainly including powerful DMA functionality; 8/16/32 KB in-system programmable flash, and 1/2/4 KB RAM; Full-Speed USB Controller with 1 KB FIFO (CC1111); 128-bit AES security coprocessor; 7-12 bit ADC with up to eight inputs; I2S interface; Two USARTs; 16-bit timer; Three 8-bit timers.



Fig. 3.10 CC1110 Module

### 3.4.4 Power Management

#### 1, Power Consumption Analysis

In order to make the sensing unit as low-power as possible, the low-power feature is required in the selection of components. In this section, the power consumption of the components adopted in the sensing unit (except the voltage regulators which will be discussed in the next section) is described. This information also justifies the adoption of the electronic components in Fig.3.2. The low power instrument operational amplifier AD620B needs a 1.3mA maximum supply current and its default supply voltage is  $\pm 12V$ . In Fig.3.2, there are three amplifiers, so that their total power consumption is around 93.6mW. The 5-order Bessel filter uses 3 quadruple operational amplifiers TLC2274 whose supply voltage is +5V and supply current is around 5mA. Their power consumption is around 75mW. In Fig3.2, the ADR431 is a voltage reference. Its supply is 800  $\mu A$  without load and its supply voltage is +5V, therefore its power consumption is near 4mW.

Table 3.1 Typical power consumption of some components

	AD620	TLC2274	ADR431
Supply Current	1.3mA	5mA	800uA (No load)
Supply Voltage	$\pm 12V$	+5V	+5V
Power Consumption	31.2mW	25mW	4mW
Number	3	3	1
Total consumption	172.6mW		

Typical power dissipation of the ADS8343 is 8mW at a 100 kHz throughput rate and a +5V supply, but it includes a shutdown mode which reduces power dissipation to under 15 $\mu$ W. The low-power RF SoC CC1110 has a flexible power management strategy which allows power consumption optimization. It has 1 active mode (AM) and 4 power modes (from PM0 to PM3). In the PM2, the current consumption is only 0.5  $\mu$  A. The required supply current of the AM depends on the specific configuration. In AM with low CPU activity, the typical current consumption is 5mA when the system clock is set to 26MHz and no peripheral is running; In AM with Radio in RX (Receiving State, 433MHz, 250KHz) , it is 20.5mA; In AM with Radio in TX (Transmitting State, 433MHz, +10dBm), it is 33.3mA.

Table 3.2. The Power Consumption of CC1110 &amp; ADS8343

	CC1110 (+3.3V)	ADS8343 (+5V)
Minimum Power Consumption	1.65uW PM2	15uW Shut down
Maximum Power Consumption	110mW AM/Tx/433MHz / +10dBm	8mW 100KHz throughout

The power requirement of the three types of sensors is given in Table 3.3.

Table 3.3. The Power Consumption of the Three Sensors

	FBA-11	FBA-EST	CXL01LF3
Supply Voltage	$\pm 12\text{V}$	$\pm 12\text{V}$	+5V
Supply Current	2.5mA	35mA	12mA
Power Consumption	60mW	840mW	60mW

## 2, Power Management

Considering the required voltages, the wireless sensor is designed to be power supplied by 3 AA batteries in series providing a voltage of near 4.5V. The components of the wireless sensor need some supply voltages such as  $\pm 12\text{V}$ , +5V and +3.3V. As shown in Figure 3.2, the  $\pm 12\text{V}$  supply voltage is for the sensors and their signal amplifiers, the +5V is for the filter and the ADC, and the +3.3V is for the RF transceiver. The power management module mainly consists of some voltage regulators and is responsible for the conversion.

In order to make the unit suitable for both low-power sensors (CXL01LF3) and non-low-power sensors (FBA-11 and FBA-EST), there are four main aspects to be considered in the design of the power management module: Highly efficient power conversion; Adjustable output voltage; Medium output power; Ability to sleep with very little power consumption.

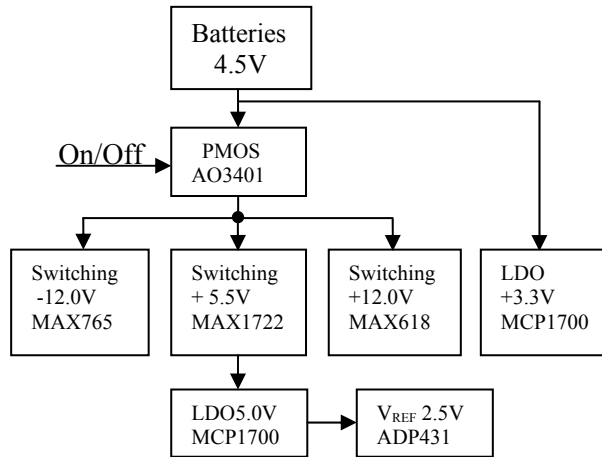


Fig. 3.10 Block Diagram of the Power management.

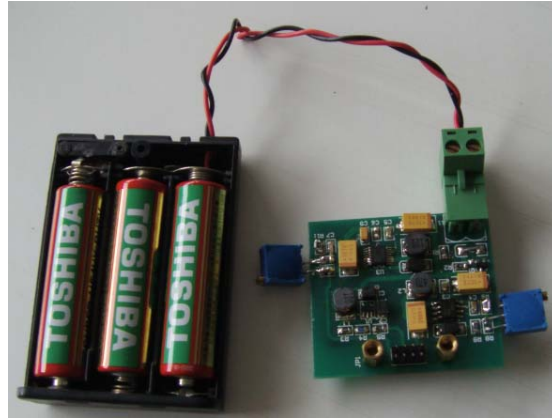


Fig. 3.11 Prototype Power Management Module.

According to the requirement, the power management is designed as shown in Fig.3.10 and Fig.3.11. The power management is implemented by 1 electronic switch (AO3401), 1 ultralow noise voltage reference (ADP431), and two types of voltage regulators: LDO (low dropout regulator, MCP1700) and switching regulators (MAX1722, MAX618 and MAX765).

The batteries directly supply power to the first +3.3V LDO regulator for the SoC RF transceiver CC1110, and supply power to other regulators through the electronic switch which is controlled by the microcontroller inside CC1110. Therefore, only the power supply of CC1110 is not switchable, since it is the controller of the whole unit.

The 5.0V voltage supply is for filter and ADC which are sensitive to noise, so that it is implemented by a switching regulator MAX1722, which has a switching noise, followed by a second +5.0V LDO MCP1700 which acts as an active filter to filter the noise. In addition, the 5.0V is used as the power supply of the ultralow noise +2.5V voltage reference for the ADC.

When the electronic switch is off, in the wireless sensor only the CC1110 is powered. The overall supply current from the batteries consists of the quiescent current of the MCP1700 (only  $1.6 \mu\text{A}$ ) and current drawn by the CC1110 which has 4 power modes (PM). In PM2, the current supply is only  $0.5 \mu\text{A}$  and the microcontroller can be woke up by the internal timer.

According to the abovementioned aspects, the key parameters for the selection of voltage regulators of LDO and switching style are quiescent current, conversion efficiency, output power and output adjustability.

#### (1) Low Dropout Regulator

A low dropout (LDO) regulator is a DC linear voltage regulator which can operate with a very small input–output differential voltage. The efficiency of LDO regulators depends on input–output voltage drop and quiescent current ( $I_Q$ ) which is the difference between the input and output currents. Since the voltage drop is very small, the  $I_Q$  is the key parameter that limits the efficiency. Therefore, in the selection of the LDO, the low  $I_Q$  ( $1.6 \mu\text{A}$ ) LDO MCP1700 produced by MICROCHIP is chosen.

In addition to low  $I_Q$  and low dropout, another feature of MCP1700 is that the output current can be up to 250 mA. Therefore, it is very suitable for this application. Its application circuit is shown in Figure 3.12. Only 2 external capacitors are required.

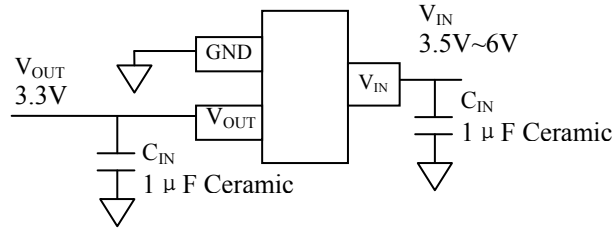


Fig. 3.12 Typical application circuit of MCP1700

In the wireless unit, 2 MCP1700s with output voltage of +3.3V and +5.0V separately are adopted. Since they are not intended to supply power to sensors, the output adjustability is not necessary.

## (2) Switching Regulator

Compared to the linear regulator, the switching regulator has a much higher efficiency on power conversion, because its pass transistor operates on switching state instead of linear mode. In switching mode, the pass transistor output either negligible voltage or negligible current and therefore consumes little power. In linear mode, the pass transistor is subject to the difference of input and output voltage and the load current, so that the power usually from the product of the voltage drop by the load current will be dissipated in the form of heat. In the wireless unit, three switching regulators which have excellent efficiency are adopted: MAX1722, MAX618 and MAX715. Their main features are shown in Table 3.4.



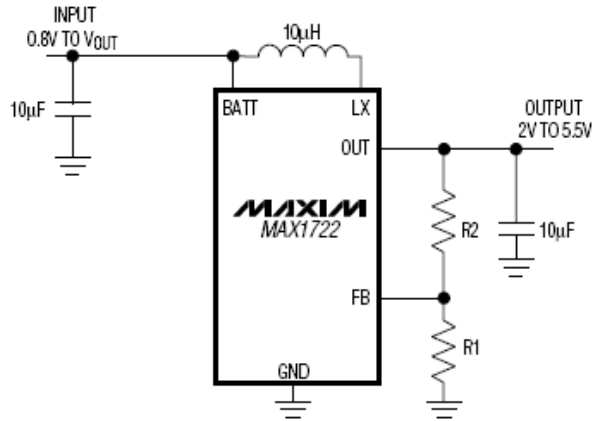


Fig. 3.13 Adjustable Output Application Circuit of MAX1722

The Max1722 is high-efficiency step-up DC-DC converter which features an extremely low quiescent supply current to ensure the highest possible light-load efficiency. As shown in Fig. 3.13, its output voltage can be adjusted from 2V to 5.5V using the resistors R1 and R2 and determined by the following equation (3.6) where the feedback resistor R2 should be in the 100K  $\Omega$  to 1M  $\Omega$  range and the  $V_{FB}$  is 1.235V.

$$R_2 = R_1 \left( \frac{V_{OUT}}{V_{FB}} - 1 \right) \quad (3.6)$$

The Max618 is also a step-up DC-DC converter that generates output voltages up to +28V and accepts inputs from +3V to +28V. As shown in Fig. 3.14, two external resistors (R1 and R2) set the output voltage. First, select a value for R2 between 10K  $\Omega$  and 200K  $\Omega$ . Calculate R1 with the following equation (3.7) where the  $V_{FB}$  is 1.5V.

$$R_1 = R_2 \left( \frac{V_{OUT}}{V_{FB}} - 1 \right) \quad (3.7)$$

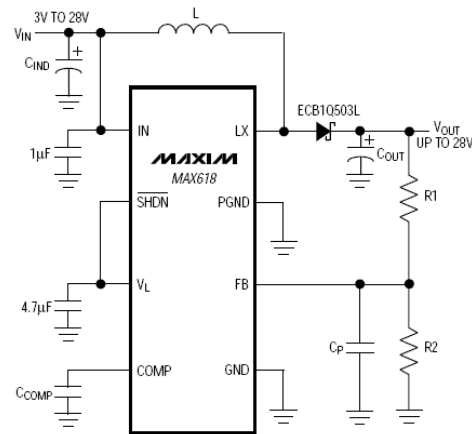


Fig. 3.14 Adjustable Output Application Circuit of Max618

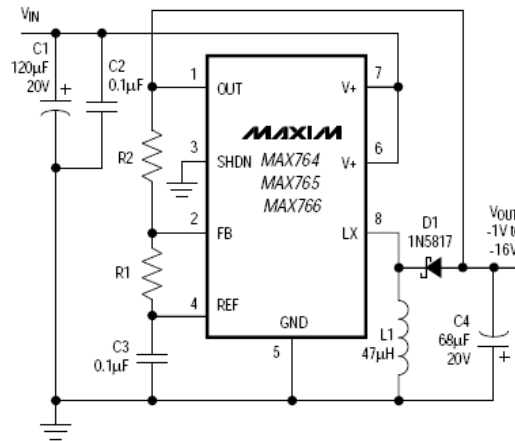


Fig. 3.15 Adjustable Output Application Circuit of Max765

Table 3.4. The Features of Power Management Components

	<b>MAX618</b>	<b>MAX765</b>	<b>MAX1722</b>
Input voltage	+3V to +28V	+3V to +16V	0.8V to 5.5V
Output voltage	Up to +28V	-1V to -16V	2.0V to 5.5V
Output current	Up to 500mA at +12V	Up to 250mA	Up to 150mA
Quiescent Current	500μA	120μA	1.5μA
Shutdown Current	3 A	5μA	N/A
Conversion Efficiency	Up to 93%	Around 80%	Up to 90%

The Max715 is an adjustable low  $I_Q$  DC-DC inverting switching regulator which are highly efficient over a wide range of load currents, delivering up to 1.5W. Its output voltage can be adjusted from -1.0V to -16V using external resistors R1 and R2, configured as shown in Figure 6. A feedback resistor R1 of 150K  $\Omega$  is recommended. The R2 is given by the following equation (3.8) where the  $V_{REF}$  is 1.5V.

$$R2 = R1 \left| \frac{V_{OUT}}{V_{REF}} \right| \quad (3.8)$$

### (3) Electronic switch

The PMOS (P-Channel MOSFET, metal-oxide-semiconductor field-effect transistor) power transistor AO3401 is used as electronic switch which can completely cut off the power supplies of sensor and some components of the sensing unit so as to minimize the power consumption when the wireless sensor is in sleep mode. The symbol of AO3401 is shown in Figure 3.16 where G is the gate for control, D is the drain and S is the source. In a sensing unit, S is directly connected to batteries, D is directly connected to the input of the switching regulators, and the G is connected to the output pin of the CC1110. When G is pulled down to 0V, the channel between S and D will be open.

When G is pulled up close to the voltage of batteries, the channel between S and D will be close.

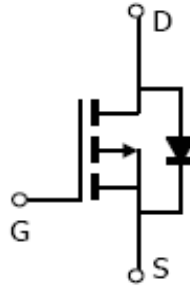


Fig. 3.16 the PMOS AO3401

### ***3.5 Software Design of the Wireless Sensing Unit***

#### **3.5.1 Integrated Development Environment**

An integrated development environment (IDE) is a software application that provides comprehensive facilities to computer programmers for software development. An IDE normally consists of: (1) a source code editor; (2) a compiler; (3) an assembler; (4) a linker; (5) a debugger. The IDE used for developing the embedded software of the CC1110 is IAR Embedded Workbench, as shown in the Fig. 3.17. The language chosen for programming is the C language which is broadly adopted in embedded system development.

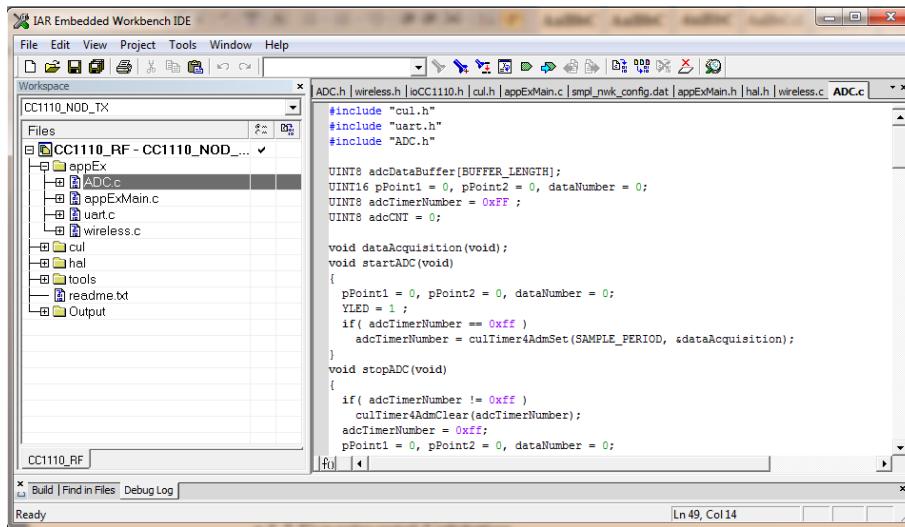


Fig. 3.17 Interface of the IAR Embedded Workbench IDE.

The CC1110 includes an on-chip debug module which communicates over a two-wire interface. The debug interface allows programming of the on-chip flash. It also provides access to memory and registers contents, and debug features such as breakpoints, single stepping, and register modification. In order to connect the software debugger in IAR Embedded Workbench IDE and the debug module in CC1110, a hardware debugger (C51RF-PS EM2.0) is required, as shown in Fig. 3.18. The C51 RF-RS EM2.0 mainly has a USB debug port to communicate with IDE, a virtual RS232 port to communicate with PC, a socket to mount a CC1110 module, a debug port for external wireless module.

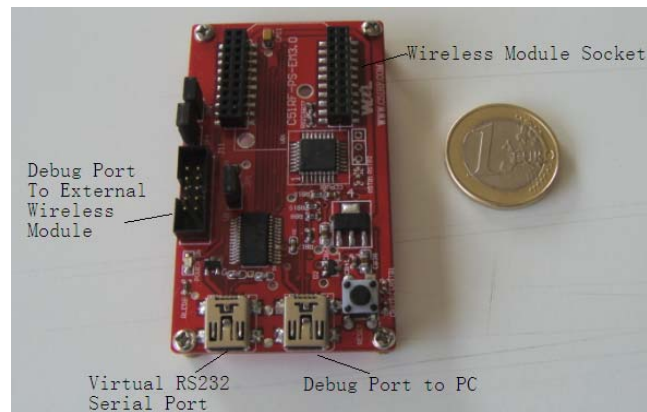


Fig. 3.18 CC1110 Debugger C51RF-PS EM2.0

Through the IAR Embedded Workbench and the C51RF-PS EM2.0 debugger, the user not only can write, compile and download the program into the CC1110, but also can debug the program, including breakpoints, single stepping, and memory and register access.

### 3.5.2 Communication Protocol

The communication protocol adopted in the wireless sensing unit is based on data packet transmission supported by the hardware packet handler in CC1110. Two communication modes are available: unreliable and reliable modes.

#### (1) Data Packet

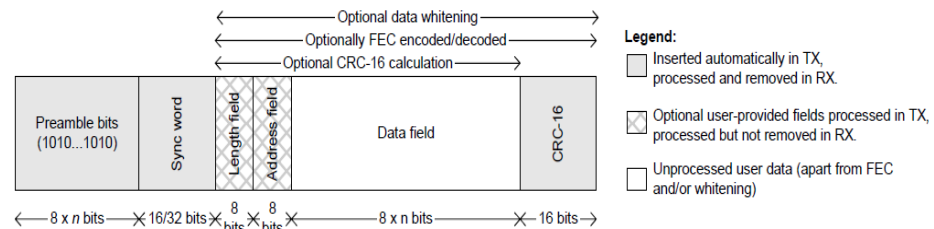


Fig. 3.19 CC1110 Packet Format

The CC1110 has built-in hardware support for packet oriented radio protocols. The data packet format is shown in the Fig. 3.19 above.

In transmit mode, the packet handler can be configured to automatically add the following elements to the packet: (1) A programmable number of preamble bytes; (2) a two byte synchronization (sync) word which can be duplicated to give a 4-byte sync word (recommended). It is not possible to only insert preamble or only insert a sync word; (3) A CRC checksum computed over the data field. In addition, the following can be implemented on the data field and the optional 2-byte CRC checksum: (1) Whitening of the data with a PN9 sequence; (2) Forward error correction (FEC) by the use of interleaving and coding of the data (convolutional coding).

In receive mode, the packet handling support will de-construct the data packet by implementing the following (if enabled): (1) Preamble detection; (2) Sync word detection; (3) CRC computation and CRC check; (4) One byte address check; (5) Packet length check (length byte checked against a programmable maximum length); (6) De-whitening; (7) De-interleaving and decoding. Optionally, two status bytes with RSSI value, Link Quality Indication, and CRC status can be appended to the received packet.

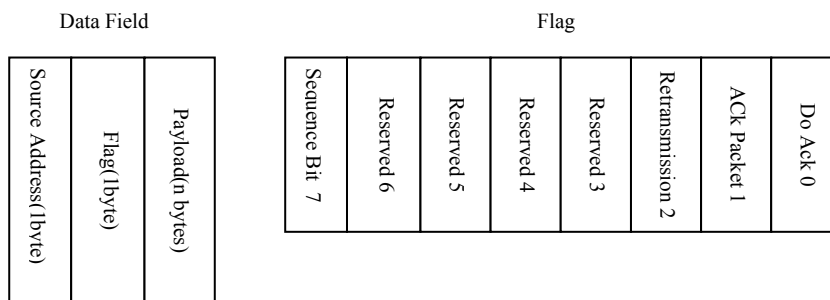


Fig. 3.20 The data field format

Based on the CC1110 packet handling hardware, the data field format of the protocol packet is designed as shown in the above Fig. 3.20.

The first byte of data field is a source address which indicates the receiver where the packet is from.

The second byte of data field is a flag byte which consists of 8 mark bits. The bit 7 is the sequence bit which is for preventing that the data packet is received twice by the receiver. It alters its status when a new data packet is sent and

maintains its status when the last data packet is retransmitted. The bits from 6 to 3 are reserved. The bit 2 is the retransmission mark. This bit is set to 1 for a retransmitted data packet, while it is set to 0 for a new data packet. The bit 1 is an ACK packet mark. When this bit is set to 1, it means that the packet is an ACK packet, not a data packet. The bit 0 is Do ACK mark for transmitter. When this bit is set to 1, the transmission is in reliable mode.

The other bytes are the payload which could contain command and its parameters.

## (2) Unreliable and reliable Communication

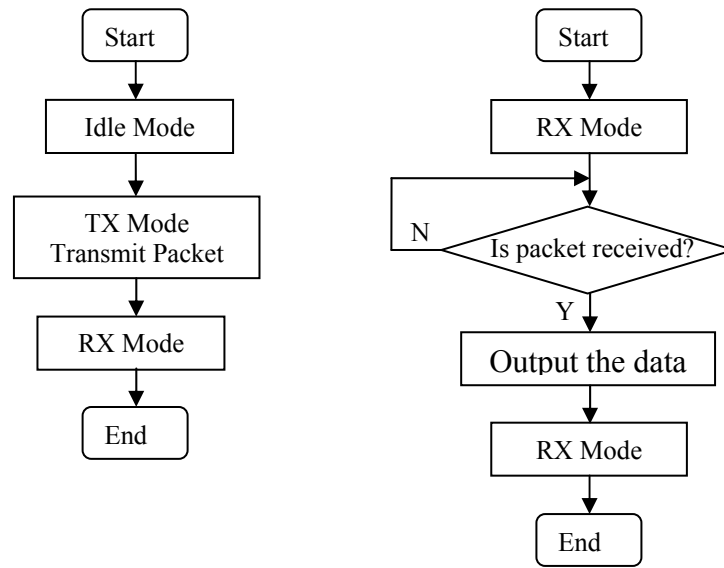


Fig.3.21 Unreliable Communication: transmission (left) and reception (right)

In the unreliable mode, a data packet transmission is completed regardless of if it is successfully received by the receiver. When interference exists or communication distance is too long, errors occur easily in receive state resulting in high receive failure probability. However, this mode has low communication delay, thus it can be used in the case that high communication speed is required and some data loss is acceptable.



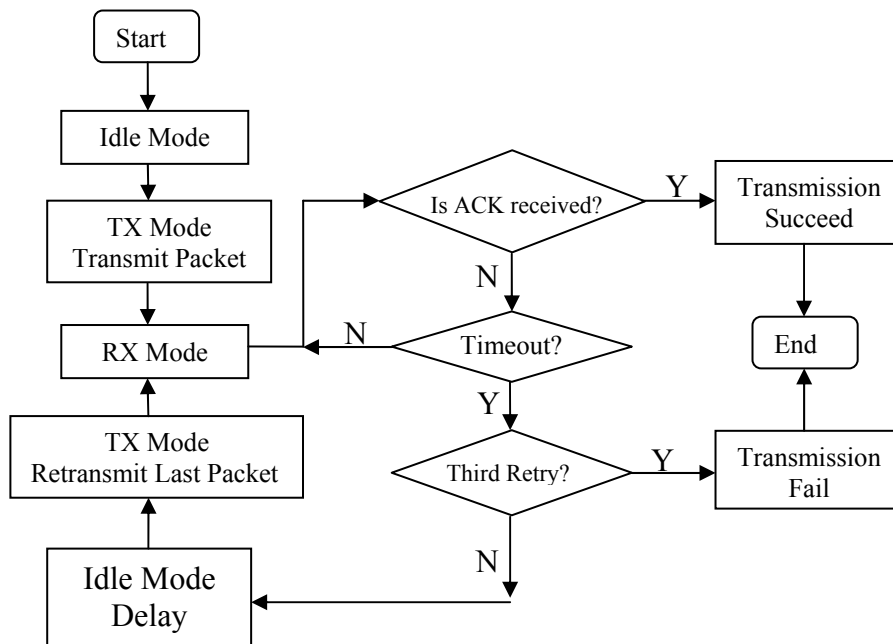


Fig. 3.22 transmitting a packet in reliable mode

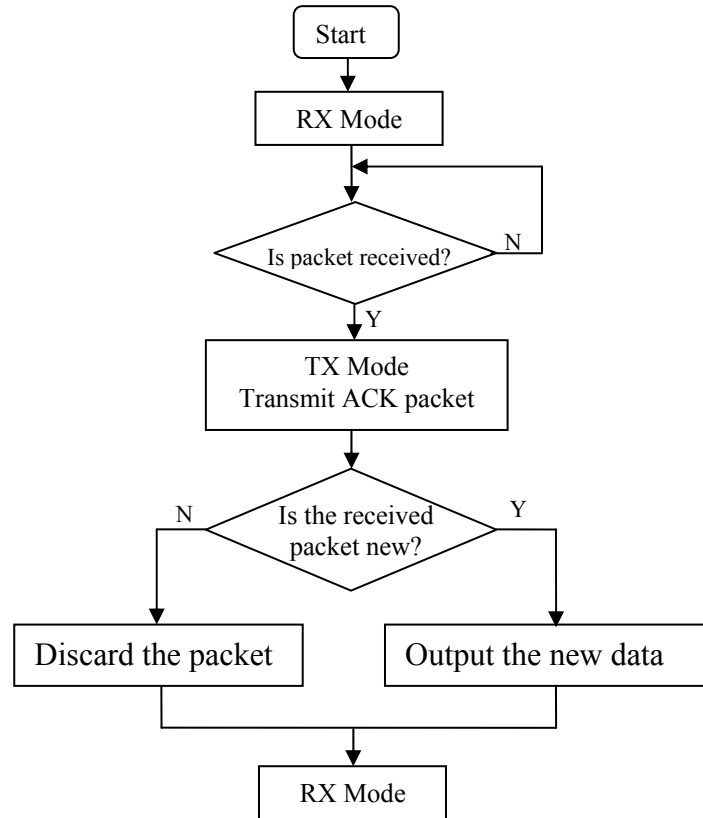


Fig. 3.23 Receiving a Packet in Reliable Mode

In reliable mode, an acknowledgement and retry mechanism is used to ensure a data packet is successfully received by the receiver.

When a data packet is sent out, the transmitter will enter receive (RX) mode and wait for an acknowledgement (ACK) packet from the receiver. If the ACK packet is not received in time, the transmitter will enter and stay in the IDLE mode for a delay time and then will go to TX mode and retransmit the packet again. The maximum retransmission time is set to 3 times. When the third retransmission still fails, the transmission data packet will be reported to fail.

When a data packet is received, the receiver will immediately go to TX mode and send an ACK packet to the transmitter. Then, the receiver will check if this packet is new or not according to the sequence bit in the flag byte of the data

packet. If the sequence bit is the same as the one of last packet, it will be regarded as a repeatedly received packet and be discarded.

### 3.5.3 Sampling and Data transmission

#### 1, Wireless Sensing Unit

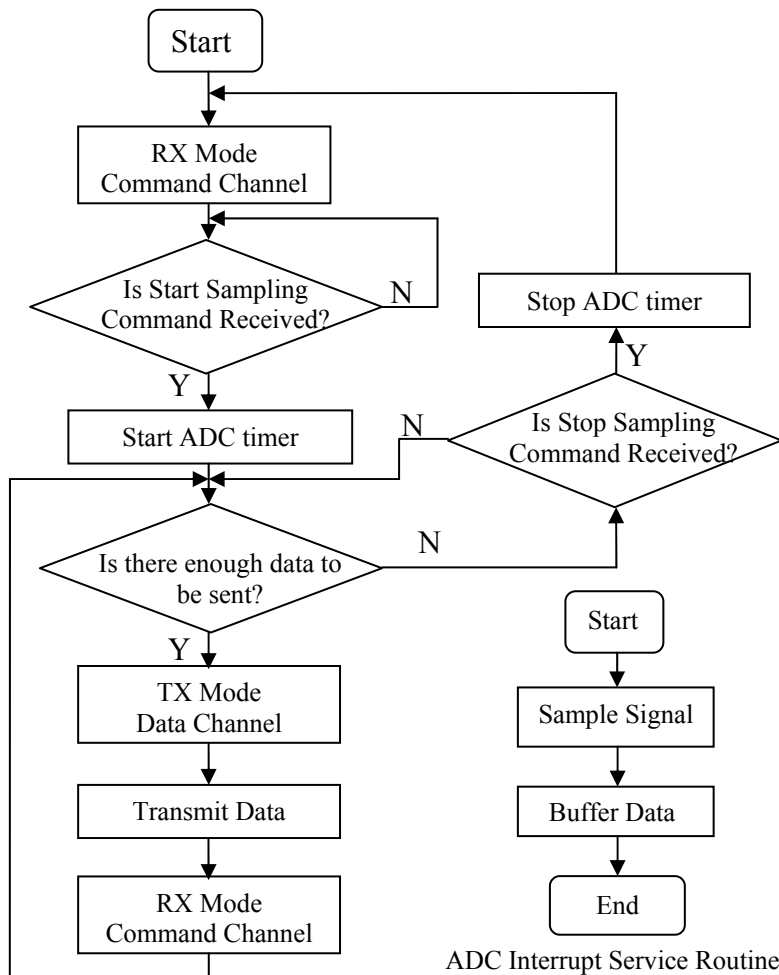


Fig. 3.24 Wireless Sensing Unit Software Flowchart

The wireless sensing unit mainly performs three tasks: waiting for a start and stop sampling command in command channel, sampling the signal in a timer interrupt service routine, transmitting the sampled data to base station unit in data channel. Indeed, each wireless sensing unit has two operating channels, its own data channel and the common command channel. As shown in Fig. 3.24, the wireless sensing units stay in command channel RX mode waiting for the starting sampling command from the command unit. Once they receive the start command, they turn on a timer designated for ADC. In the timer interrupt service routine, the signal sampling by ADC is executed to acquire the data which are then saved in a data buffer. When the data number in the buffer exceeds a threshold, the wireless sensing unit will pack the data into a data packet, enter data channel TX mode and then transmit the packet to the corresponding base station unit by the reliable communication mode. Once the packet is sent out, the wireless sensing units will switch to command channel waiting for the stop sampling command. When a stop sampling command is received, the wireless sensing unit will turn of the ADC timer and will stay in command channel RX mode waiting for the start sampling command. The start/stop sampling command is broadcast in command channel through unreliable mode.

## 2, Base Station Unit

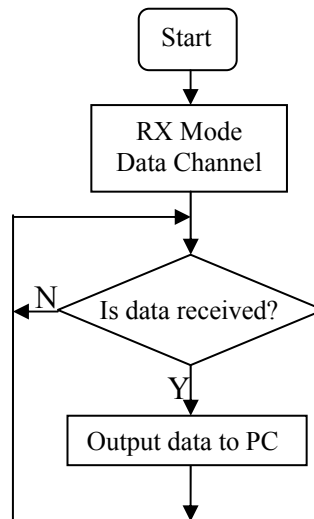


Fig. 3.25 Base Station Unit Software Flowchart

As shown in Fig.3.25, the base station units mainly receive the data transmitted from their corresponding wireless sensing unit and pass the received data to PC HyperTerminal through virtual COM implemented by a UART-USB bridge.

### 3, Command Unit

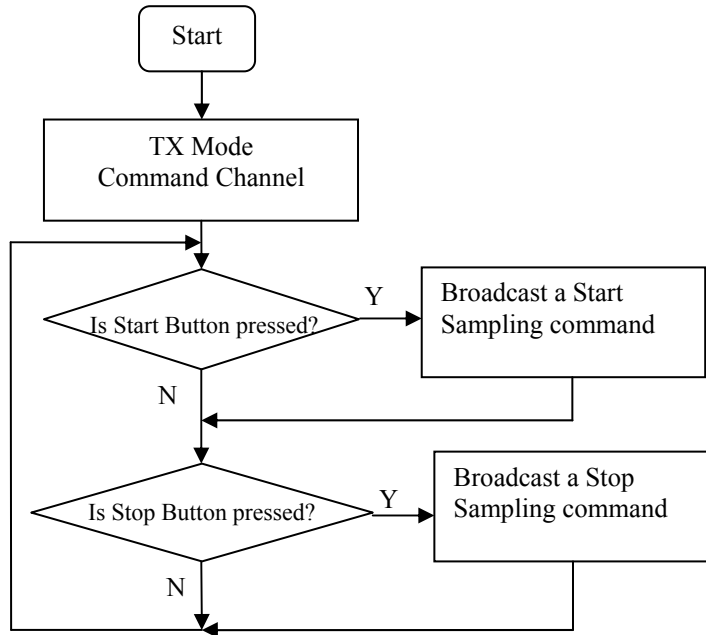


Fig. 3.26 Command Unit software flowchart

The command unit is designed to manually start, stop and synchronize wireless data acquisition from the sensors. It operates in a preset command channel and has two buttons, one is for starting sampling and the other one is for stopping sampling. When one of the buttons is pressed, the corresponding wireless command will be broadcast to all the wireless sensors. Each wireless sensor has two operating channels, one is the common command channel and the other channel is its private channel. Each wireless sensor will switch to the command channel right after finishing transmitting a data packet to its base

station unit, and will return to its private channel when a new data packet is ready to be sent.

### **3.6 Experimental Validation**

To validate the developed wireless structural monitoring system, a laboratorial test is conducted using a reduced-scale, 3-storey steel frame mounted on a shaking table. A mono-axial accelerometer FBA-11 is installed on each floor of the structure. The shaking table is configured to move in a sinusoidal mode with the frequency of 1 Hz and the amplitude of 2 mm. The acceleration response of the third floor is simultaneously acquired, with a sampling rate of 250 Hz, via two wireless sensing units and a wired DAQ system serving as reference.

In Figures 3.27-3.29, the acquired data are plotted together and aligned using MATLAB. The data from the wireless sensing units 1 and 2 are labeled as “WSU1” and “WSU2”, respectively, and they are compared with the ones obtained from the wired DAQ system. From Fig. 3.27, the waveforms resulting from the two wireless sensing units are basically consistent between each other and with the waveform from the wired system. From the enlargements in Fig.3.28 and Fig.3.29, the waveforms from the wired DAQ are characterized by a “saw-tooth” trend, because the corresponding ADC is 12 bit and the reference voltage is 10 V, thus resulting in a sampling resolution of 0.00488V. Instead, the ADC on the wireless sensing unit is 16 bit and its reference voltage is 2.5 V, resulting in a sampling resolution of 0.0000763 V. Therefore, its waveform is very smooth even when the signal amplitude is very small. The slight differences in the signal amplitudes are mainly due to small differences in the circuit parameters such as the gain and the reference voltage.

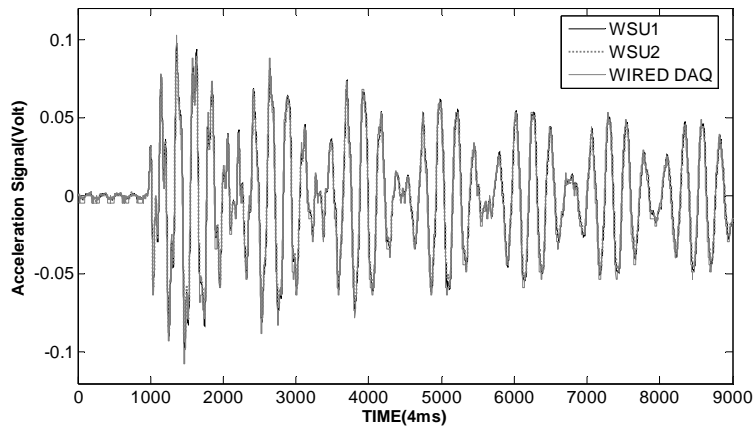


Figure 3.27. The complete waveforms acquired from “experiment1”.

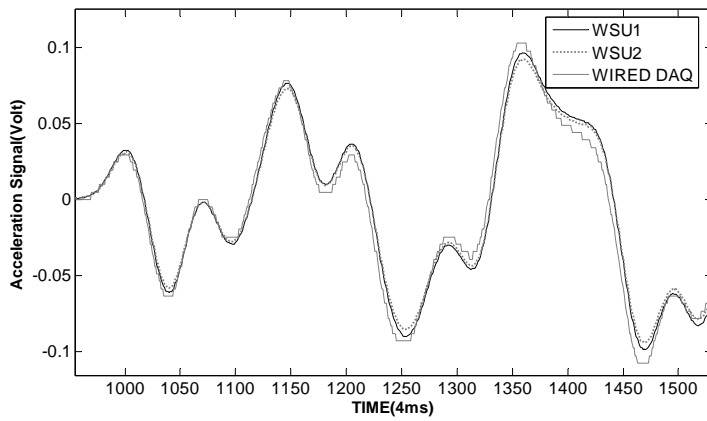


Figure 3.28. Enlargement of the initial part of Figure 3.27

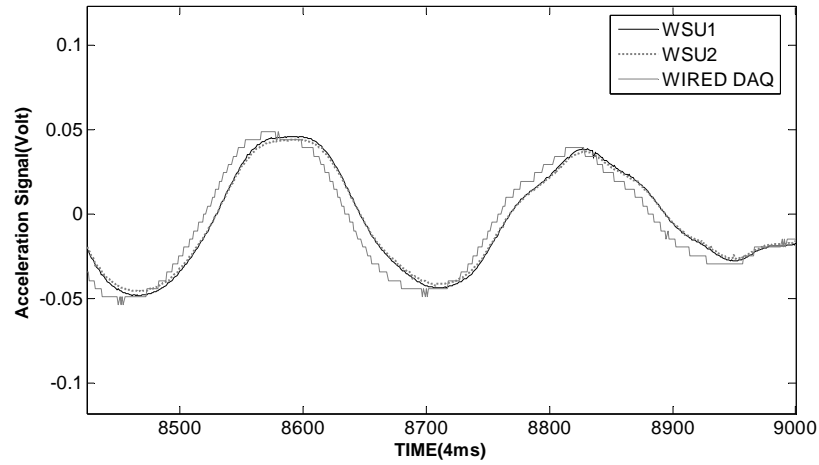


Figure 3.29. Enlargement of the ending part of Figure 3.27

The phase consistency is another important aspect to be analyzed. In Figure 3.28, the initial phases of the three signals are exactly the same. In Figure 3.29, where only the ending part of the waveform is plotted, a small phase difference between the wireless sensing units and the wired DAQ system is observed, while the phases between the two wireless units are still exactly the same. The detected phase discrepancy between the two kinds of communication systems can be justified by a small error in the sampling rate. In order to confirm this reasoning, another experiment is carried out.

In the new experiment, the wired DAQ system still operates with a sampling rate of 250 Hz, while the wireless system is intentionally adjusted to sample the data at about 249 Hz so that the resulting sampling rate is not exactly equal to 250 Hz. Only one wireless unit is deployed in this second experiment, since no phase difference is observed between different wireless units. The operating parameters of the shaking table are the same as the ones adopted for the previous experiment. Similar figures are obtained by plotting the acquired data (Figures 3.30-3.32). By comparing the ending part of the waveform represented in Figure 3.32 with the one plotted in Figure 3.29, it can be observed that the phase difference between the signals from the wireless and wired systems is increased, as expected. This result demonstrates that errors in the sampling rates can result in a phase difference between the data transmitted to the central computer



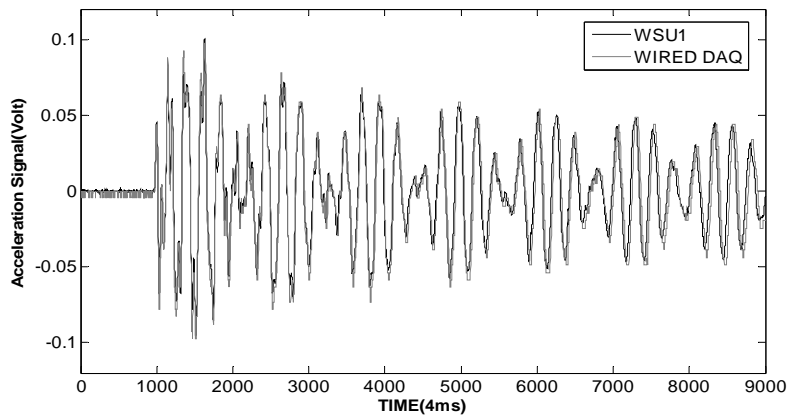


Figure 3.30. The complete waveforms acquired from “experiment2”

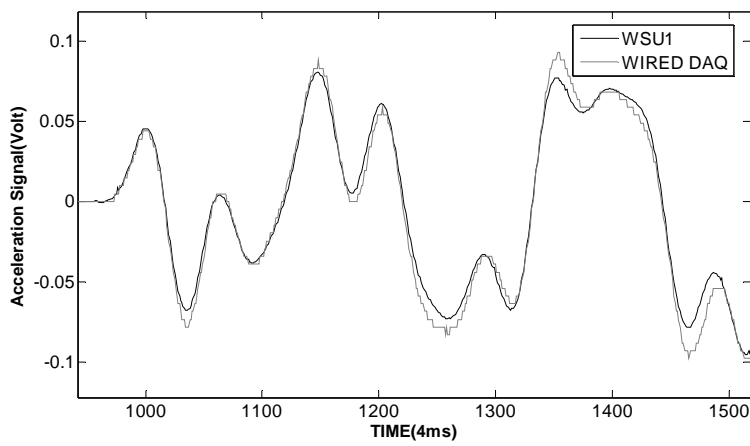


Figure 3.31. Enlargement of the initial part of Figure 3.30

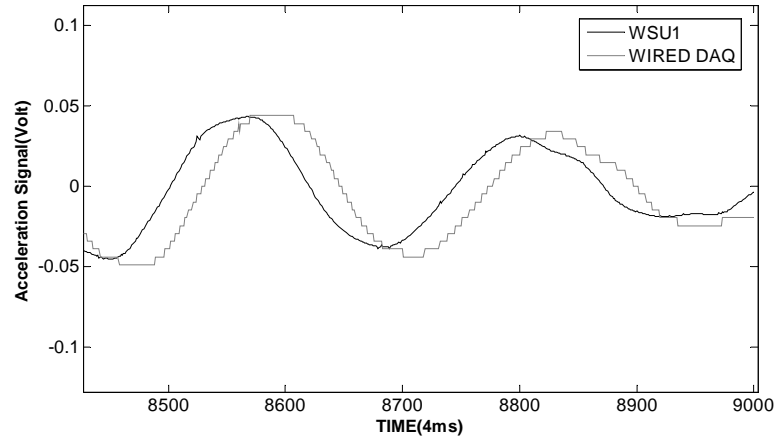


Figure 3.32. Enlargement of the ending part of Figure 3.30

### 3.7 Summary

In this chapter, a wireless structural monitoring system adopting frequency division multiplexing is presented. This system consists of sensors, wireless sensing units, base station units, a command unit, a USB hub, a computer and HyperTerminal. Using FDM, each wireless sensor has a private base station unit and a private data channel. All of the wireless sensors share a common command channel receiving the broadcasted command to start/stop sampling. When having enough data to transmit, the wireless sensors stay in data channel and TX mode; otherwise it will stay in command channel and RX mode.

The frequency division multiplexing wireless communication is implemented by the Texas Instrument SoC RF transceiver CC1110 which can operate in Sub-1GHz ISM frequency bands. Due to the similarity, another SoC RF transceiver CC2510 can be adopted to replace CC1110 for making the wireless sensing unit operating in 2.4GHz ISM frequency band. The channels of the FDM wireless communication depends on the available frequency band and data rate.

The low power feature of the wireless sensing unit is guaranteed by the selection of low-power electronic components, especially the power management components like the LDO and the switching regulators which feature a low quiescent current, a highly efficient power conversion, an adjustable output voltage and a medium output power. The wireless sensor is

able to work with high power efficiency and to sleep with very little power consumption. The overall duration of the wireless sensor powered by batteries depends on the duty cycle and the capacity of the batteries.

In order to make the wireless sensing unit compatible with various traditional sensors, the power management and signal conditioning module were carefully designed. The wireless sensing unit has multiple or adjustable power supplies to meet the requirement of sensors. The wireless sensing unit has a flexible signal conditioning module which can be adaptive to various output range and offset of sensors,

The wireless sensing unit has reliable and unreliable communication modes. The reliable modes adopt acknowledgement-retry mechanism to ensure a data packet can be successfully received by receiver. Reliable mode is used in data transmission. In the unreliable mode, a data packet transmission is completed regardless of if it is successfully received by the receiver. The start/stop sampling command is broadcast in unreliable mode.



## **Chapter 4**

### **an Active Mass Damper using a digital DC motor PID controller and wireless sensors**

#### ***4.1 Introduction***

In the last twenty years, many attempts to introduce structural control in civil engineering (characterized by systems with large masses) were done (Spencer and Nagarajaiah 2003; Casciati, Rodellar et al. 2011).

Among others, one of the main inconveniences was associated with the network connecting the sensor units (necessary to provide the control feedback) to the managing computer (i.e., the brain elaborating the sensor signals) and from here to the actuators. This physical connection among parts far away across the building is in conflict with the architectural constraints. Furthermore, damages to this network put the control system out of service.

Wireless sensor network could be a convenient alternative. Nevertheless, they were developed without the constraint of real time transmission. In other words wireless systems are designed to store a set of sensor readings to send the entire pack to the receiver. So a first required modification is to guarantee a real time transmission. (Casciati, Faravelli and Chen 2010e; Chen and Faravelli 2011; Casciati, Faravelli and Chen 2011b)

In this chapter, a previously deigned active mass damper (AMD) structural control system for a simple three-storey frame is updated by replacing its coaxial cables with a wireless sensing system and replacing its analog DC motor PID controller with an digital one. Finally, a laboratory test is performed to validate the system.

#### ***4.2 Active Mass Damper***

The typical active structural control system shown in Fig. 4.1 consists of the sensors which measure the response of the controlled structure, a controller which processes the data from the sensors according to the associated algorithm and determines the control output signal, and an actuator which receives the

signal from the controller and then generates the control force to be applied to the structure. Therefore, if the controlled structure is regarded as a closed loop system, the structural control system represents the feedback branch.

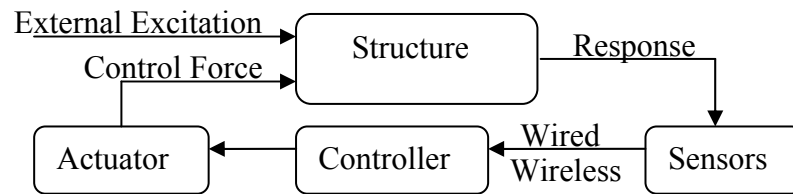


Fig. 4.1 The active structural control system



Fig.4.2 the 3-Storey Frame



Fig.4.3 the one axis shaking table

In the laboratory to which the author has access , a 3-story steel frame (as shown in Fig. 4.2) of reduced size controlled by an AMD structural control system is placed on a shaking table (as shown in Fig. 4.3) whose motion is used as excitation (Battaini 1999). The sensors are 4 uniaxial accelerometers, Kinematics FBA-11, installed on each floor separately. The actuator is an Active Mass Damper (AMD) installed at the top of the steel frame. The controller (see Fig. 4.4, excluding the dotted block, and Fig.4.5) was implemented mainly by the microcontroller C8051F007 which integrates with 4 analog to digital (ADC) input channels and 2 DAC (digital to analog) output channels(Casciati and Rossi 2004). Two control algorithms, linear control and fuzzy control, were implemented. The firmware has been designed with the easiness of use as the main concern. It has been implemented as a terminal shell. On the computer, the software HyperTerminal is used to access the embedded shell interface exposed by the board.

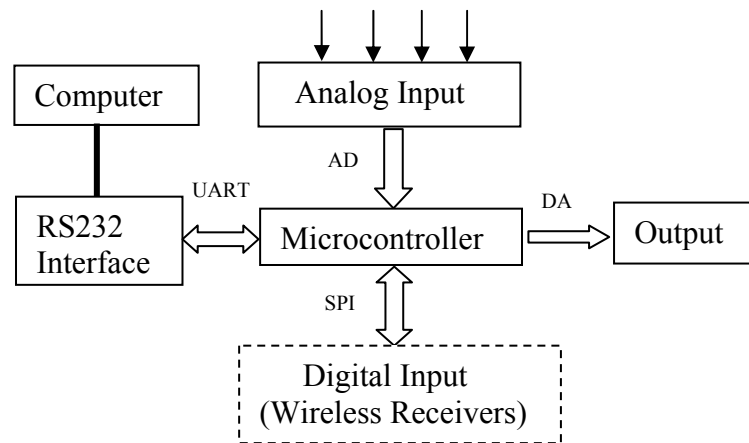


Fig.4.4 Block diagram of the controller



Fig.4.5 the structural controller

In order to introduce wireless sensors to this structural control system, the controller is slightly modified. As shown in Fig. 4.4 a dotted block which consists of wireless transceivers connected to the microcontroller via SPI interface is added. The wireless transceivers are used to command the wireless sensors and collect the data from them as well. The user can choose the wireless or the wired signal input through the computer.

The active mass damper used in this experiment consists of a uni-axial moving mass. The mass is attached to a cart which is driven by a Direct Current (DC) motor through a gear. Control of the position of the moving mass is achieved by a proportional derivative (PD) servo controller based on a



displacement measurement, given by a potentiometer attached to the moving cart.



Fig.4.6 the Analog PD controller of Quanser Consulting

The position servo controller of the DC motor was originally designed and implemented by the Quanser Consulting. The authors replaced the old electronics with a new one based on a digital proportional integral derivative (PID) control method and a pulse width modulation (PWM) driving scheme. This is achieved by using the H Bridge LMD18200T which is more power efficient than linear amplifier. Compared to the current motor controller, the new one resulted to be much smaller and more power efficient.

### ***4.3 Real Time Wireless Sensing***

The wireless sensing system is conceived to replace the cable connections between the four sensors and the structural controller, which requires a real-time and continuous data acquisition from the sensors. The conventional time division multiplexing (TDM) method encounters the problem of a high transmission delay when many channels are required. Such an observation suggested the authors to adopt a frequency division multiplexing (FDM) approach. In the FDM communication, different signal channels operate on different frequency bands, so that the data transmission can occur simultaneously without conflicts. As shown in Fig. 4.7, each channel of the wireless sensing system is formed by a pair of transceivers, one of which is mounted on the wireless sensing unit and the other is connected to the structural controller by the SPI bus. In the SPI bus, the structural controller is the master end and the other transceivers are the slave ends. In other words, only the structural controller can issue the communication.

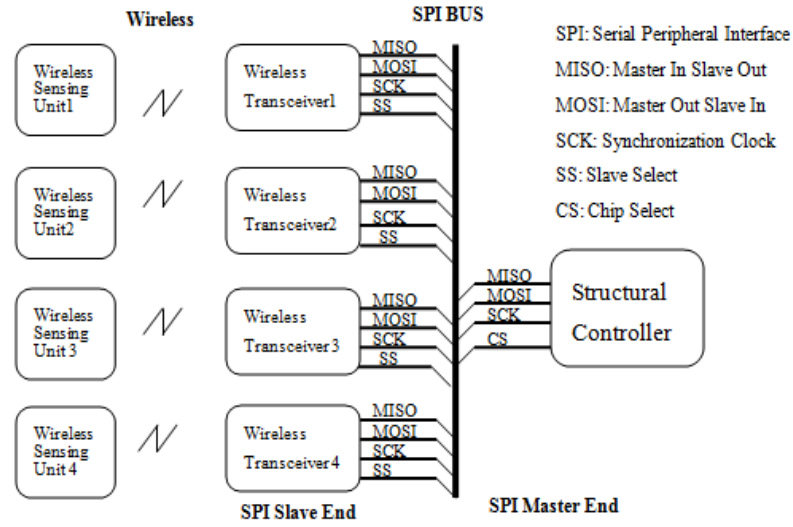


Fig. 4.7 Architecture of the wireless sensing system designed for structural control applications

In one cycle of remote data sampling, the controller broadcasts a command to the transceivers which then send the wireless request to the corresponding Wireless Sensing Units (WSUs). When the request is received, the WSUs start to perform the AD conversion, and they send the sampled data back to the corresponding base station transceiver. In this manner, the synchronization of the sensing system is guaranteed. To achieve the sampled data, the structural controller communicates with the four transceivers in turns, during predetermined time intervals.

#### 4.4 PID Position Controller for a DC motor

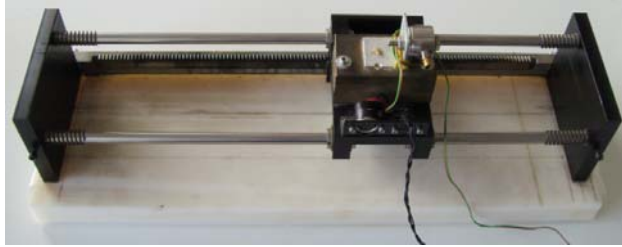


Fig. 4.8 Photo of the Active Mass Damper

As shown in Fig. 4.8, the active mass damper used in this experiment consists of a uniaxial moving mass. The mass is attached to a cart which is driven by a DC motor through a gear. The control of the position of the moving mass is achieved by a newly designed proportional integral derivative (PID) controller based on the displacement measurement, given by a potentiometer attached to the moving cart. The maximum stroke is  $\pm 15\text{cm}$  with a nominal maximum acceleration of  $5g$ . The total moving mass is  $1.7\text{Kg}$ , making the moving mass approximately 1.2 percent that of the total mass of the structure.

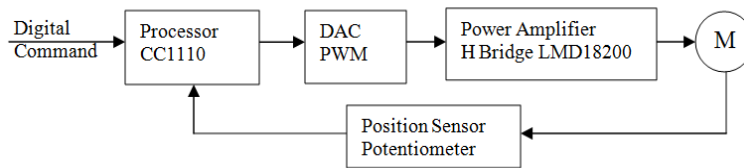


Fig.4.9 Block diagram of the servo position control system

As shown in Fig. 4.9, the motor servo control system consists of a processor CC1110 which implements a PID algorithm, a digital to analog converter in the form of pulse width modulation (PWM) which uses the duty cycle to represent the magnitude of the signal, a power amplifier LMD18200 which is a H bridge for driving the motor, and a position sensor in the form of potentiometer.

The block diagram of the PID algorithm is shown in the Fig. 4.10 in which the  $U(k)$  is the error, at step  $k$ , between the set point position and the actual

position,  $Y(k)$  is the output to the PWM, the  $Z^{-1}$  operator indicates a one sample time delay and the saturation represents the input range of the PWM. The optional anti-windup logic is used to stop the action of integrator when the output is saturated for avoiding excessive oscillation.

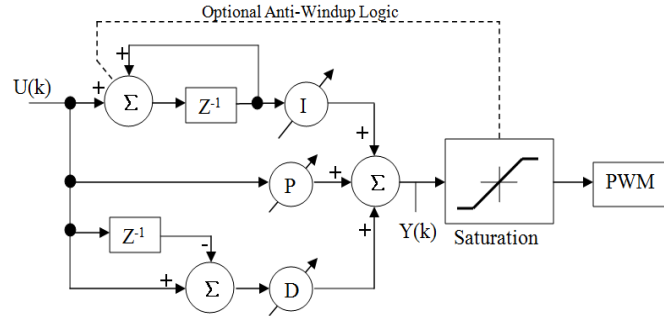


Fig.4.10 Block diagram of the digital PID algorithm

The processor inside the CC1110 is an enhanced 8051 core able to operate on a system clock up to 26MHz. Thanks to the high speed, the time required to perform one sample time PID calculation will be very small, for instance, few hundred microseconds allowing one to control at sample frequency of 1 KHz.

The PWM is supported by the 16 bits timer1 of the CC1110. It forms a very efficient power D/A converter when coupled to a switching power stage. The frequency of clock source of the timer can be up to 26MHz as well, which means that the resolution is 38 ns. Therefore, it can provide high resolution duty cycle even for short-period PWM signal. In the application of the driving motor, in order to avoid audible noise from motor, the frequency of the PWM signal should be close to or greater than the human hearing limit 20 KHz. When the PWM period is fixed to 20 KHz and the 26 MHz timer clock source is selected, the resolution of the PWM is still up to 10bits.

The motor responds to a PWM output stage by time averaging the duty cycle of the output. Most motors react slowly, having an electrical time constant of 0.5 ms or more and a mechanical time constant of 20.0 ms or more. A 20 kHz PWM output is effectively equivalent to that of a linear amplifier.

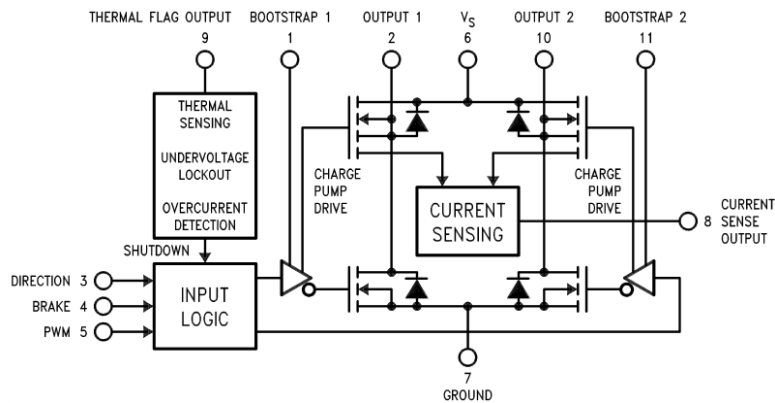


Fig. 4.11 Functional block diagram of LMD18200

The power amplifier after the PWM is implemented by the LMD18200. The LMD18200 is a 3A H-Bridge designed for motion control applications. The device is built using a multi-technology process which combines bipolar and CMOS (Complementary Metal Oxide Semiconductor) control circuitry with DMOS (Double-diffused Metal–Oxide–Semiconductor) power devices on the same monolithic structure. Ideal for driving DC (Direct Current) and stepper motors, the LMD18200 accommodates peak output currents up to 6A. An innovative circuit which facilitates low-loss sensing of the output current has been implemented. As shown in Fig. 4.11, LMD18200 is highly integrated and has the following features which are commonly concerned in designing a motor driver.

- (1) Delivers up to 3A continuous output
- (2) Operates at supply voltages up to 55V
- (3) Low RDS(ON) typically 0.3 ohm per switch
- (4) TTL and CMOS compatible inputs
- (5) No “shoot-through” current
- (6) Thermal warning flag output at 145°C
- (7) Thermal shutdown (outputs off) at 170°C
- (8) Internal clamp diodes
- (9) Shorted load protection

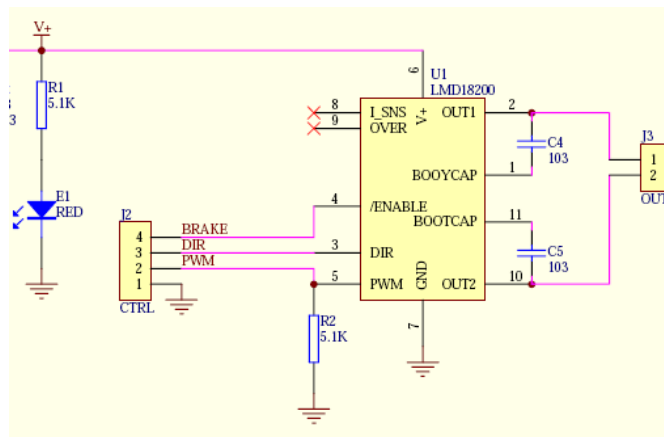


Fig. 4.12 Schematic of the LMD18200 Driver Module

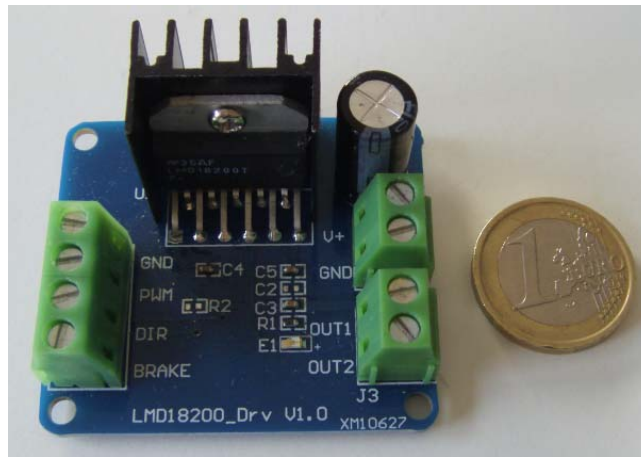


Fig. 4.13 Photo of the LMD18200 Driver Module

Due to the high integration LMD18200, the motor driver module is simple and small, as shown in Fig. 4.12 and Fig. 4.13. Its interface is also quite simple. There are only 3 control signals input to be interfaced with the controller together with the ground signal GND, PWM for controlling the magnitude of the average driving voltage of motor, DIR for controlling the polarity of the driving voltage on motor and BRAKE for quickly stopping the power supply to motor in case of accident. The “V+ GND” connector is for the only power

supply to module which can be up to +55V depending on the requirement of the motor. The “OUT1 OUT2” connector is for the DC motor.

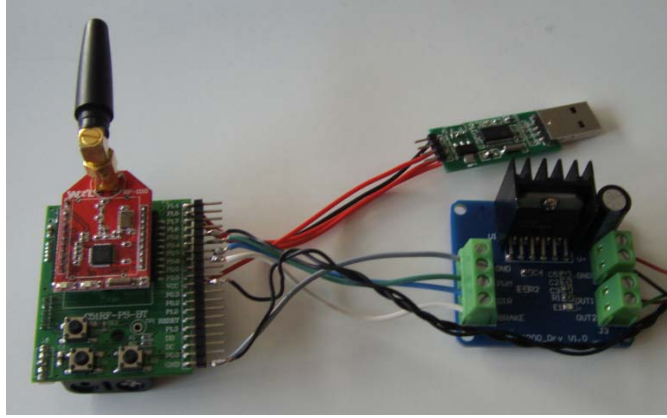
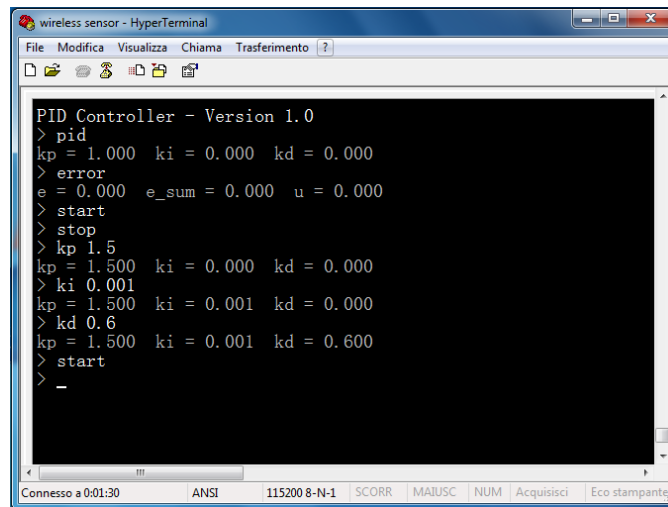


Fig. 4.14 the whole controller prototype

The whole controller prototype is shown in Fig. 4.14 where in addition to the driver module one can also see the CC1110 module mounted on its battery board and a UART (Universal Asynchronous Receiver/Transmitter) to USB (Universal Serial Bus) virtual RS232 module for communication with the configuration software in computer.

In order to configure the parameters of the PID controller in the computer, the controller is implemented as data terminal equipment (DTE), the software HyperTerminal is adopted as the terminal emulation as shown in Fig. 4.15 and the ANSI (American National Standards Institute) emulation is adopted. Some commands useful for the configuration are realized. For instance, the command ‘pid’ is to view the PID parameters; ‘error’ is to view the error input, the summation of error and control output of the PID algorithm; ‘kp’, ‘ki’ and ‘kd’ is to set the value of corresponding parameter. ‘start’ and ‘stop’ is to start and stop the PID control.



```

PID Controller - Version 1.0
> pid
kp = 1.000  ki = 0.000  kd = 0.000
> error
e = 0.000  e_sum = 0.000  u = 0.000
> start
> stop
> kp 1.5
kp = 1.500  ki = 0.000  kd = 0.000
> ki 0.001
kp = 1.500  ki = 0.001  kd = 0.000
> kd 0.6
kp = 1.500  ki = 0.001  kd = 0.600
> start
>
-

```

Fig. 4.15 the Configuration Interface for the PID controller

## 4.5 Experimental Validation

In this section, some experiments are performed to validate the controller prototype in Fig. 4.10. The AMD actuator is installed on the top of a 3-storey, steel frame which stands on a uniaxial shaking table used as excitation source. An accelerometer FBA-11 is positioned on each floor to provide the feedback acceleration signal. The excitation is a sinusoidal movement with a frequency of 1.25Hz and amplitude of 2mm. The value of 1.25Hz is close to the first natural frequency of the frame.

The first goal of the experimental tests consists of validating the data acquisition via wireless sensors. Therefore, a wired DAQ device from National Instrument simultaneously acquires the data and is used as reference for comparison. The acceleration data acquired by both approaches are plotted together and partly shown in Fig. 4.16, where the good agreement between them is evident, even when considering the records collected at the ground floor where the noise is dominant.



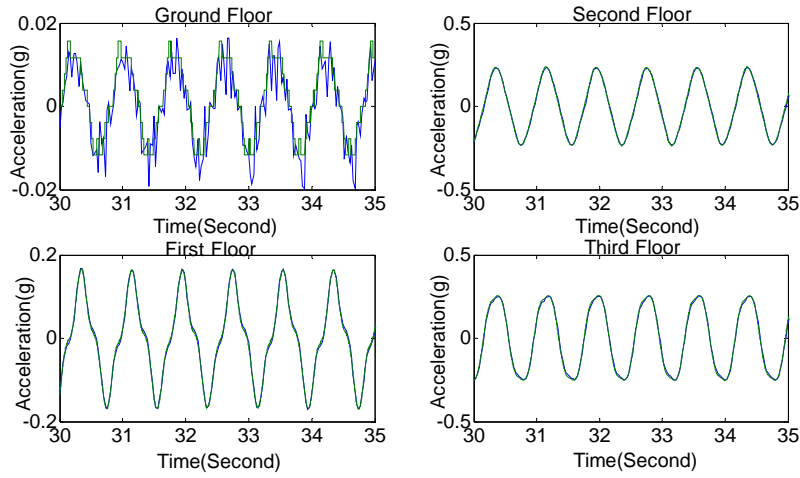


Fig.4.16 Comparison of the data acquired by wireless sensor and wired DAQ device. The blue line is the wired data while the green line is the wireless data.

The second task is to validate the effectiveness of the AMD. As previously mentioned, the excitation is a sinusoidal movement at a frequency of 1.25Hz, which is close to the first natural frequency of the structure. Therefore, when the excitation starts, the frame without AMD will resonate and the amplitude of the top floor acceleration will become higher and higher (as shown in the top left subplot of Fig. 4.17). In order to avoid destroying the frame, the excitation is stopped when the amplitude is close to 0.6V. As the excitation ends, the frame response is damped in a very slow manner (as shown in the top right subplot of Fig. 4.17).

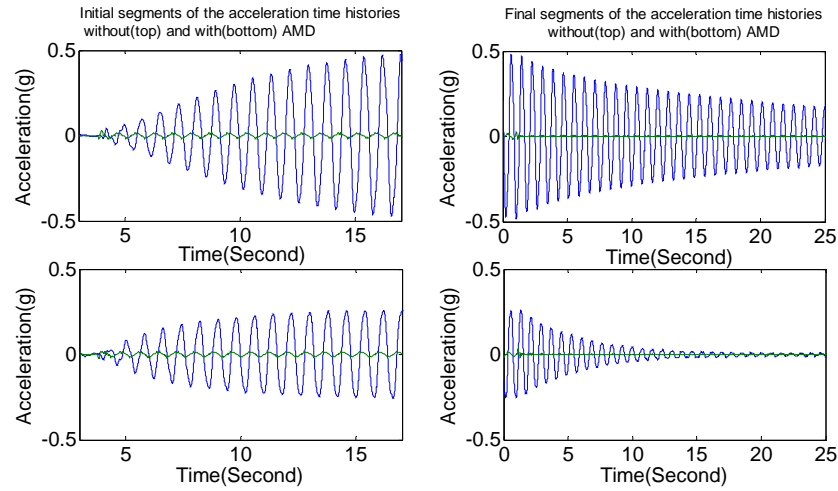


Fig. 4.17 Response Comparison of the controlled and uncontrolled frame under the same excitation: initial (right) and final (left) segments of the acceleration time histories, without (top) and with (bottom) ADM The blue line is the shaking table acceleration while the green line is the top floor acceleration.

Instead, when the excitation starts, the frame with the AMD will also resonate, but the amplitude of the top floor acceleration will tend to become stable at around 0.3V (as shown in the bottom left subplot of Fig. 4.17). When the excitation ends, the frame response is quickly damped (as shown in the bottom right subplot of Fig. 4.17).

## 4.6 Summary

In the applications of structural control, continuous and real-time sensing techniques are required. Wireless connections between the sensors and the structural controller are desirable in order to reduce the high cost and the labor-intensive installation related to the cables deployment. In this chapter, the analog cables are replaced by a customized prototype of a wireless sensing system which is based on the SoC single-chip transceivers. This solution offers high performance at low cost. The continuous and real-time wireless transmission is achieved by implementing a Frequency Division Multiplexing (FDM) approach.

The newly designed PID controller is validated to be effective and efficient in driving an AMD. The overall system is validated by carrying out laboratory tests.



## Chapter 5

### Energy Harvesting and Storage

#### 5.1 Introduction

Currently, most wireless sensor networks are powered by batteries which has the disadvantages that there is the need of either replacing or recharging them periodically. One possibility to overcome this power limitation is to harvest energy from the environment to either recharge a battery, or even to directly power the electronic device. This emerging concept is known as energy harvesting (also known as power harvesting or energy scavenging). It is the process that energy is derived from external sources (e.g., light, heat, motion, Radio Frequency), captured, and stored. Although macro energy harvesting technology has been around for a long time in the form of windmills, watermills and passive solar power systems and they can feed the grid, typically adding kilowatts or megawatts to the power distribution system, only the micro energy harvesting for low-power electronics like wireless sensor networks will be discussed in this dissertation. A typical micro energy harvesting system consists of energy harvester, power management and energy storage. It only can provide micro power to low power electronics. A typical energy-harvesting based wireless sensor node is illustrated in the following Fig. 5.1.

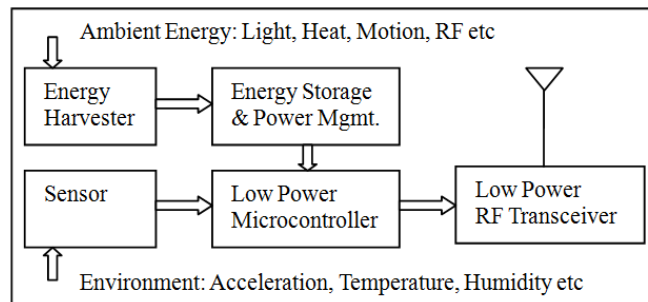


Fig. 5.1 Block diagram of a typical wireless sensor node with energy harvester.

This chapter first gives an overview of using energy harvesting and storage technologies for wireless sensor network. Then a prototype designed in the laboratory to which the author has access is described.

## 5.2 Ambient Energy Source and Harvester

The most promising micro-harvesting technologies extract energy from light, temperature differentials and vibration. A fourth possibility – scavenging energy from RF emissions – is interesting, but the energy availability is at least one order of magnitude less than that of the first three classes. The following table shows the approximate amount of energy per unit available from four micro-harvesting sources.

Table 5.1 Energy Harvesting Estimate(Texas Instruments 2010)

Energy Source	Harvested Power
<b>Vibration/Motion</b>	
<b>Human</b>	4 $\mu$ W/cm <sup>2</sup>
<b>Industry</b>	100 $\mu$ W/cm <sup>2</sup>
<b>Temperature Difference</b>	
<b>Human</b>	25 $\mu$ W/cm <sup>2</sup>
<b>Industry</b>	1-10mW/cm <sup>2</sup>
<b>Light</b>	
<b>Indoor</b>	10 $\mu$ W/cm <sup>2</sup>
<b>Outdoor</b>	10m W/cm <sup>2</sup>
<b>RF</b>	
<b>GSM</b>	0.1 $\mu$ W/cm <sup>2</sup>
<b>WiFi</b>	0.001 $\mu$ W/cm <sup>2</sup>

1, Light

Solar energy harvesting using photovoltaic cells represents one of the most mature and reliable techniques available for utilizing ambient energy. Approximately 1mW of average power can be harvested from each 1cm<sup>2</sup> photovoltaic cell. Typical efficiency is roughly 10 percent and the capacity factor of photovoltaic sources (the ratio of average power produced to power

that would be produced if the sun was always shining) is about 15 to 20 percent. (Texas Instruments 2010)

The operation process of photovoltaic cell is composed of three steps: (1) photons in sunlight hit the solar panel and are absorbed by semiconducting materials, such as silicon; (2) electrons are knocked loose from their atoms, allowing them to flow through the material to produce electricity. Due to the special composition of solar cells, the electrons are only allowed to move in a single direction. (3) An array of solar cells converts solar energy into a usable amount of direct current (DC) electricity.

When a photon is absorbed, its energy is given to an electron in the crystal lattice. Usually this electron is in the valence band, and is tightly bound in covalent bonds between neighboring atoms, and hence unable to move far. The energy given to it by the photon "excites" it into the conduction band, where it is free to move around within the semiconductor. The covalent bond that the electron was previously a part of now has one fewer electron — this is known as a hole. The presence of a missing covalent bond allows the bonded electrons of neighboring atoms to move into the "hole," leaving another hole behind, and in this way a hole can move through the lattice. Thus, it can be said that photons absorbed in the semiconductor create mobile electron-hole pairs.

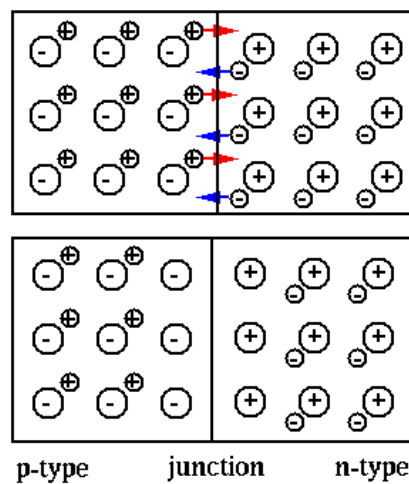


Fig. 5.2 silicon PN junction

The most commonly known solar cell is configured as a large-area p-n junction made from silicon, as shown in Fig. 5.2. The p-n junction limits the

electron only able to move in one direction, from p-type silicon to n-type silicon. As a simplification, one can imagine bringing a layer of n-type silicon into direct contact with a layer of p-type silicon. In practice, p-n junctions of silicon solar cells are not made in this way, but rather by diffusing a n-type dopant into one side of a p-type wafer (or vice versa). If a piece of p-type silicon is placed in intimate contact with a piece of n-type silicon, then a diffusion of electrons occurs from the region of high electron concentration (the n-type side of the junction) into the region of low electron concentration (p-type side of the junction). When the electrons diffuse across the p-n junction, they recombine with holes on the p-type side. However, the diffusion of carriers does not happen indefinitely because charges build up on either side of the junction and create an electric field. The electric field creates a diode that promotes charge flow (known as drift current) that opposes and eventually balances out the diffusion of electrons and holes. This region where electrons and holes have diffused across the junction is called the depletion region because it no longer contains any mobile charge carriers. It is also known as the *space charge region*.

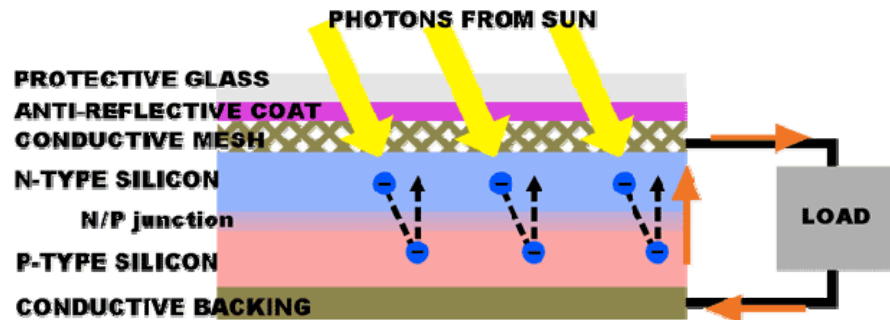


Fig. 5.3 Architecture of a photovoltaic module

The basic construction of a photovoltaic module is illustrated in Fig. 5.3. Since the voltage produced by a photovoltaic cell is around the diode voltage, the cells within a module are normally connected in series to increase the overall voltage of the module. The modules can then be connected in parallel to increase the output current. To prevent electricity from flowing back into the solar module, a blocking diode is commonly used between the module output and its target input.



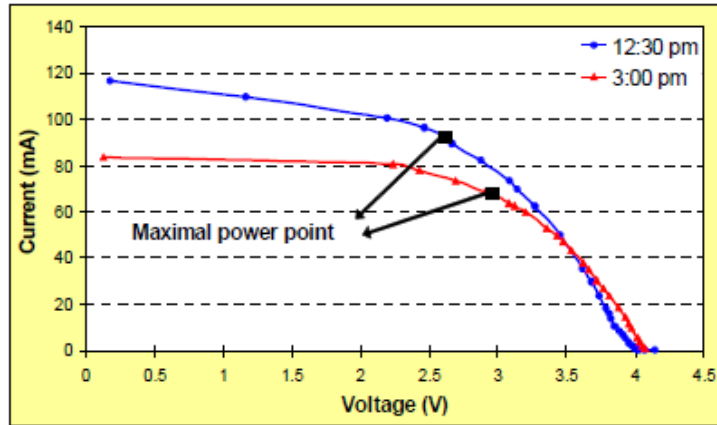


Fig. 5.4 Measured V-I characteristics of the Solar World 4-4.0-100 solar panel

In the usage of a solar panel, it is crucial to understand their voltage and current characteristics. A 3.75" x 2.5" panel from Solar World Inc., the 4-4.0-100 is characterized by (Raghunathan, Kansal, Hsu, Friedman and Srivastava 2005). This panel is typical of the commercially available panels, and the results of the study can be extended to similar panels. In the study, the authors noted that panels are characterized by two parameters, the open circuit voltage and the short circuit current. These two parameters are found on the x- and y- intercepts of the V-I curve shown in Fig. 5.4. From Fig. 5.4, a few observations are made. First, it is evident that the solar panel behaves as a voltage limited current source. Additionally, an optimal operating point exists, meaning that power output from the panel is maximized at that point. Finally, as the amount of solar radiation decreases, the short circuit current decreases; however, the open circuit voltage remains nearly constant. Understanding these characteristics is beneficial in achieving an effective solar energy harvesting system.

## 2, Heat

Thermoelectric harvesters exploit the Seebeck effect, which states that voltage is created in the presence of a temperature difference between two different metals or semiconductors. A thermoelectric generator (TEG) consists of thermopiles connected thermally in parallel and electrically in series. The latest TEGs are characterized by an output voltage of 0.7 V at matched load,

which is a familiar voltage for engineers designing ultra-low-power applications. Generated power depends on the size of the TEG, the ambient temperature, and (in the case of harvesting heat energy from humans), the level of metabolic activity.

### 3, Motion

Commercially available kinetic energy systems also produce power in the milliwatt range. Energy is most likely to be generated by an oscillating mass (vibration). But electrostatic energy harvested by piezoelectric cells or flexible elastomers is also classified as kinetic energy. Vibrational energy is available from structures such as bridges and in many industrial and automotive scenarios. Basic kinetic harvester technologies include: (1) a mass on a spring; (2) devices that convert linear to rotary motion; and (3) piezoelectric cells. An advantage of (1) and (2) is that voltage is not determined by the source itself but by the conversion design. Electrostatic conversion produces voltages as high as 1,000 V or more.

### 4, RF

In cities and very populated areas, there is a large amount of electromagnetic energy around us transmitted by such sources as radio and television broadcasting, cell phone networks, Wifi, satellite communication systems and so on. By scavenging this ambient energy from the air around us, the technique could provide a new way to power networks of wireless sensors, microprocessors and communications chips. The conversion is based on a rectifying antenna (rectenna), constructed with a Schottky diode located between the antenna dipoles. A special case of this concept is RFID tags, which can receive RF energy from a nearby reader and also perform wireless communication with it.

The Georgia Tech School of Electrical and Computer Engineering announced a device to capture ambient electromagnetic energy to drive small electronic devices. The device uses an ultra-wideband antenna which can exploit a variety of signals in different frequency ranges, providing greatly increased power-gathering capability.

### 5.3 Power Management

Since the power from the abovementioned harvesters is unregulated and intermittent, power management circuit is required before the harvested energy can be used to charge the storage element or power the application circuit. The energy produced by the harvester is first rectified (in the case of vibration harvesters). Then a dedicated DC - DC converter transfers the power to an energy storage element, for instance a secondary battery, matching the voltage level at the harvester output with the voltage level needed to charge the battery. For example, in the MicroStrain EH-Link energy harvesting wireless sensor node (Arms, Townsend, Hamel, Distasi and Galbreath 2010), there are two types of DC-DC converter: step down (LTC3588) and step up (LTC3108). The input range of the LTC3588 is from 3 to 20V AC or 3 to 20 V DC, supporting the piezoelectric harvester, inductive harvester and photovoltaic harvester). The input range of the LTC3108 is from 20 to 600mV DC, supporting thermoelectric harvester.

Maxim release the industry's first complete power-management IC dedicated to Energy Harvesting, MAX17710 which can charge a low-capacity cell with overcharge protection and an LDO regulator output with over-discharge protection. This chip can facilitate the design of power management in energy-harvesting solution. (MAXIM, 2011)

In order to maximize the power transfer from the harvester, a function called maximum power point tracking (MPPT) is also pursued, which can regulate the load offered to the harvester so that it matches the electric impedance of the generator. (Raghunathan and Chou 2006)

## 5.4 Energy Storage

Table 5.2 Characteristics of typical energy storage options(Blyler 2009)

	Li-Ion Battery	Thin Film Battery	Super Cap
Recharge cycles	Hundreds	Thousands	Millions
Self-discharge	Moderate	Negligible	High
Charge Time	Hours	Minutes	Sec-minutes
Physical Size	Large	Small	Medium
Capacity	0.3-2500 mAHr	12-1000 $\mu$ AHr	10-100 $\mu$ AHr
Environmental Impact	High	Minimal	Minimal

The harvested electrical energy should be buffered or stored in storage element, such as Li-ion battery, thin-film battery, super-capacitor etc. The characteristics of the three typical storage options are listed in the above Table 5.2. Capacitors are used when the application needs to provide huge energy spikes. Batteries leak less energy and are therefore used when the device needs to provide a steady flow of energy.

## 5.5 Low Power Electronics

Since the energy harvested from environment is very low in a micro-energy harvesting solution, the power requirement of the application electronic should be as low as possible. For example, in a wireless sensor node, the necessary components including microcontroller, sensor and RF transceiver should be of low power. The lifetime of an energy harvesting based WSN can be extended by two approaches: one is to raise the harvested energy; the other is to reduce the energy consumption in wireless sensor node.

The microcontroller products from Texas Instrument (MSP430 series, ultra low power) and Microchip (PIC series, extremely low power) are of relatively lower power. Both these products feature low standby current, low active current, low operating voltage and short wake up time.

Many microelectronics companies have low power RF transceiver series products which support the various license-free ISM frequency bands and are easy-to-use due to high integration, such as Texas Instrument, Microchip,

Nordic, Silicon Labs etc. In recent years, the concept of System on Chip (SoC) is emerging. The SoC transceiver integrates a low power microcontroller so that the cost and size of the application unit can be reduced, such as IEEE802.15.4-compliant CC2430 for ZigBee application from TI. The Texas Instrument's series product is representative and commonly used in many WSN.

Compared to traditional sensor, micro-electromechanical systems (MEMS) sensors have the advantages: low power, low cost and small size. Therefore, it is suitable for the energy harvester based WSN. The Crossbow CXL-LF series accelerometer is based on this technology.

### 5.6 Hardware Design and Implementation of a Smart Energy Harvesting and Storage Unit Prototype

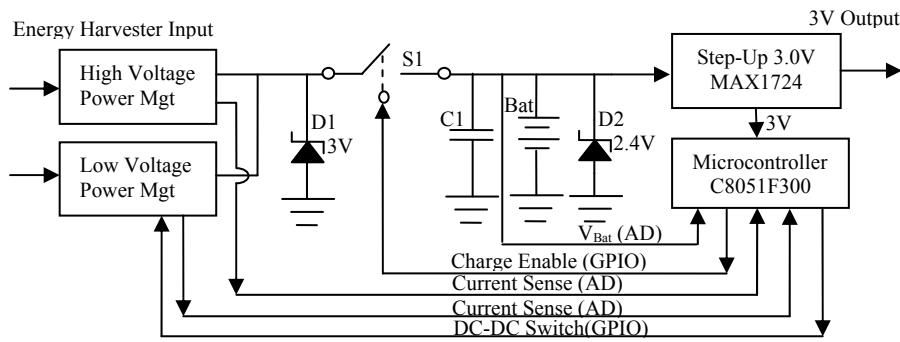


Fig. 5.5 Functional Block Diagram of the Energy Harvesting Unit (Mgt: management, Bat: battery, AD: analog to digital pin, GPIO: general purpose input and output pin)

In this section, a smart energy harvesting and storage unit is designed to manage the power from energy harvesters, as shown in Fig.5.5. The unit has a high voltage AC/DC and a low voltage DC energy harvester input. The unit outputs a regulated 3V voltage through the step-up converter MAX1724.

A super capacitor or a rechargeable battery can be used as the energy storage element. In order to protect the energy storage element from being overcharged and damaged, two Zener diodes (D1 and D2) are used. When the voltage from the energy harvester is higher than the reverse breakdown voltage (D1: 3V, D2: 2.4V), the diode will allow a high current to flow, thus limiting the voltage at the reverse breakdown voltage.

In this unit, there is a low power microcontroller to manage the power conversion. The microcontroller can enable and disable charging through the electronic switch S1. It also can monitor the charging voltage and current through its internal ADC.

In the low voltage power management module, there is a DC-DC step-up voltage converter whose switching frequency is controlled by the microcontroller. Thus its output voltage can be controlled by the microcontroller. In the high voltage power management module, there is a full wave rectifier formed by 4 diodes. The rectifier can convert an alternating current (AC), which periodically reverses direction, to a direct current (DC) which flows in only one direction. At the output of both the power management modules, there is a 1ohms resistor in series. The charging current is monitored by indirectly monitoring the voltage of the resistor, since the charging current is equal to the current flowing through the resistor.

Based on the abovementioned hardware, the firmware in the microcontroller can monitor the charging current and voltage, thus estimating the harvested power and energy. The firmware can be aware of if the storage element is fully charged or not, by monitoring the voltage of storage element. If the storage element is fully charged, the firmware turn off the switch S1 to disable the charging.

The performance of this energy harvesting and storage unit with an EM energy harvester was reported by (Casciati and Rossi 2007).

## **5.7 Summary**

Energy harvesting and storage is a promising solution for the power supply limitation of wireless sensor network. In this chapter, some typical micro ambient energy sources and their corresponding harvesters are introduced, including light, motion, heat and radio frequency. Since ambient energy is unregulated and intermittent, an energy storage element is required to store the harvested energy and power management circuits are required to match the harvester output with the energy storage element input and the power requirement of load circuits. The power consumption of the electronics using the harvested energy should be as low as possible. At last, a smart energy harvesting and storage unit prototype is introduced.

## **Chapter 6**

### **Summary, Conclusions and Future Directions**

Using wireless sensors in structural monitoring and control system may greatly reduce the installation cost while greatly increasing the flexibility of the system architectures. This thesis has described the development and validation of a wireless sensing unit. Based on the wireless sensing unit, a wireless structural monitoring system is constructed and a structural control system is updated to be wireless. This chapter first provides the summary and conclusions of the thesis, and then discusses future research directions.

#### ***6.1 Summary and Conclusions***

The main work of this dissertation is designing a general wireless sensing unit compatible with the typical sensors in the application of structural health monitoring and control system to replace the coaxial cables and the centralized data acquisition device. The real-time multi-channel wireless communication is implemented by the frequency division multiplexing. Based on the designed wireless sensing unit, a wireless structural monitoring system and a wireless structural control system are constructed.

##### **(1) Wireless Sensing Unit**

The wireless sensing unit is based on the SoC RF transceiver CC1110 operating in the sub-1GHz license-free ISM frequency band with a proprietary communication protocol. It was validated by laboratorial test.

The compatibility with various sensors is mainly associated with the power management and signal conditioning modules. The flexible power management module based on the LDO linear voltage regulator and switching voltage regulator of high-efficiency, low quiescent current, and adjustable output make the wireless sensing unit capable of providing flexible power supplies to various

sensors for monitoring structural dynamics, such as accelerometers, strain gage, load cell, laser distance sensor and so on. The signal conditioning module based on an instrument operational amplifier with differential input and adjustable gain and offset make the wireless sensing unit compatible with the different outputs of various sensors.

The SoC RF transceiver CC1110 has packet handling hardware which greatly facilitates the implementation of packet-based wireless communication. Two communication modes are available: reliable mode and unreliable mode. In the reliable mode, the acknowledgement and retry mechanism is adopted to ensure that a data packet is successfully received.

### (2) Wireless Structural Monitoring System

Based on the wireless sensing unit, a real-time multi-channel wireless structural monitoring system is designed. The wireless structural monitoring system consists of pairs of wireless sensor and base station unit, a USB hub and a computer and the software tool HyperTerminal which can receive data from the RS232 port and display and save the received data into TXT file. The base station unit mainly consists of a CC1110 module and a UART to USB adapter for implementing a virtual RS232 in computer through the USB connection.

The real-time multi-channel features are implemented by the frequency division multiplexing method which is supported by the CC1110 transceiver through the configurable frequency synthesizer and receiver band pass filter. The channel number is limited by the available frequency band. One wireless channel is constructed by a pair of CC1110 transceiver modules, one of which is in the wireless sensing unit and the other is in the base station unit.

### (3) Wireless Structural Control System

In a wireless structural monitoring system, real time wireless transmission is optional, while it is required in a wireless structural control system. Based on the FDM method, a real-time four-channel wireless sensing system is designed and integrated into a wired active mass damper structural control system to



extend 4 wireless data input channels. The wireless sensing system is validated by laboratory tests.

In addition, a digital PID position controller for DC motor is developed to replace the analog PD controller in the previous AMD system. The digital controller mainly consists of a CC1110 transceiver module, where a digital PID algorithm is implemented, and a power amplifier H bridge LMD18200 module. Compared to the analog controller, the digital controller is of high power efficiency, small size and more flexible.

#### (4) Energy Harvesting and Storage

Although wireless sensor can avoid the drawbacks of wired sensor, its advantage is compromised by the fact that the batteries power supply need to be periodically replaced. Energy harvesting and storage is a promising solution for this problem. In this dissertation, some typical micro ambient energy sources and their corresponding harvesters are investigated including light, motion, heat and radio frequency. Since the ambient energy is usually limited, unregulated and intermittent, an energy storage element is required to store the harvested energy and some power management circuits are required to match the harvester output with the energy storage element input and the power requirement of load circuits. Furthermore, the power consumption of the electronics using the harvested energy should be as low as possible.

## ***6.2 Future Directions***

The wireless sensing unit presented in this paper is mainly based on the CC1110 operating in Sub-1GHz ISM frequency band. Compared to Sub-1GHz ISM frequency band which is regional and has a limited bandwidth, the 2.4GHz ISM frequency band is global, has a larger bandwidth (83.5MHz) and allow a higher RF transmitting power. Therefore, to have more channels and larger communication range, the future development of the wireless sensing unit should adopt the 2.4GHz transceiver.

Although the license-free bandwidth of 2.4GHz is large, many wireless devices are working on this band, like WiFi and Bluetooth. Thus, the

interference from these wireless devices should be considered. In addition, the signals from different frequency channels, especially the adjacent channels, might interfere with each other. Thus, a deeper study on possible interference should be performed.

## Bibliography

Andrejašić, M. (2008). "MEMS Accelerometers." from [http://mafija.fmf.uni-lj.si/seminar/files/2007\\_2008/MEMS\\_accelerometers-koncna.pdf](http://mafija.fmf.uni-lj.si/seminar/files/2007_2008/MEMS_accelerometers-koncna.pdf).

Arms, S. W., C. P. Townsend, M. J. Hamel, S. J. Distasi and J. H. Galbreath (2010). Energy Harvesting Wireless Sensor Networks for Embedded Structural Health Monitoring. Proceedings of fifth European Workshop on Structural Health Monitoring, Sorrento, Italy.

Battaini, M. (1999). "Controlled Structure System, Design and reliability." Structural Control and Health Monitoring **6**(1): 11-52.

Blyler, J. (2009). "Energy Scavenging And Storage Must Work Together." from <http://chipdesignmag.com/lpd/blog/2009/07/16/energy-scavenging-and-storage-must-work-together/>.

Casciati, F. and Z. C. Chen (2009). Using GPS sensors in Structural Mechanics. Proceedings of the 1st Japan-Austria Joint Workshop on Mechanics and Model Based Control of Smart Materials and Structures. H. Irschik, M. Krommer, K. Watanabe and T. Furukawa, SpringerWienNewYork.

Casciati, F., J. Rodellar and U. Yildirim (2011). Active and Semi-active Control of Structures: A Review of Recent Advances. the 8th International Conference on Structural Dynamics, Leuven, Belgium.

Casciati, F. and R. Rossi (2004). Fuzzy chip controllers and wireless links in smart structures. Jadwisin, Poland, Springer Verlag.

Casciati, F. and R. Rossi (2007). "a Power Harvester for Wireless Sensing Applications." Structural Control and Health Monitoring **14**(4): 649-659.

Casciati, S. and Z. C. Chen (2011). "A multi-channel wireless connection system for structural health monitoring applications." Structural Control and Health Monitoring **18**(5): 588-600.

Casciati, S., L. Faravelli and Z. C. Chen (2009a). A design of multi-channel wireless sensing system for structural monitoring. ECCOMAS Thematic Conference on Computational Methods in Structural Dynamics and Earthquake Engineering. Rhodes, Greece, 22-24 June, 2009.

Casciati, S., L. Faravelli and Z. C. Chen (2009b). Design of a Multi-channel Real-time Wireless Connection System for Analog Cable Replacement Application. 7th International Workshop on Structural Health Monitoring. Stanford, CA USA, September 9-11, 2009.

Casciati, S., L. Faravelli and Z. C. Chen (2010a). A multi-channel wireless transmission system for structural monitoring. The 4th International Conference on Structural Engineering, Mechanics and Computation. Cape Town, South Africa, Sept. 6-8, 2010.

Casciati, S., L. Faravelli and Z. C. Chen (2010b). A Real-time Multi-channel Wireless Sensing Network for Structural Monitoring Applications. The 10th International Conference on Motion and Vibration Control. University of Tokyo, Japan, Aug. 17-20, 2010.

Casciati, S., L. Faravelli and Z. C. Chen (2010c). A Real-time Multi-channel Wireless Sensing System for Analog Cable Replacement Application. The 5th Edition of European Workshop on Structural Health Monitoring. F. Casciati and M. Giordano. Sorrento, Naples, Italy, June 29-July 02, 2010: 1188-1195.

Casciati, S., L. Faravelli and Z. C. Chen (2010d). Frequency Division Multiplexing Wireless Connection. The 6th International Conference on Wireless Communications, Networking and Mobile Computing. Chengdu, China, Sept.23-25, 2010.

Casciati, S., L. Faravelli and Z. C. Chen (2010e). Multi-channel Cable Replacement for Structural Control Applications. The 5th World Conference on Structural Control and Monitoring. KEIO PLAZA Hotel, SHINJUKU, Tokyo, Japan, Jul.12-14, 2010.

Casciati, S., L. Faravelli and Z. C. Chen (2011b). Power Harvesting and Management for Structural Control Application. Engineering Mechanics Institute 2011. Northeastern University , Boston, MA, June 2-4, 2011.

Chen, Z. C. and L. Faravelli (2011). Wireless Sensors for Structural Control 8th International Conference on Structural Dynamics. Leuven, Belgium, Jul. 4-6 2011.

Faravelli, L. and Z. C. Chen (2009). Time Issues in a Wireless Network. 15th International Workshop on Dynamics and Control. CIMNE, Barcelona.

Farrar, C. R. (2001). Historical Overview of Structural Health Monitoring. Lecture Notes on Structural Health Monitoring Using Statistical Pattern Recognition. Los Alamos Dynamics, Los Alamos,NM.

Feltrin, G. (2010). Data intensive long-term monitoring with wireless sensor networks. Workshop on Monitoring Technologies. June 7-8, Troyes (FR).

Feltrin, G., J. Meyer, R. Bischoff and M. Motavalli (2009). Modular Wireless Sensor Network for Long-Term Structural Health Monitoring. 4th International Conference on Structural Health Monitoring of Intelligent Infrastructure (SHMII-4) Zurich, Switzerland.

Freescale Semiconductor (2007). "Accelerometer Terminology Guide."

IEEE Computer Society (2007). "IEEE802.15.4a-2007." from <http://standards.ieee.org/getieee802/download/802.15.4a-2007.pdf>.

Jiang, X. D., Y. L. Tang and Y. Lei (2009). Wireless Sensor Networks in Structural Health Monitoring Based on ZigBee Technology. Proceedings of the 3rd international conference on Anti-Counterfeiting, security, and identification in communication, HongKong, China.

Kim, S., M. Spenko, S. Trujillo, B. Heyneman, V. Mattoli and M. R. Cutkosky (2007). Whole body adhesion: hierarchical, directional and distributed control of adhesive forces for a climbing robot. 2007 IEEE International Conference on Robotics and Automation. Roma, Italy.

KYOWA. "what is a strain gage."

Liu, H., H. Darabi, P. Banerjee and J. Liu (2007). "Survey of Wireless Indoor Positioning Techniques and Systems." IEEE TRANSACTIONS ON SYSTEMS, MAN, AND CYBERNETICS—PART C: APPLICATIONS AND REVIEWS **37**(6): 1067-1080.

Lynch, J. P. (2006). "A Summary Review of Wireless Sensors and Sensor Networks for Structural Health Monitoring." The Shock and Vibration Digest **38**(2): 91-128.

Lynch, J. P., Y. Wang, R. A. Swartz, K. C. Lu and C. H. Loh (2008). "Implementation of a closed-loop structural control system using wireless sensor networks." Structural Control and Health Monitoring **15**(4): 518-539.

Meyer, J., R. Bischoff, G. Feltrin and M. Motavalli (2007). A Low Power Wireless Sensor Network for Long Term Structural Health Monitoring. 3rd International Conference on Structural Health Monitoring of Intelligent Infrastructure. Vancouver.

MicroStrain. "G-LINK\_mXRS\_Datasheet\_Rev\_1.00.". from [http://www.microstrain.com/product\\_datasheets/G-LINK\\_MXRS\\_Datasheet\\_Rev\\_1.00.pdf](http://www.microstrain.com/product_datasheets/G-LINK_MXRS_Datasheet_Rev_1.00.pdf).

Raghunathan, V. and P. H. Chou (2006). Design and Power Management of Energy Harvesting Embedded Systems. Proceedings of the 2006 international symposium on Low power electronics and design, Tegernsee, Bavaria, Germany.

Raghunathan, V., A. Kansal, J. Hsu, J. Friedman and M. Srivastava (2005). Design Considerations for Solar Energy Harvesting Wireless Embedded Systems. IEEE International Conference on IPSN.

Saunders, A., D. Goldman, R. Full and M. Buehler. (2006). The RiSE Climbing Robot:Body and Leg Design. Proceeding of SPIE Defense&Security Symposium, Unmanned Systems Technology, Orlando, FL.

SignalGeneriX. "WiseSPOT." from [http://www.signalgenerix.com/index.php?option=com\\_content&view=article&id=11&Itemid=23](http://www.signalgenerix.com/index.php?option=com_content&view=article&id=11&Itemid=23).

Spencer, B. F. and S. Nagarajaiah (2003). "State of the Art of Structural Control." Journal of Structural Engineering **129**(7): 845-856.

Spencer, B. F., M. E. Ruiz-Sandoval and N. Kurata (2004). "Smart Sensing Technology:Opportunities and Challenges." Structural Control and Health Monitoring **11**: 349-368.

Swartz, R. A. and J. P. Lynch (2006). A Multirate Recursive ARX Algorithm For Energy Efficient Wireless Structural Monitoring. Proceedings of the 4th World Conference on Structural Control and Monitoring, San Diego, CA, USA.

Swartz, R. A. and J. P. Lynch (2009). "Strategic Network Utilization in a Wireless Structural Control System for Seismically Excited Structures." ASCE J. Struct. Engg **135**(5): 596-608.

Texas Instruments (2010). "Ultra Low Power Meets Energy Harvesting." from <http://focus.ti.com/general/docs/lit/getliterature.tsp?baseLiteratureNumber=slyy018&fileType=pdf>.

Unver, O., M. P. Murphy and M. Sitti (2005). Geckobot and Waalbot: Small-Scale Wall Climbing Robots. AIAA 5th Aviation, Technology, Integration, and Operations Conference.

Wang, Y., J. P. Lynch and K. H. Law (2005). Design of a Low-Power Wireless Structural Monitoring System for Collaborative Computational Algorithms. Proceedings of SPIE 12th Annual International Symposium on Smart Structures and Materials. San Diego, CA.

Wikipedia. "wireless sensor network." from <http://en.wikipedia.org/wiki/WSN>.

Zhu, D., X. Yi, Y. Wang, K. M. Lee and J. Guo (2010). "A Mobile Sensing System for Structural Health Monitoring: Design and Validation." Smart Materials and Structures **19**: 055011.